DISSERTATION

THE ROLE OF GALACTOSYLECERAMIDES IN FLAVIVIRUS INFECTION

Submitted by

Hannah Laurence

Department of Microbiology, Immunology, and Pathology

In partial fulfillment of the requirements

For the Degree of Doctor of Philosophy

Colorado State University

Fort Collins, Colorado

Spring 2025

Doctoral Committee:

Advisor: Rushika Perera

John Belisle
Punya Nachappa
Greg Ebel

ABSTRACT

THE ROLE OF GALACTOSYLECERAMIDES IN FLAVIVIRUS INFECTION

Mosquito-borne flaviviruses are an intensifying threat to global health without specific antiviral therapies or a widely available vaccine. Between 2000 and 2019, there was a 10-fold surge in dengue virus cases reported globally [1]. 2024 was a record year with more than 14 million dengue cases reported worldwide [2]. Flaviviruses are reliant upon host cell membranes to complete their life cycle. Preliminary data for this work included an siRNA loss of function screen of each enzyme in the sphingolipid metabolic pathway performed in liver cells (Huh7) infected with dengue virus 2. This screen identified numerous enzymes of interest in the metabolic pathway. This dissertation investigates the roles of two key enzymes in the sphingolipid metabolic pathway that affect synthesis and degradation of galactosylceramides, UDP-galactosyltransferase 8 (UGT8) and galactocerebrosidase (GALC), and how they affect flavivirus infections in vitro. We studied how modulating the expression of UGT8 and GALC during infection with dengue virus, serotype 2 (DENV2) and Zika virus (ZIKV) impact the virus life cycle in human hepatoma cells (Huh7). We additionally studied how UGT8 knockdown affected ZIKV titer in neuroblastoma cells (SH-SY5Y). Chapter 2 focuses on the effect of UGT8 during DENV2 infection of Huh7 cells. We showed that with UGT8 knockdown, there was an increase in titer, while overexpression caused a decrease in titer. Mechanistic studies demonstrated that modulating UGT8 expression affected entry and release of DENV2 particles. We did not observe any effect on DENV2 genome replication or the specific

infectivity of the virus particles. We hypothesized that modulation of UGT8 expression alters the cell and viral membranes to influence virus release and virus entry. Chapter 3 focuses on GALC, which performs the reciprocal reaction as UGT8 and degrades galactosylceramides in the lysosome. We discovered that GALC knockdown increased both extracellular and intracellular DENV2 titers, but did not affect genome replication or specific infectivity. This suggested that GALC knockdown caused an increase in the efficiency of viral assembly. We proposed that the oxidative stress resulting from loss of function of the GALC enzyme upregulated sphingomyelinases to increase cellular pools of ceramide, resulting in an increase in efficiency of viral assembly. Chapter 4 explored the effects of UGT8 in ZIKV infection of both Huh7 cells and SH-SY5Y cells. Modulation of UGT8 expression in these cells showed a similar phenotype to DENV2. Together, the findings in this dissertation highlight the importance of sphingolipid metabolism in flavivirus infections and provides new insights into the roles of these specialized lipids during infection. Hypothesis of the study: The flavivirus life cycle is critically influenced by the balance of galactosylceramide synthesis and degradation, processes regulated by UDP-galactosyltransferase 8 (UGT8) and galactocerebrosidase (GALC) respectively.

ACKNOWLEDGEMENTS

I would like to express my utmost gratitude to my advisor, Dr. Rushika Perera, for her guidance during my doctoral journey. She gave me the opportunity to work in her lab, provided me mentorship and character-building, and supported me through the tough times I had during graduate school. Her expertise in virology and metabolism has been invaluable in shaping this research. I greatly appreciated the opportunity to have worked under her supervision which has contributed significantly to my growth as a scientist.

I would like to also thank the members of my graduate committee: Drs. Punya Nachappa, John Belisle, and Greg Ebel. They saw me through some of the lowest points of grad school and helped me to emerge in one piece on the other side.

To all the members, past and present of the Perera lab, thank you for your support and for helping me to find joy and new knowledge in all of our failures. A special thank you to Oshani, for laughing with me at all hours of the day and night in the lab. And to Kaitlyn, who taught me what it means to be a good mentor, and who will soon be starting her own journey in graduate school. To Paul, who shared grad school life advice and good music. To Irma, without whom I would have been completely lost in mosquito-land.

To my family, who have been by my side and always a phone call away as I finally get to be done with school after the 27th grade ☺ Thank you for believing in me, even when I didn’t believe in myself.

TABLE OF CONTENTS

Chapter 1: Literature Review

1.1 Introduction

Infectious diseases are a significant threat which present challenges to human health and the global economy, with vector-borne diseases accounting for greater than 17% of all human infectious diseases [3,4]. Mosquito-borne diseases alone are responsible for approximately 700 million cases globally and over a million deaths annually [5,6]. In 2023, there was a record year for dengue virus, with 6.5 million cases and 7,300 dengue-related deaths recorded [5]. These staggering case numbers underscore the need for continued research to develop improved prevention strategies and therapeutics to address these urgent global health issues.

To stay ahead of the next pathogen with epidemic potential, we must focus our efforts on both clinical research, to understand the medical consequences of diseases, and also basic science and virology research, to understand the mechanisms of infection and develop therapeutic targets. While significant effort has gone into studying infectious diseases on a molecular level, focusing on changes to nucleic acids and proteins, there is a growing need for a detailed understanding of the metabolism of infectious diseases to complete the puzzle. Changes in metabolites reflect changes in a cell's metabolism, which can provide a complete picture of all the pathways being affected by a given stimulus. Among the components involved in host cellular metabolism, lipids are emerging as critically important yet historically overlooked part of the puzzle. Recent advances have begun to shed light on the fundamental roles of lipid metabolism in viral infection, providing new perspectives on our understanding of disease pathogenesis.

Cellular lipids, which have long been recognized as structural components in cells, have in recent years gained recognition for their roles in disease pathogenesis. Lipids are versatile molecules that perform a myriad of functions that can be usurped during infection. In the context of viral infection, lipid metabolism may be altered to mediate pathogen recognition and attachment, how the viral and host membranes fuse together, or may affect signaling pathways. In this dissertation, the roles of lipids in viral infection will be extensively discussed. Elucidating the functions of lipids during viral infection and the impact of infection on lipid metabolism could reveal novel approaches for developing treatment and prevention strategies.

First, an overview of the two viruses studied in this dissertation work will be presented, followed by an examination of flavivirus biology, host cell lipid structure, function and metabolism, and how those two topics intersect.

1.2 Overview of Flaviviruses

Flaviviruses (FVs) are a diverse family of viruses which include dengue viruses (DENV), Zika virus (ZIKV), West Nile virus (WNV), and yellow fever virus (YFV), among many others. Within the family Flaviviridae are four genera: Hepacivirus, Flavivirus, Pegivirus, and Pestivirus. The majority of viruses within the Flavivirus genus are arthropod-borne and are vectored by either mosquitoes or ticks.

1.3 Dengue viruses

Global disease burden

Dengue viruses (DENVs) are a group of mosquito-borne viruses comprising four serotypes that affect humans around the world. The four serotypes circulate concurrently in tropical and subtropical regions. The World Health Organization estimates that 390 million dengue infections occur each year and up to 100 countries are affected [5]. In 2013, there were global economic losses of up to 8.9 billion US dollars attributed to an estimated 58 million symptomatic cases of dengue virus worldwide [7]. As cases have increased over the years, the CDC now estimates that there are between 100-400 million cases of dengue virus each year [5,8]. This increases the burden on public health and the global economy. In 2024 there was a surge of dengue cases in the Americas with over 7 million cases reported by April. In just a few months this far surpassed the total number of cases in the Americas in 2023 which reached 4.6 million [2]. Many countries where dengue is endemic do not have robust systems for detection and reporting of cases, so the numbers reported are thought to likely underrepresent the true number of cases.

Clinical disease

Following the bite of a dengue virus-infected mosquito, the an incubation time in the human host ranges from 4-7 days and symptoms may last 3-10 days [9]. Patients affected by dengue viruses may exhibit a wide range of symptoms, resulting in different disease states that are classified as dengue fever, dengue hemorrhagic fever, and dengue shock syndrome. Dengue fever is characterized by mild disease, ranging from subclinical to self-limiting flu-like illness that typically lasts 3-7 days and often includes

headaches, fever, musculoskeletal pain, ocular pain, nausea, and a characteristic skin rash [5,8–11]. Dengue hemorrhagic fever patients often experience similar symptoms but additionally have bleeding problems, including bruising and skin and/or oral cavity hemorrhages. Left untreated, dengue hemorrhagic fever patients have a mortality rate of up to 10-20%, whereas with medical care the mortality rate is much lower at 2.5% [9]. A small proportion of patients progress to the most severe disease state, dengue shock syndrome. Dengue shock syndrome is characterized by hemodynamic shock, circulatory collapse, and ultimately multi-organ failure, which may lead to death [5,8–12]. Dengue virus infection is diagnosed using reverse-transcription polymerase chain reaction or NS1 antigen-capture enzyme-linked immunosorbent assays (ELISA) [13]. There are no antiviral drugs to treat patients who become infected with dengue viruses, and medical providers must rely on supportive care to manage symptoms.

In a clinical setting there is no simple way to predict which patients will progress to the severe disease states. Patients who have previously been infected with one serotype and become infected a second time with a different serotype are at increased risk of severe disease due to antibody-dependent enhancement (ADE) [14–16]. ADE occurs when non- or sub-neutralizing antibodies to the first serotype bind virus particles during the second infection, resulting in increased entry of virus into monocytes, macrophages, and dendritic cells. With more entry comes increased replication, and ultimately a more severe disease state.

ADE has significantly stymied vaccine development, as the methodology behind most vaccines is to expose the recipient to a part of the pathogen to promote the development of immunity [17] Because previous exposure to a different serotype can

precipitate severe disease, this has made vaccine development complicated, and required creativity and innovation.

One of the early dengue vaccines was Dengvaxia, a live attenuated tetravalent vaccine which was developed and introduced by Sanofi Pasteur in 2015 [18,19]. One of the issues with Dengvaxia was that it had a wide range of efficacy depending on the serotype of dengue: for DENV3 and DENV4 it was 81.9% and 90.0% effective, respectively, but for DENV1 it was 61.2%, and for DENV2 it was only 3.5% effective [19]. This was especially concerning as DENV2 was the predominant circulating strain in the areas where the clinical trial was deployed. In addition, there were only a small number of blood samples collected from trial participants before the clinical trial, making it difficult to study serostatus as a metric in how the vaccine performed. Retrospective analysis of the participants revealed that those who were seronegative and received the vaccine had a 2-4 fold higher risk of hospitalization related to severe disease as compared to seropositive participants [19]. We learned a lot from the Dengvaxia trial, namely the importance of prescreening participants to understand their serostatus, and it has helped inform the development of new vaccine candidates.

There are two promising tetravalent vaccine candidates currently: TAK-003 from Takeda and Butantan-DV developed by Instituto Butantan in Brazil, the NIH, and Merck [20,21]. As of May 2024, TAK-003 was pre-qualified by the World Health Organization and recommended it for use in children ages 6-16 years old in regions with high endemic dengue levels [22]. TAK-003 had a cumulative efficacy after 3 years following administration of 62.0% against dengue infection and 83.6% efficacious at preventing hospitalization related to severe dengue [21]. It was noted that efficacy against dengue

infection declined over the years and evaluation of the effects of a booster dose is ongoing.

As of January 2024, the Butantan-DV vaccine was in phase 3 clinical trials which included vaccinating 10,259 people with the vaccine and 5,976 with the placebo across 16 centers in Brazil representing 5 different regions. The results are very promising: at the two-year post-inoculation mark, the vaccine was shown to be 89% effective in preventing infection for people with prior dengue infection, and 79.6% effective in preventing infection for people without prior infection. It must be noted that in these regions of Brazil that only DENV1 and DENV2 have been circulating during the years of the trial, so efficacy against DENV3 and DENV4 in this population is not yet known. The Butantan-DV vaccine is an exciting advancement relative to other dengue vaccines on the market as it has shown to be safe and efficacious for people without prior dengue infection [20]. While the challenges associated with ADE have made vaccine development difficult, these two new vaccine candidates, TAK-003 and Butantan-DV, offer hope for improved dengue prevention strategies going forward.

1.4 Zika virus

Global disease burden

Zika virus was first identified and named in 1947 in the Zika forest of Uganda and has been the cause of sporadic and unpredictable outbreaks worldwide ever since [23–25]. The next major outbreak did not occur until 2007 in the island of Yap, which was then closely followed by an outbreak in French Polynesia in 2013 [23]. The outbreak that resulted in Zika virus being widely known was the 2015 outbreak in Brazil. The World

Health Organization declared the Brazilian outbreak a global health emergency due to its rapid spread through a densely populated region, its links to birth defects, and the possible neurological sequelae. There was also concern for rapid spread given how common the Aedes mosquito vector is in the region [25,26]. Since then, sporadic yet smaller outbreaks have occurred in various countries in the Americas, southeast Asia, and Africa, but none as severe as the Brazilian outbreak [27]. It has been hypothesized that the Brazilian outbreak was larger than other outbreaks due to a perfect storm of many factors, including increases in international travel to and from Brazil related to preparations for the Olympics, high population density of seronegative people in the affected region, and suboptimal water management and vector control strategies [23,28,29].

Clinical disease

Zika virus, similar to dengue viruses, is acquired through the bite of an infected mosquito with an incubation time in the human host of 3-14 days. Many patients with Zika virus are asymptomatic. Those who develop symptoms typically experience rash, fever, conjunctivitis, myalgia, malaise and headaches [24,30]. However, the most concerning aspect of Zika virus is its potential to disrupt normal fetal development. It can cause microcephaly when pregnant individuals are infected, particularly during the first trimester when brain development is critical [31,32]. Diagnosis of Zika virus infection is made using quantitative reverse transcription PCR to detect Zika virus RNA in a blood sample [33].

The 2015 Zika epidemic in Brazil showcased the severity of this issue: One study reported that during the outbreak there were 4,180 babies with suspected microcephaly

reported by the end of the year [31]. Another publication reported 1,950 confirmed cases of fetal microcephaly in babies born to mothers who previously were diagnosed with Zika virus [32]. Given limited health infrastructure, these case numbers likely underestimate the number of babies infected. A recent study utilizing a mouse model of congenital Zika infection shed light on possible mechanisms of microcephaly. It showed the mice mount a robust immune response along with downregulation of genes that are crucial in brain development. Furthermore, they showed a negative correlation between Zika virus polyprotein abundance and host cell-cycle inducing proteins that had previously been causally associated with human microcephaly cases [34].

In rare instances (approximately 1 in 4,000), adult patients can develop Guillain-Barre syndrome (GBS) days to weeks after symptoms first present [30,35]. GBS involves the development of autoantibodies to glycolipids found on the surface of peripheral nerves, causing damage to myelin and axon [36]. This damage results in delayed or interrupted nerve signaling, which can cause loss of sensation, painful tingling sensations, muscle weakness, and uncoordinated gait [35,37]. GBS is considered a medical emergency, as the autoantibody induced damage can continue without treatment and may progress to affect nerves necessary for cardiovascular function [37]. These findings highlight the multifaceted and complex consequences of Zika virus infection which prompts further research into mechanisms and options for prevention and treatment.

1.5 Flavivirus life cycle

The FV life cycle is a complex, multi-step process where the virus uses the host cell machinery and membranes to replicate its genetic material and form new progeny virions. FVs have an 11kb genome that is a single-stranded, positive sense RNA which encodes for a single polyprotein [11,38,39]. The genome codes for three structural proteins, capsid (C), pre-membrane (prM), and envelope (E), and seven non-structural proteins, NS1, NS2A, NS2B, NS3, NS4A, NS4B and NS5. The viral genome is contained within a viral capsid, host-derived lipid envelope, and viral glycoproteins (M and E), which together form an icosahedral virus particle [8,38]. The following section details each stage of the FV life cycle:

Attachment and entry

While some viruses display tropism for specific cell types, FVs have broad cellular tropism and can bind to a wide variety of receptors on many different cell types [40–42]. DENVs have been detected in the liver within hepatocytes, Kupffer cells, and endothelium, in the spleen within macrophages, multinucleated cells, and lymphoid cells, in the lung within macrophages and endothelium, in the kidney within the tubular epithelial cells, and the blood within peripheral monocytes and lymphocytes [43,44]. On the other hand, Zika has been found in the placenta within Hofbauer cells, trophoblasts, and endothelium, in the brain within neural progenitor cells, mature neurons, and astrocytes, in the eye within the aqueous humor, cornea, neuronal cells in the retina, the testes within spermatogonia, Sertoli cells, Leydig cells, and in the vagina within epithelial cells, and in the blood within dendritic cells and macrophages [45,46]. The ability of FVs to infect so many cell types make it difficult to design strategies to combat infection.

At the start of infection, the viral E protein recognizes and binds to a cellular attachment molecule on the plasma membrane [38,40,42,47]. Single particle tracking of DENVs has revealed that the virus diffuses along the cell surface until it finds a clathrin-coated pit [48]. The pit then deepens into a membrane invagination which is subsequently made into a vesicle by dynamin-mediated membrane fission. Once formed, the vesicle detaches from the plasma membrane and the clathrin coat is shed [42].

The virus-containing vesicle is then delivered to the early endosome, a process which typically occurs within five minutes of the initial plasma membrane contact for DENVs and WNV [48,49]. As the early endosome matures into a late endosome, the environment becomes more acidic. This pH change triggers a critical conformation change in the E protein, exposing the previously inaccessible internal fusion peptide [50]. Upon exposure, the E proteins on the virus surface change from homodimers that lay flat on the surface to homotrimers that extend outward from the virus. This event allows for the virus surface to be in close proximity to the endosomal membrane [51]. This facilitates fusion of the virion with the endosomal membrane, depositing the viral RNA into the cytoplasm [38,42,47,49,52].

The prM protein plays a protective role in this process, covering the E protein to prevent premature fusion [53]. For DENVs, fusion has been reported to occur within 10-13 minutes from the start of infection [48,54]. Interestingly, the lipid composition of the endosome membrane appears to play a role in fusion efficiency. In one study on endothelial cells infected with DENV, lysobisphosphatidic acid, a lipid that is enriched in the late endosome membrane, was shown to aid in fusion [55]. Increasing the cholesterol content of the endosomal membrane has been shown to enhance WNV fusion with the

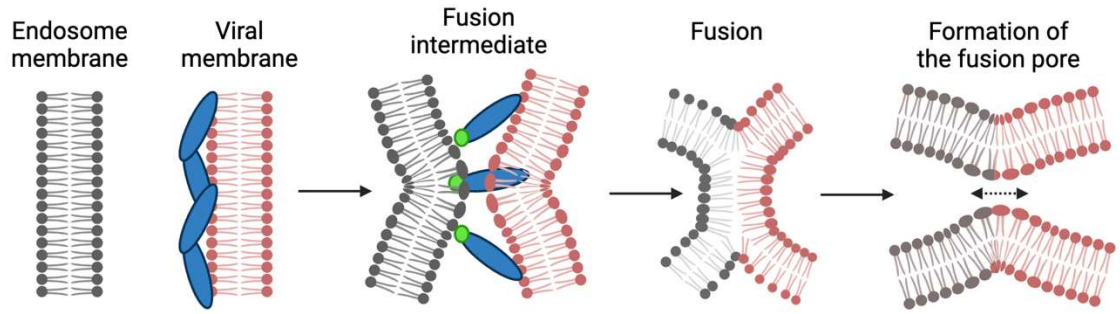

Figure 1.1. Viral fusion with the endosome membrane. A mature flavivirus particle has 180 viral envelope (E) proteins on its surface, arranged as 90 E protein homodimers that lie flat in a herringbone pattern. After the virus enters the cell through receptor-mediated endocytosis, it encounters the acidic environment of the endosome. The reduction in pH triggers a series of structural changes in the E proteins. First, the E protein homodimers dissociate. Then, the fusion peptide, previously hidden at the dimer interface, becomes exposed. Subsequently, the E proteins rearrange to form homotrimers, which extend outward from the viral surface. These conformational changes facilitate the insertion of the fusion peptide into the endosomal membrane. The E protein homotrimers then fold back on themselves, bringing the viral and endosomal membranes into close proximity. This process culminates in the formation of a fusion pore, allowing the viral RNA genome to be released into the host cell cytoplasm. Figure was made with Biorender.

membrane [56,57]. In Alphaviruses, the cholesterol molecules in the membrane appear to directly interact with the E protein, however, in FVs this does not appear to be the case. It is hypothesized that the cholesterol-induced changes in the membrane fluidity and physico-chemical characteristics may facilitate FV fusion [57,58].

Translation and virion assembly

Positive sense RNA viruses have a unique advantage: their genomes can act as mRNA and begin translation upon reaching the ribosome. The flaviviral open reading frame is translated into one long polyprotein that is then cleaved into the ten individual viral proteins [38]. Some viral proteins dramatically alter the cellular membranes, inducing extensive membrane rearrangements of the ER. The membrane rearrangements in the ER form structures called convoluted membranes, which are sites where translation of new viral proteins occurs [38,59,60]. Genome replication and assembly occur in replication compartments (RCs) which are invaginations in the ER membrane [38,59,61–

63]. At the ER, viral protein NS1 is a cofactor for replication of viral RNA and the C protein aids in packaging the viral RNA into new virions [38]. NS1 is unique in that it can also be secreted from infected cells in oligomers of 2, 4, or 6 NS1 proteins arranged around a central lipid core [64,65]. The NS1 protein has also been causally associated with the perivascular leakage syndrome seen in dengue patients [66]. NS2A is a transmembrane protein that aids in viral RNA replication and in assembly [38,67]. NS3, activated by its co-factor, NS2B, functions as a serine protease, helicase, and nucleotide triphosphatase, and processes the viral polyprotein [38,68]. NS4A and NS4B are responsible for the formation of the convoluted membranes and, in conjunction with NS2A and NS2B, form the scaffold for replication complex [38,69]. Once all of the components are assembled in the RC, the invagination extends inward toward the ER lumen and the virus particle buds off, taking the ER membrane as the outer membrane of the virus particle. These virus particles then travel in vesicle packets to the Golgi apparatus for maturation. This highly complex and coordinated processes of membrane rearrangements, protein synthesis, and genome replication, ensure efficient production of viral progeny.

Maturation and release

Following assembly, multiple immature virions travel together in large vesicular structures called vesicle packets (vp) which fuse with the Golgi apparatus membrane where particle maturation occurs [38,70,71]. When immature virus particles arrive in the Golgi, they are approximately 60 nm in diameter and have 90 prM-E heterodimers which form 60 trimeric spikes on the surface of the particle [38]. During the maturation process, several structural rearrangements of the surface proteins of the particle occur. The trans-

Golgi has a low pH which triggers the conversion of the 90 prM-E heterodimers to dissociate and form 90 E protein homodimers, which lay flat against the membrane surface, reducing the particle diameter to approximately 50 nm. From here, the prM protein is accessible, allowing for furin-mediated cleavage of prM to form pr and M protein. This cleavage event separates the pr protein from the M protein. The cleaved pr fragment remains associated with the particle, covering the fusion peptide of the E protein until the particle is released from the cell. The neutral pH of the extracellular environment allows the pr fragments to fully dissociate from the particle [38]. While many particles achieve prM cleavage, reaching the full maturity, some particles miss this cleavage step, giving them the immature spiky phenotype, which can result in decreased infectivity [38,71].

1.6 Flavivirus reliance on host cell membrane dynamics and lipid composition

Lipid composition of membranes

Lipids play many different roles in the host cell, including energy storage, maintaining membrane integrity, second messengers in signal transduction, and may serve as recognition receptors. Lipids in a membrane can also control how proteins and other lipids aggregate or disperse within the membrane [72]. The majority of structural lipids in eukaryotic membranes are glycerophospholipids such as phosphatidylcholine, phosphatidylethanolamine, phosphatidylserine, phosphatidylinositol, phosphatidic acid and phosphotidylglycerol [72]. Glycerophospholipids are composed of a diacylglycerol backbone which forms their hydrophobic component and then a hydrophilic headgroup such as phosphate, choline, ethanolamine, serine, inositol, or glycerol. Phosphatidylcholine makes up approximately 50% of the phospholipids in eukaryotic

membranes, has a cylindrical shape, and is organized into planar bilayers. In contrast, phosphatidylethanolamine has a conical shape due to the relative small size of its polar headgroup, and when it is incorporated in a phosphatidylcholine bilayer, it creates curvature [72,73]. Most phospholipids have two hydrocarbon tails, and one is typically saturated and the other is unsaturated[74]. This curvature is utilized for normal cell functions such as budding, fission, and fusion. The phospholipid composition of the two leaflets of a lipid bilayer are maintained by bi-directional transport undertaken by lipid flippase proteins [75].

Another important group of lipids that determine membrane structure are the sphingolipids. These are discussed in depth in section 1.7, but briefly, they are composed of a ceramide backbone which is made up of two parts, a sphingoid base and a fatty acid which is linked to the base via an amide bond [72,76,77]. Sphingolipids typically have saturated hydrocarbon tails so they are taller and narrower than phosphatidylcholines, allowing them to cluster more densely and form a gel phase [72]. The gel phase decreases lateral mobility of lipids in the leaflet. Decreasing the ability of lipids to move results in an area of the membrane that has increased rigidity and width relative to areas that are not in a gel phase [78]. The length of the hydrocarbon chain can affect the structure of the sphingolipid molecule. An area of a membrane that is composed of lipids with shorter hydrocarbon tails favors positive curvature, whereas an area of a membrane with lipids with longer hydrocarbon chains favors negative curvature [79]. Finally, the third important lipid that confers structure to a membrane are sterols. Unlike glycerophospholipids and sphingolipids, sterols are non-polar and are found throughout eukaryotic membranes [72].

Membrane structure and function

The ability of a membrane to bend depends on the lipid composition of the membrane and the structures of the lipid molecules [72,80,81]. To be able to fuse two membranes together, the two membranes must bend dramatically towards each other, which requires energetically unfavorable intermediates [80–82]. The energy to form these positions is derived from the elastic energy of the bent membranes [81]. Lipids that are cylindrical in shape create a flat or planar shaped membrane [72,80,81]. Lipids with a large polar headgroup favor positive membrane curvature, which means that the membrane bends away from the headgroup forming a convex shape, whereas lipids with a polar headgroup that has smaller cross-sectional area than their hydrocarbon tails favor negative membrane curvature, which means that the membrane bends towards the headgroup forming a concave shape [80,81,83]. One group used liposomes to study the difference in membrane dynamics between two sphingolipids, sphingomyelin and ceramide. They reported that when they treated the liposomes with sphingomyelinase to convert the sphingomyelin into ceramide, they observed spontaneous endocytosis of parts of the liposome membrane [83]. This suggests that the presence of ceramides in a membrane may favor the membrane bending to form invaginations, which could be beneficial to processes like viral entry and formation of the replication compartments in the ER.

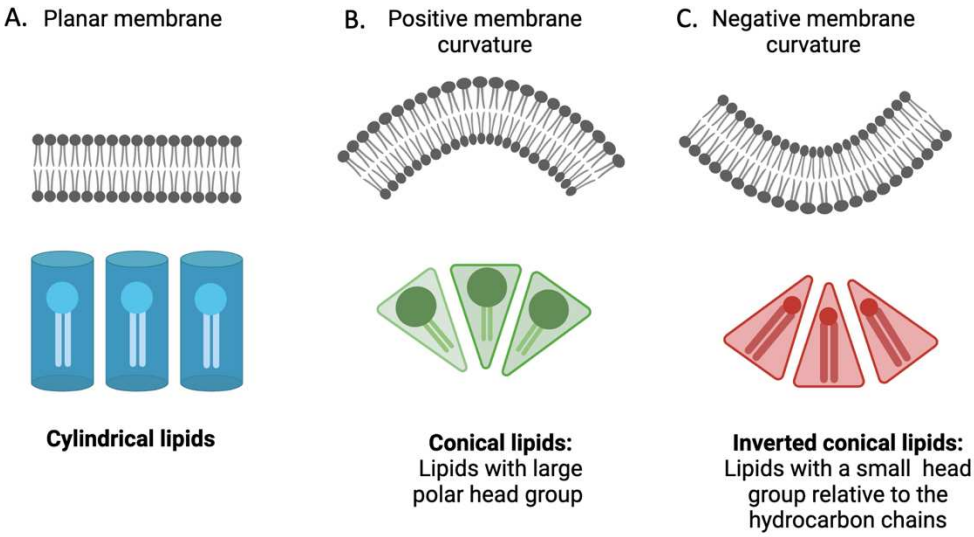

Figure 1.2. The shape of lipid molecules in a membrane affect the membrane curvature. **A.** Membranes composed predominantly of cylindrical-shaped lipids form a planar or flat membrane shape. **B.** Membranes with a high proportion of conical lipids, which are lipids that have a large polar head group, form positive membrane curvature. Positive curvature denotes the convex shape of the membrane as it bows away from the center of the cell. **C.** Membranes with a high proportion of inverted conical lipids, which are lipids with a relatively small head group in comparison to the length of their hydrocarbon chains, form negative membrane curvature. Negative curvature denotes the concave shape of the membrane where it bends inwards towards the center of the cell. Figure was made with Biorender.

Before we discuss the differences in the organelle membranes, it is important to understand that not all lipid bilayer leaflets are the same. In the ER, the distribution of lipids is symmetrical, whereas in the Golgi, endosome, and plasma membrane, the distribution is asymmetrical [72,75]. Specifically, glycosphingolipids and sphingomyelin are enriched on the non-cytosolic side of the Golgi and endosome or the outer leaflet of the plasma membrane, while phosphatidylserine and phosphatidylethanolamine are enriched on the cytosolic or inner leaflet [72]. There are specific functional consequences to the leaflet lipid composition - for example, lipid translocation from the non-cytosolic to the cytosolic leaflet can cause a structural imbalance and facilitate membrane bending needed for vesicle budding [75]. Structural imbalances in the two leaflets may confer an advantage during viral infection, as multiple stages rely on the bending of membranes and budding. Additionally, the distribution of lipids in the membrane leaflets impacts

numerous cellular processes, including signaling, molecule trafficking, and functions specific to each organelle; all of which can be exploited by various viruses.

The virus life cycle depends on the lipids of each cellular organelle

The FV life cycle is intimately associated with cellular membranes. Infection has been shown to alter host cell lipid metabolism to support the extensive membrane morphological changes viral proteins induce for viral replication and assembly [84–87]. The membrane of each cellular organelle is enriched in specific lipids which support its structure and function (Figure 1.3). In turn, flaviviruses use each of these membranes to their advantage to support the virus life cycle [38].

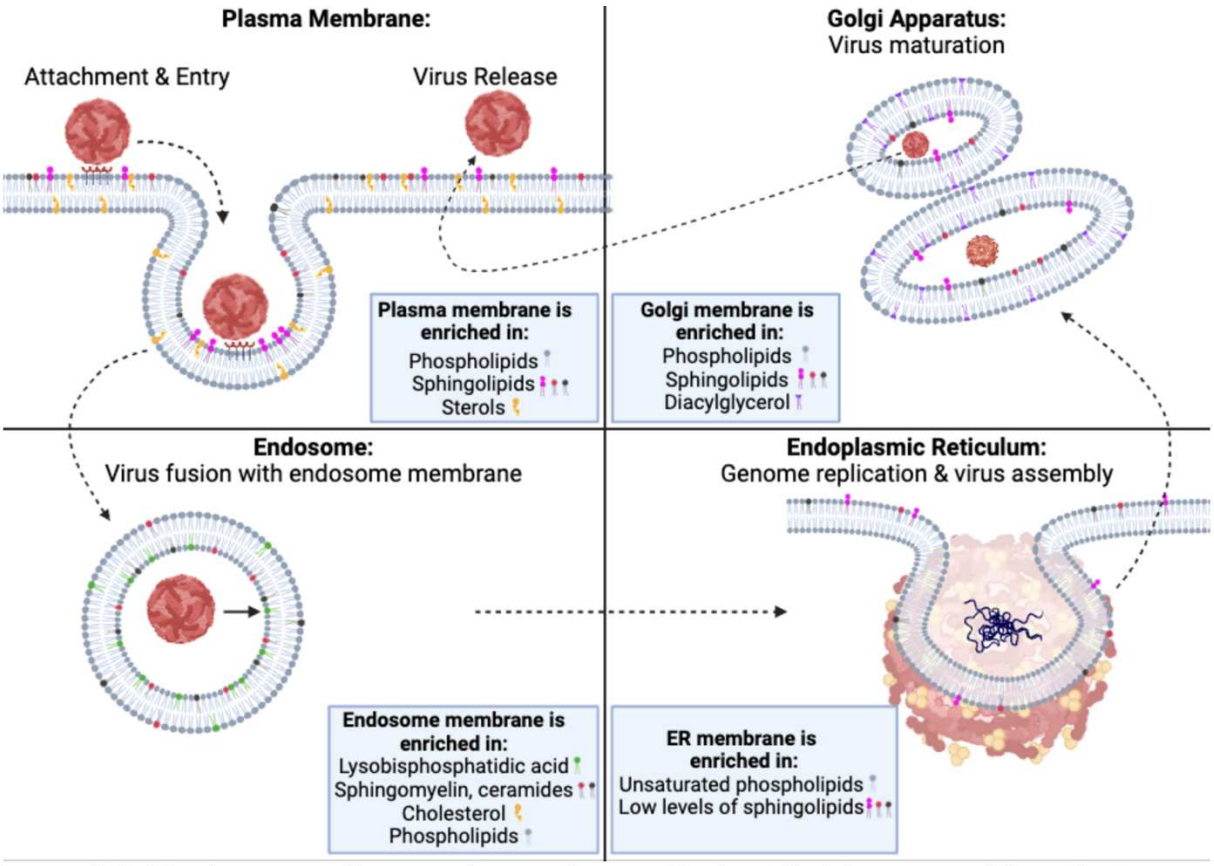

Figure 1.3. Each organelle membrane has a distinct lipid composition that supports different stages of the virus life cycle.

Figure was made with Biorender.

Plasma membrane –Viral entry and egress

The plasma membrane is enriched in phospholipids, sphingolipids, and sterols, which can facilitate endo- and exocytosis along with maintenance of the barrier function to safeguard cellular contents [88,89]. The plasma membrane composition affects both virus entry and virus release.

Cholesterol is a sterol commonly utilized by many viruses. For example, HIV-1 has been shown to use gp120 to bind CD4 and reorganize lipid rafts to bring co-receptor molecules such as CXCR4 or CCR5 closer to facilitate entry. Furthermore, depletion of cholesterol in the plasma membrane and dispersing lipid rafts has been shown to reduce HIV-1 entry into cells in vitro [90]. As mentioned in section 1.5, increasing cholesterol concentration in the endosome has also been shown to increase fusion of WNV to the endosomal membrane [57]. For DENVs, the enrichment of the late endosomal membrane in lysobisphosphatidic acid is advantageous and the virus uses these lipids to gain access to the cytoplasm [55].

Another sterol important in viral pathogenesis is 25-hydroxycholesterol (25HC), the product of cholesterol oxidation catalyzed by the cholesterol-25-hydroxylase enzyme. The cholesterol-25-hydroxylase gene is considered an interferon stimulated gene due to its involvement in antiviral response pathways. The presence of the product, 25HC, in a membrane increases the availability of cholesterol to extracellular interactions by altering the position and orientation of cholesterols molecules [91]. Oxysterols can also trigger the translocation of cholesterol from the plasma membrane to the ER. In the context of viral pathogenesis, addition of exogenous 25HC has been shown to decrease entry of multiple flaviviruses, including DENV, WNV, and YFV, as well as SARS-CoV-2 [92,93]. Knockout

of cholesterol-25-hydroxylase in A549 cells (pulmonary adenocarcinoma cells) using a CRISPR-Cas9 system increased ZIKV titer, while overexpression had an opposing effect [93]. Furthermore, they found that ZIKV infection induced expression of cholesterol-25-hydroxylase in infected cells, further demonstrating the effect of 25HC on viral pathogenesis. The literature focuses on 25HC having a role in immune-activation during viral infection. However, the structural membrane changes, such as increased availability of cholesterol to extracellular molecules and its movement from the plasma membrane to the ER, may also play a role in viral pathogenesis.

Studies from the membrane biology field show that conversion of sphingomyelin to ceramide in the plasma membrane of macrophages (J774 cells) by addition of neutral sphingomyelinases has been shown to cause rapid formation of membrane invagination and budding [94]. If viruses are able to alter the ceramide composition of the plasma membrane, that could potentially facilitate viral entry via enhancing the endocytic capacity of the membrane. A publication on ZIKV used lipidomics to show that ceramide is upregulated at 24 and 48 hours post-infection in Huh7 cells (human hepatoma cells) relative to mock cells [95]. They subsequently demonstrated that ceramides are redistributed to sites of ZIKV replication in the ER, suggesting it affects formation of the replication complexes. The impact of ceramides in the plasma membrane were not specifically investigated.

Endoplasmic reticulum – Genome replication and assembly

In contrast to the plasma membrane, the endoplasmic reticulum is enriched in unsaturated phospholipids with relatively lower levels of sphingolipids. This composition results in a thinner and more flexible membrane which may facilitate the formation of viral replication compartments [96,97]. While the exact mechanism of replication compartment formation remains unclear, is likely involves the interplay between viral and host proteins as well as the lipid composition of the ER membrane [61,98].

The ER membrane plays a critical role in FV assembly, as immature virus particles bud into the ER lumen, deriving their lipid envelope from this organelle [84]. As previously mentioned, during ZIKV infection of human liver cells, an increase in ceramides was observed, which may assist in the formation of replication complexes by facilitating membrane invagination and budding [95]. Ceramides are an inverted conical shaped lipid which favor negative membrane curvature. Following sphingomyelinase treatment of vesicles and liposomes, sphingomyelin is hydrolyzed to form ceramide, and has been shown to generate membrane invagination and vesicle formation [83,94,99–101]. Similarly, WNV infection of HeLa cells causes significant increases in multiple species of phospholipids, ceramides, and sphingomyelin [102].

To understand the impact of sphingolipid metabolism on the FV life cycle, one group treated cells with a neutral sphingomyelinase inhibitor, which reduces the conversion of sphingomyelin to ceramide. This treatment decreased infectious WNV released from two mammalian and one mosquito cell line, demonstrating that it is broadly applicable in both the host and the vector [102]. This phenotype was validated using siRNA to silence neutral sphingomyelinase and the same phenotype was observed.

Additional investigations revealed inhibition of neutral sphingomyelinase reduced the amount of plaque forming units (PFUs) in the extracellular environment, however, the intracellular PFUs were not significantly altered [95]. Interestingly, the extracellular viral RNA copies were significantly decreased, while the intracellular viral RNA copies were significantly increased. These observations suggested that virus release and/or maturation were affected when the conversion of sphingomyelin to ceramide was reduced. Furthermore, transmission electron microscopy of the inhibitor-treated cells showed that while the diameter of the virus particles in the ER was unchanged, the number of virus particles inside each vesicle packet was significantly reduced [95]. This led researchers to propose that alterations in the ER membrane composition resulted in decreased virion assembly without impacting genome replication, which ultimately caused fewer infectious particles to be released. This study showed the importance of the balance between ceramide and sphingomyelin in the ER and the impacts on FV assembly and release. It demonstrates how specific changes to the membrane composition may significantly alter the virus life cycle and underscores the importance of sphingolipid metabolism in FV infections.

Golgi Apparatus - Maturation

The Golgi apparatus has high levels of phosphocholine along with enrichment of sphingolipids, particularly sphingomyelin and glycosphingolipids, along with phosphatidylinositol 4-phosphate, and diacylglycerols [89,103]. Our understanding of how Golgi lipids support virion maturation is limited. One publication reported on the role of the cis-Golgi protein, acyl-coenzyme A binding domain containing 3 (ACBD3), and how it

supports efficient virus replication by assisting in the trafficking of immature tick-borne encephalitis (TBEV) virions from the ER to the Golgi [104]. ACBD3 is a protein that functions in trafficking of cellular cargo from the ER to the Golgi. They discovered that depletion of ACBD3 decreased virus release and that the number of cells positive for E protein was reduced in cells with ACBD3 knockout. While this protein aids in virion trafficking, it is not thought to directly affect viral maturation processes. Additional studies are needed to improve our understanding of how Golgi lipids and membranes impact virion maturation and trafficking through the Golgi towards egress.

1.7 Sphingolipids: An overview of metabolism and biological relevance

Sphingolipids are a diverse and essential class of lipids which play roles in numerous biological processes within the cell and form structural components of membranes. Sphingolipids are versatile molecules composed of a sphingoid base attached by an amide bond to a fatty acid chain which can vary in length. While they are produced in the ER and Golgi, they are most enriched in the plasma membrane and endosome membrane [97,105,106].

After phospholipids, sphingolipids are the second most abundant structural lipid in the plasma membrane of mammalian cells, underscoring their importance in membrane architecture and function [89]. Plasma membrane lipid composition varies depending on species and cell type. For example, in mouse intestinal epithelial cells, 50% of the plasma membrane sphingolipids are glucosylceramides [107], whereas in yeast the predominant sphingolipid species of the plasma membrane include inositolphosphoceramide, mannosylinositol-phosphoceramide, and mannosyldiinositol-phosphoceramide [108].

While comprehensive characterization of the lipid composition of the plasma membrane of different cell types in the literature is limited, emerging research suggests that composition affects both structure and function. For example, glycosphingolipids have been proposed as a mediator of transcytosis in hepatocytes, suggesting that sphingolipids have cell-specific roles beyond membrane structure [109]. As discussed later in section 1.8, glycosphingolipids are an important component of lipid rafts which are portals of entry for FVs [110,111]. The diverse and cell-specific composition of sphingolipids within the plasma membrane not only determines membrane structure but also plays crucial roles in cell-specific functions.

Ceramides

The sphingolipid metabolic pathway is centered on the molecule ceramide which plays a key role in numerous cellular processes. Ceramides are a prolific group of molecules that participate in intracellular signaling, cell cycle arrest, apoptosis, senescence, stress responses, and maintenance of membrane structure [77,112–115]. They are the backbone of more complex sphingolipids such as sphingomyelin, cerebrosides, and gangliosides [116].

The properties of ceramide species depend on the length of the fatty acid hydrocarbon chain [117]. The hydrocarbon chain, regardless of length, facilitates stacking of ceramides into tight layers, increasing a membrane's rigidity [118,119]. The literature largely reports ceramides as being inverted conical shaped lipids which facilitate negative membrane curvature [83,100,101,117]. However, one publication states that ceramides with longer hydrocarbon chain (C18 or greater) can increase the membrane permeability

while facilitating negative membrane curvature, whereas ceramides with a shorter hydrocarbon chain (less than C18) could promote positive membrane curvature [116]. This is due to the relative length of the hydrocarbon chains and their effect on the shape of the molecule. As ceramides with shorter hydrocarbon chains are much less abundant in a mammalian organism, they are not as well studied as those with longer hydrocarbon chains. As previously discussed in section 1.6, the shape of ceramides and their recruitment to the ER during ZIKV infection is hypothesized to play a role in formation of viral replication complexes during viral assembly [95]

Ceramides as a whole are highly abundant in the central nervous system, with C18 ceramides being the most abundant ceramide species [116]. In other sites in the human body, chain length differences are the result of the level of expression of the ceramide synthase (CerS) enzymes, of which there are six isoforms (CerS1 through 6) which each favor different lengths of fatty acid. The expression of each of these isoforms varies depending on the cell type and the metabolic needs of the tissue [120]. In the liver and kidney, where there is high expression of CerS2, longer-chain ceramides (C20-C26) are most abundant, whereas medium chain ceramides (C18-C20) are made by CerS4 in the skin, white blood cells, and liver. CerS3 is highly expressed in the testis and skin where it produces very long chain ceramides (C20-C26) [120]. The myriad roles of ceramides in cellular processes, membrane structure, and the tissue-specific expression of ceramide synthases highlight the significance of sphingolipid metabolism in the maintenance of homeostasis and function across the different organ systems.

Though our understanding of the mechanism remains limited, levels of ceramides in a given cell are thought to be tightly controlled. This to assure that production of

complex sphingolipids can occur quickly as needed based on homeostatic needs and responses to stimuli [112,121]. In addition, careful regulation of ceramides make sense as they can activate a signaling cascade in apoptosis [122]. In addition, as mentioned in section 1.6, ceramides have an inverted conical shape, and increasing the proportion of ceramides in a membrane has been shown to facilitated membrane invagination and formation of vesicles [83,94,101]. In the context of viral infection, this change in the ER could facilitate formation of viral replication complexes. Ceramides are involved in many distinct cellular processes and current research is focused understanding their complex regulatory mechanisms and why their structure is suited to their specific functions in different cell types.

Sphingolipid Metabolism

The sphingolipid metabolic pathway is comprised of three main parts: 1) De novo ceramide synthesis, 2) the hydrolytic pathway, and 3) the salvage pathway [77,112,113]. This intricate network permits cells to alter sphingolipid composition in different cellular compartments to maintain homeostasis and respond to stimuli. The de novo pathway makes ceramides in the ER from non-sphingolipid precursor molecules. Once synthesized, ceramides are transported to the cytosolic leaflet of the Golgi membrane by vesicular trafficking and ceramide transport protein (CERT) [123,124]. In the Golgi, ceramides may serve as building blocks for more complex sphingolipids. Glucose can be added to ceramides to form glucosylceramides which then translocates from the cytosolic side of the membrane to the luminal side where it may be further processed into more complex lipids. Alternatively, when ceramide is still in the ER, galactose can be added to

form galactosylceramide (GalCer), a reaction catalyzed by UDP-galactosyltransferase 8 (UGT8), which is the focus of chapter 2 of this dissertation. Following formation of GalCer, it is translocated to the Golgi and then to the plasma membrane where it forms part of the outlet membrane leaflet. Additionally, ceramides can combine with phosphatidylcholine in the trans-Golgi to form sphingomyelin, an important structural lipid, which also plays roles in cell growth and survival [125]. Glucosylceramide and galactosylceramide are discussed in greater depth in the section below titled 'Glycosphingolipids.'

The hydrolytic and salvage pathways operate in distinct cellular compartments to fulfill specific cellular needs. The hydrolytic pathway produces ceramides in the plasma membrane. This process occurs when sphingomyelinases perform a hydrolysis reaction to generate ceramides [112,125,126]. In contrast, the salvage pathway operates in the lysosome to recycle breakdown products. It is here that ceramides are catabolized and broken into a sphingoid base and a fatty acid [114,127]. These breakdown products are then transported to the ER. In the ER, a new fatty acid can be added to the sphingoid base in a process called re-acylation to form ceramides [114]. This complex metabolic network, involving the de novo, hydrolytic, and salvage pathways that function in the different cellular compartments, showcases the dynamic and adaptable nature of sphingolipid regulation, which is critical for maintaining cellular homeostasis and responding to stimuli (Figure 1.4, adapted from [128])

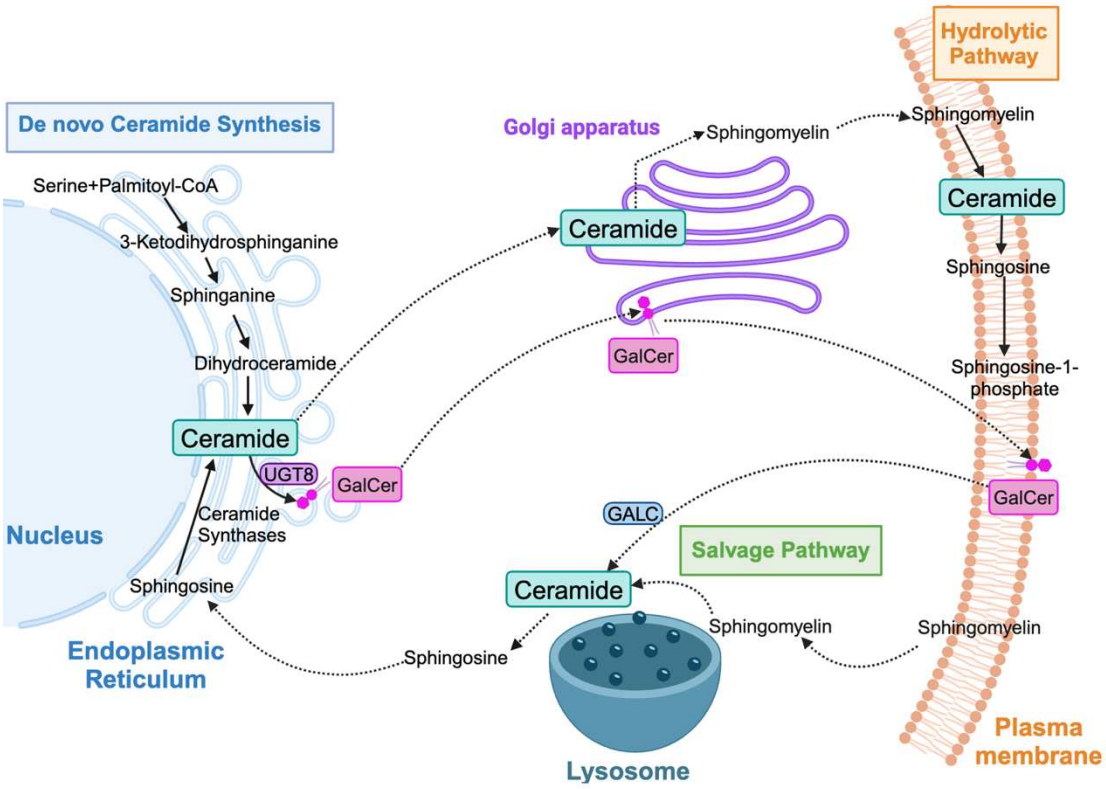

Figure 1.4. The sphingolipid metabolic pathway. The metabolic pathway is composed of three parts: De novo synthesis, the hydrolytic pathway, and the salvage pathway. The de novo pathway for ceramide synthesis occurs in the ER, beginning with condensation of L-serine and palmitoyl-CoA to form 3-ketodihydrosphinganine. 3-ketodihydrosphinganine is reduced to form sphinganine, which is then acylated by a ceramide synthase enzyme to form dihydroceramide, which is then converted to ceramide. From here, ceramides can be sent to the Golgi for production of complex glycosphingolipids, such as sphingomyelin, or they can be made into galactosylceramide (GalCer) in the ER. Following synthesis, GalCer is transported to the Golgi and then to the outer leaflet of the plasma membrane. The hydrolytic pathway (also referred to as the sphingomyelinase pathway) occurs in the plasma membrane where sphingomyelin is hydrolyzed by sphingomyelinases to form ceramide, which can then be further degraded into sphingosine and sphingosine-1-phosphate. The salvage pathway serves to recycle molecules to support synthesis of new ceramides. Sphingomyelin and other glycosphingolipids are transported to the lysosome where they are degraded to form ceramide. Ceramides are then further degraded into sphingosine and fatty acids, and sphingosines are transported back to the ER for de novo ceramide synthesis. This figure was adapted from Bautista-Pérez, R.; Franco, M.; Donis-Maturano, L. Sphingolipid Catabolism. Encyclopedia. Figure was made with Biorender.

Glycosphingolipids

Glycosphingolipids (GSLs) are complex molecules composed of ceramides bound to carbohydrate moieties (Figure 1.5, adapted from [129,130]). These lipids reside in the late Golgi and the plasma membrane where they play crucial roles in cellular functions and membrane structure. In the Golgi they form dense clusters while in the plasma membrane they form organized structures called glycosphingolipid-enriched

microdomains (GEMs) or more commonly, lipid rafts [76]. GEMs are highly dynamic membrane domains that are enriched with cholesterol, saturated phospholipids, and sphingolipids, and often other sphingolipid species such as sphingomyelin [131,132]. GEMs in the plasma membrane can concentrate or isolate specific proteins and lipids to regulate their interactions with extracellular stimuli. Some viruses have been found to utilize GEMs to facilitate attachment and entry, including influenza virus, measles virus, Ebola virus, dengue viruses, human hepatitis C virus, Japanese encephalitis virus, and West Nile Virus [99,133]. The widespread usage of lipid rafts by different viruses points to them as a key part of the virus entry process.

GEMs also play a number of critical roles for the cell, including regulation of signal transduction, receptor activation, host-pathogen and cell-cell interactions, membrane permeability, and intracellular lipid and protein trafficking [99,131,132,134]. Within GEMs, GSLs, particularly ceramides, can act as second messengers in signal transduction in response to stress, apoptotic triggers, and inflammation [135]. GSLs also modulate cell-cell interactions by altering lipid raft organization, which can expose or activate receptors that can interact with the extracellular environment [131,132]. GEMs with high ceramide and GSL content exhibit unique physical characteristics, including a gel-like consistency, increased rigidity, and greater thickness. These features can negatively impact membrane permeability [136,137]. Furthermore, GEMs are often more ordered relative to the surrounding areas of the plasma membrane, and are typically less fluid as a result [138,139]. The unique attributes of GEMs allow them to alter the structure and function of the plasma membrane.

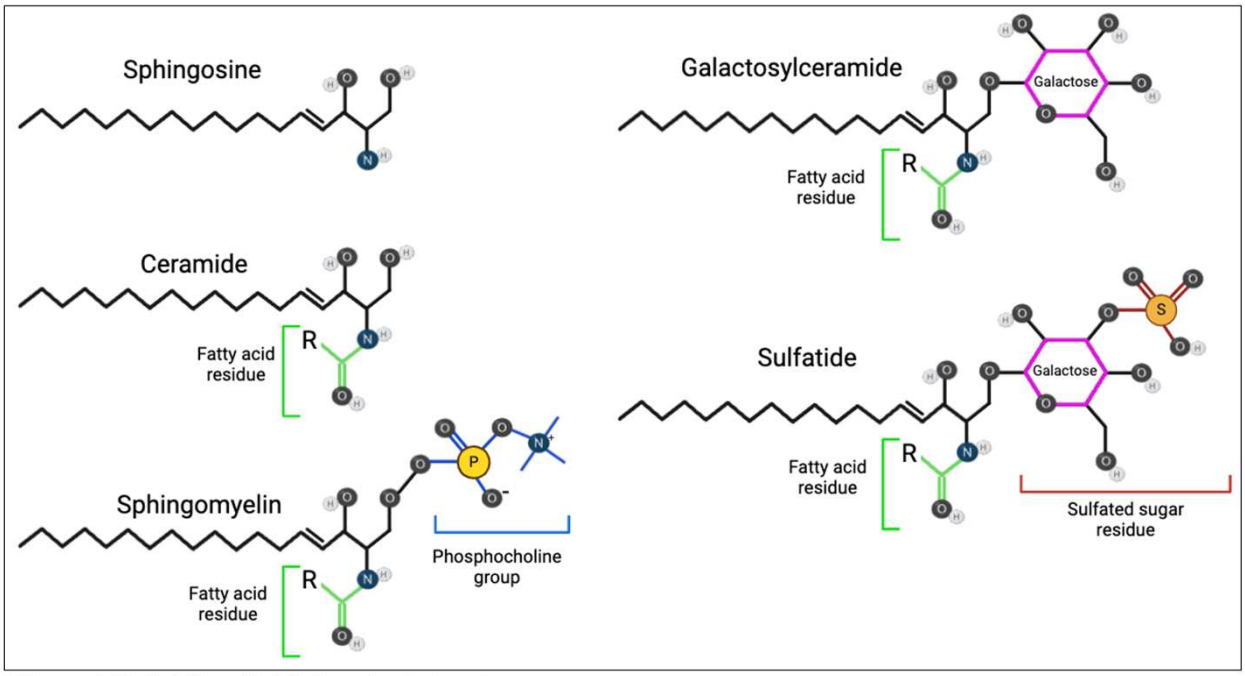

Figure 1.5. Sphingolipid chemical structures.

Figure was made with Biorender.

GSLs are categorized as neutral or acidic based on the absence or presence of a negatively charged head group [76,116]. Neutral GSLs include glucosylceramide (GlcCer), galactosylceramide (GalCer), and lactosylceramide (LacCer). GlcCer and GalCer are additionally categorized together and referred to as cerebrosides. LacCer is made by the addition of a galactose onto a GlcCer molecule via a β-1,4-glycosidic linkage [76,116]. In contrast, acidic GSLs are divided into four categories: gangliosides, glucuronoglycosphingolipids, sulfatoglycoshpingolipids, and phosphoglycosphingolipids. Gangliosides have one or more sialic acid group(s), whereas the other three possess either a glucuronic acid, sulfate, or phosphate group, respectively [116]. Gangliosides are primarily found in the outer leaflet of the plasma membrane of neuronal cells where the ceramide portion of the molecule is embedded in the membrane and the oligosaccharide extends into the extracellular environment where it is poised to interact with other molecules [97,116]. These gangliosides can also have additional components, for

example, sialic acid can be attached to the oligosaccharide chain of gangliosides. Sialic acid has been implicated in numerous diseases, including viral diseases like Influenza, degenerative and nutritional diseases like atherosclerosis, and developmental diseases such as infantile sialic acid storage disease [140]. Pathogens can interact with sialic acid moieties on cells, as is the case with influenza virus, while other pathogens coat themselves with sialic acids as a form of molecular mimicry to evade the immune response [140]. The wide variety of GSLs with their diverse structures and functions play important roles in membrane structure and host-pathogen interactions, making them key players in health and disease pathogenesis.

Galactosylceramides: biosynthesis, trafficking, and recycling

From here we will focus on the GSL galactosylceramide, as the enzyme that produces it is the focus of chapter 2 and the enzyme that degrades it is the focus of chapter 3 of this dissertation. Galactosylceramide (GalCer) is formed on the luminal side of the endoplasmic reticulum by the addition of a galactose onto a ceramide molecule which is catalyzed by UDP-galactosyltransferase 8 (UGT8) [110,113,115,141]. From there, GalCer is transported to the trans-Golgi where it may be made into more complex sphingolipids, or may be transported to the outer leaflet of the plasma membrane [110]. When GalCer is ready to be recycled, it is endocytosed and transported via a vesicle to the lysosome where it is degraded by galactoceramidase (GALC) to form a sphingoid base and a fatty acid [110,142]. These components are then trafficked back to the ER to be made into new sphingolipids.

1.8 Galactosylceramides and their roles in disease

Galactosylceramides in non-infectious diseases

GalCer and other sphingolipids have been implicated in several developmental neurologic diseases that affect young children. One of the more severe and life-limiting diseases is Krabbe's disease, also called globoid cell leukodystrophy or galactosylceramide lipidosis [110,143]. This is a genetic condition with an autosomal recessive inheritance pattern. The mutation is in the galactocerebrosidase (GALC) gene, causing a lack of production or activity of galactocerebrosidase in the lysosome. This deficiency results in accumulation of GalCer and psychosine (also referred to as galactosylsphingosine) in macrophages and neural cells, specifically in oligodendrocytes and Schwann cells [110]. Psychosine is a toxic metabolite and has detergent-like properties which causes loss of structural integrity of cell membranes. When the membranes become unstable it results in oxidative stress, mitochondrial damage, and ultimately cell lysis and cell apoptosis [110]. This constellation of lesions attracts inflammatory cells and causes demyelination of axons which results in axonal dysfunction and neurologic symptoms. Patients with Krabbe disease have <10% of normal GALC function resulting in a severe phenotype [143]. Symptoms generally present in infants and toddlers and can be progressive and ultimately life-limiting.

Another developmental disease that implicates GalCer is juvenile neuronal ceroid lipofuscinosis (JNCL) which is also known a neuronal ceroid lipofuscinosis or Batten disease. This is one of the most common neurodevelopmental disorders of children [110]. The disease is caused by a mutation in the ceroid-lipofuscinosis neuronal 3 (CLN3) gene which causes accumulation of lipopigments in the lysosomes of neurons. CLN3 is a

transmembrane protein that resides in the Golgi and plasma membrane [144]. CLN3 has a GalCer binding domain and functions to transport it from the trans-Golgi to lipid rafts in the plasma membrane. In the disease, the GalCer binding site is altered, precluding the transport of GalCer by CLN3 and allowing accumulation of GalCer in the ER and Golgi [110]. This has a negative impact on the lipid rafts in the plasma membrane, deregulates ceramide levels, and causes apoptosis of affected neurons.

Galactosylceramides and their metabolites in viral diseases

Galactosylceramides and their metabolites have been implicated in viral diseases including Human Immunodeficiency Virus (HIV) and influenza virus. Galactosylceramide was discovered as an entry receptor for HIV that interacts with envelope glycoprotein 120 (gp120) in 1991 [145]. This was an exciting discovery not only because it broadened our understanding of HIV pathogenesis but it also opened our eyes to the possibility of glycolipids serving as necessary factors for viral attachment and entry. When HIV was first being studied, it was originally shown that HIV could infect CD4+ cells via the interaction of the gp120 with host cell CD4 [145–147]. The conformational change from this interaction exposes the V3 loop of gp120 to allow interactions with the coreceptors CXCR4 or CCR5 and also exposes the fusogenic domain of surface glycoprotein gp41 to facilitate entry [148]. However, it was then observed that HIV could infect a number of cells that lacked CD4 expression, including hepatocytes, natural killer cells, and colonic and brain epithelial cells [134,145,146,148,149]. This suggested that alternate methods of viral entry that did not require CD4 were possible. Further studies elucidated that galactosylceramide (GalCer) could bind the V3 loop of gp120 with high affinity and the

addition of antibodies to GalCer could block HIV attachment and entry to cells in vitro, identifying it as an alternative receptor for HIV [145,147]. Though GalCer was identified as the most commonly utilized glycolipid receptor for HIV, other related glycosphingolipids were also found to participate in HIV entry, including sulfatide, lactosylceramide (LacCer), GM3, and GD3 [150,151]. Sulfatide is a downstream product of GalCer and was shown to play a role with CD4- cells, however, LacCer, GM3, and GD3 were found to be utilized by CD4+ lymphocytes to facilitate fusion of the viral envelope to the host cell plasma membrane [150]. The discovery of GalCer and related GSLs as alternative receptors for HIV not only broadened our comprehension of mechanisms of viral entry, but also shed light on the complex interactions between viruses and cellular membranes.

Building on the importance of GSLs in viral infection, sulfatide, the downstream metabolite of GalCer, has been reported to play an important role in Influenza virus pathogenesis. Sulfatide is composed of a galactosylceramide molecule with a sulfate group added to the galactose component, giving it a more negative charge. Galactosylceramides are converted to sulfatides via the cerebroside sulfotransferase in the Golgi [150]. One group reduced sulfatide levels in COS cells (kidney fibroblasts) using siRNA against the cerebroside sulfotransferase and infected with influenza virus, they found that it reduced influenza viral titer by 60-fold. In contrast, when they utilized MDCK (kidney) clonal cell lines with stable overexpression of sulfatide and infected with influenza virus, there was a 500-3,000 times increase in titer [152]. They also infected C57BL/6 mice with influenza and administered an anti-sulfatide antibody daily and found that mice treated with the antibody had 17 times lower viral titers in their lung homogenates than control mice [152]. They determined sulfatide in lipid rafts in the plasma membrane

associated with hemagglutinin, and this interaction increased translocation of Influenza ribonucleoprotein complexes from the nucleus to the cytoplasm, dramatically enhancing viral replication.

1.9 Conclusions

In this chapter we have summarized the importance of lipids in flavivirus infection and discussed relevant background information on both the virus life cycle and sphingolipid metabolic pathway. This chapter provides the premise for the experimental questions addressed in this dissertation. We will present our findings on how modulation of galactosylceramide by manipulation UGT8 expression affects DENV2 infection in human liver cells in vitro (Chapter 2). We also explore the opposing reaction where galactosylceramide is recycled in the lysosome by galactosylceramidase (Chapter 3). From there, we begin to explore the effects of UGT8 expression on ZIKV in both human liver cells and human neuroblastoma cells in vitro (Chapter 4). While glucosylceramides have been studied in the context of viral infection, the arm of the sphingolipid metabolic pathway centered on galactosylceramide has been largely unexplored. Our research aims to advance the field by elucidating how galactosylceramides impact flavivirus infection. We anticipate these findings may be conserved in other FVs, contributing to a more global understanding of virus-host interactions associated with lipid metabolism.

We hypothesize that the balance of galactosylceramide synthesis and recycling, regulated by UGT8 and GALC, respectively, plays a pivotal role in the flavivirus life cycle in vitro.

Chapter 2: The role of UDP-Galactosyltransferase 8 in DENV2 Infection

2.1 Introduction

UDP-galactosyl transferase 8 (UGT8), also referred to as ceramide galactosyltransferase (CGT), is a key enzyme in the synthesis of galactosylceramide within the sphingolipid metabolic pathway. UGT8 catalyzes the addition of a galactose molecule on to ceramides in the ER (Figure 2.1A). UGT8 is most abundant in tissues of the central nervous system, but is also moderately abundant in the gastrointestinal tract, kidney, and gallbladder, with low levels of expression in the liver, lung, testis, female reproductive tissues, and breast tissue [153]. UGT8 belongs to a superfamily of enzymes called the UDP-glycosyltransferases which catalyze the addition of sugar residues to small lipophilic molecules. The different UGT families include UGT1, UGT2, UGT3, and UGT8. These enzymes catalyze the addition of a variety of different sugars, including glucuronic acid which can be added by UGT1 and UGT2, and UDP-N-acetylglucosamine, UDP-glucose, and UDP-xylose which can be added by UGT3 [154]. UGT8 is the only UGT enzyme that is able to utilize UDP-galactose and to our knowledge is unable to utilize any other sugars. There is approximately 45% homology between the amino acid sequences of the enzymes in the UGT families [155]. The UGT1, UGT2, and UGT3 families have a specific amino acid sequence in their sugar binding site which affect the type of sugars they can bind to. They have an aspartate followed by a glutamine motif, whereas UGT8 has an aspartate followed by a histidine. When researchers mutated this histidine to glutamine in UGT8, they found that the ability of UGT8 to utilize UDP-galactose was significantly reduced [156]. Another publication reported that performing this same mutation allowed UGT8 to bind UDP-glucose [157]. While sugar specificity is just one of the characteristics that sets the UGT families apart, UGT8 is the black sheep of the UGT superfamily due to how its primary function differs from the rest of the superfamily.

The majority of the UGTs function in pathways to conjugate drugs or metabolites to inactivate them or prepare them to be excreted, making them invaluable in detoxification, however, the role of the UGT8 family has been reported to be primarily biosynthetic rather than detoxifying [154]. The only detoxifying role of UGT8 that has been described is the galactosidation of bile acids made in the liver [156]. One publication reported that they generated human embryonic kidney (HEK293T) cell lines with overexpression of UGT8. They used these cell lines to evaluate if UGT8 could galactosidate substrates other than ceramide by exposing them to different exogenous substrates. They found that not only did UGT8 most efficiently galactosidate ceramides, but it could also galactosidate the following bile acids to varying degrees: cholic acid, deoxycholic acid, chenodeoxycholic acid, hyodeoxycholate acid, and ursodeoxycholic acid [154]. While bile acids are derived from sterols, the activity of UGT8 on other sterol or sterol-derived molecules was not examined in this publication. Interestingly, when human liver microsomes were similarly assessed for UGT8-mediated galactosidation, it was discovered that UGT8 did not galactosidate chenodeoxycholic acid or lithocholic acid, though the other bile acids tested in the HEK cell lines were not evaluated in this study [158]. In Huh7 cells, the most abundant bile acid is chenodeoxycholic acid but the cell line does not maintain high levels of bile acids in a cell culture system [159,160]. It appears possible that UGT8 could have low levels of promiscuity with the ability to galactosidate bile acids, but further investigation of these specific effects in liver cells are needed to validate these concepts. There is no report in the literature of the effects of galactosidation of bile acids on cell membranes.

While the UGT superfamily of enzymes were first discovered in maize plants in 1977, the UGT8 family was more recently discovered and was the subject of focused studies only since the 1990s [161]. The UGT8 enzyme is distinct from the other UGT molecules in that it is genetically dissimilar and comprises the only member in its own family, while the other UGT

families contain multiple enzymes [162]. All of the other UGTs are encoded by a single locus on chromosome 2 on the long arm at position 37 (notated 2q37), whereas UGT8 is located on chromosome 4 on the long arm at position 26 (notated 4q26) [162]. Given its more recent discovery, we are still learning about the roles of UGT8 in health and disease.

The roles of UGT8 in disease have been studied in cancer biology and neurobiology, but to our knowledge has not been reported in viral infection. In cancer biology, increased expression of UGT8 is reported to be a poor prognostic marker due to its association with increased aggressiveness and pro-metastatic behavior [163,164]. In breast cancer, one of the hypotheses is that increased expression of UGT8 decreases cellular pools of ceramide by converting them to galactosylceramides, resulting in less signaling by ceramides to induce apoptosis of tumor cells [164,165]. By inhibiting apoptosis of cancer cells, it allows cells to continue to proliferate and spread to new areas, forming metastases. This concept could also apply to viral infection. A reduction in ceramide levels could potentially inhibit the apoptosis signaling cascade, resulting in increased cell survival, which would be beneficial to the virus.

The roles of UGT8 in neurobiology are largely related to neurodegenerative diseases and potential therapies. The metabolite of UGT8, GalCer, is a major constituent of myelin, the lipid layer that insulates nerves and allows for smooth and coordinated electrical conduction [166]. Animal studies on lysosomal storage diseases such as Krabbe disease, caused by deficiency or dysfunction of the galactosylceramidase (GALC) gene, have shown that treating mice with a UGT8 inhibitor can decrease the severity of the disease and clinical symptoms [167]. While we have a working understanding of the roles UGT8 plays in neoplastic and neurologic diseases, UGT8 and its role in viral infection remain unclear.

Preliminary loss-of-function studies of enzymes in the sphingolipid metabolic pathway in Huh7 cells (human liver cells) identified numerous enzymes involved in the synthesis of glycosphingolipids that had a significant effects on viral titer [168]. From this screen, we

observed an increase in virus titer following knockdown of the enzyme UDP-galactosyltransferase 8 (UGT8). We hypothesized that UGT8 played an antiviral role in DENV2 infection of liver cells. In this thesis, we investigated the role of UGT8 in DENV2 infection and the mechanism of how UGT8 affects the virus life cycle.

2.2 Results

2.2.1 Modulating UGT8 expression affects DENV2 titer

To understand the role of UGT8 in DENV2 infection, we first validated the loss of function studies using an siRNA pool against UGT8 in Huh7 cells followed by infection with DENV2, strain 16681 at an MOI of 0.3 for 24 hours. A negative control siRNA (IRR) with no homology to human genes was used to control for off-target effects of siRNA treatment and a siRNA targeting the DENV2 genome was used as a positive control [169,170]. Following siRNA knockdown, we observed that UGT8 mRNA expression was significantly reduced by 81% (Figure 2.1B). We titrated the virus on baby hamster kidney (BHK) cells and determined that UGT8 knockdown resulted in a significant increase in DENV2 titer by 2.9-fold (Figure 2.1C). None of the siRNA treatments were cytotoxic (Figure 2.1D). This experiment was repeated for a minimum of three independent replicates with three technical replicates and representative data from a single experiment is shown. We validated this knockdown phenotype in human pulmonary adenocarcinoma (A549) cells and observed a 2-fold increase in titer following siRNA knockdown (Supplemental Figure A.1). We then wanted to determine if the effect on titer in Huh7 cells was sustained beyond peak replication at 24 hours. We repeated the knockdown and collected supernatants at 48 hours. The phenotype at 48 hpi remained consistent, with a 1.6-fold increase in cells with UGT8

knockdown (Supplemental Figure A.2A). However, this was a smaller magnitude of change than the 24 hpi time point.

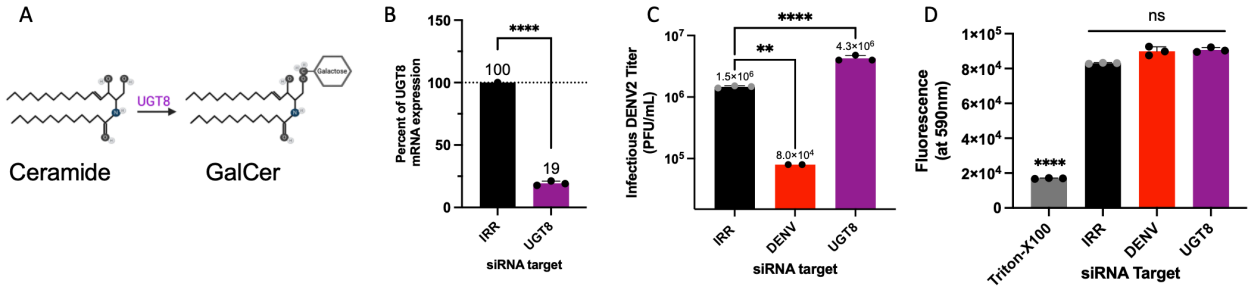

Figure 2.1. Modulating UGT8 expression affects DENV2 titer A. UGT8 adds a galactose onto ceramide to form galactosylceramide. This figure was made with Biorender. **B.** Huh7 cells were transfected with four siRNAs targeting UGT8, a negative control irrelevant siRNA (IRR), or a positive control siRNA specific to the dengue virus used for infection (DENV). Cells were mock infected and collected 24 hours post-transfection to confirm mRNA knockdown. qRT-PCR was performed, and results were normalized to the RPLP0 housekeeping gene. **C.** 48 hours following transfection, cells were infected DENV2 (MOI = 0.3) for 24 hr. At 24 hpi, viral supernatants were collected and analyzed via plaque assays. Viral titer was significantly increased by 65% following UGT8 knockdown. **D.** Cell viability following siRNA transfection and mock infection was assessed using an Alamar Blue Cell Viability Assay. Fluorescence at 590 nm corresponds to the cells' metabolic activity. The positive control, Triton-X100, is toxic to the cells, and shows decreased fluorescence, indicating decreased metabolic activity. No siRNA treatment significantly affected cell viability. (B-D one-way ANOVA with Dunnett's multiple comparison's test: ns = $p \geq 0.05$ * = $p \leq 0.05$, ** = $p \leq 0.01$, **** = $p \leq 0.0001$; results are expressed as mean values with standard deviation indicated by error bars) [Abbreviations: IRR, irrelevant, non-targeting siRNA; DENV, DENV2-specific siRNA; UGT8, UDP-galactosyltransferase 8].

In conjunction with loss of function, we performed transient overexpression of UGT8 by transfecting in a plasmid containing the UGT8 gene. An empty vector plasmid (EV) served as the negative control. Overexpression was confirmed using qRT-PCR which showed a 39% increase in UGT8 mRNA expression (Figure 2.2A). With transient overexpression, we observed a 1.5-fold decrease in viral titer at 24 hpi (Figure A.2B). At 48 hpi, the titer was not significantly different than the negative control (Supplemental Figure A.2B). There were no significant cytotoxic effects of the plasmids (Figure 2.2C). This experiment was repeated for a minimum of three replicates and representative data from a single experiment is shown.

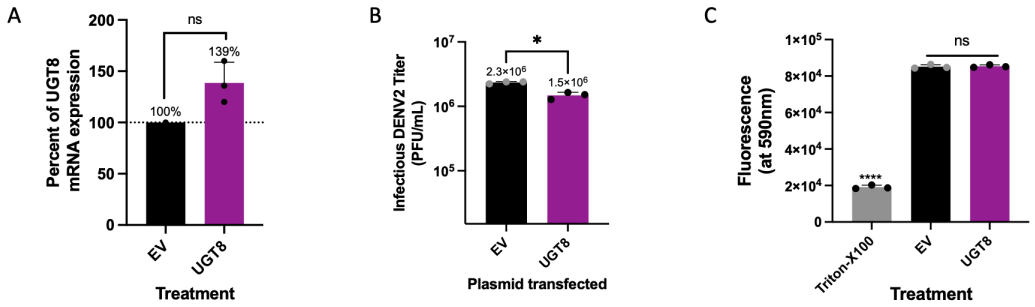

Figure 2.2 Modulating UGT8 expression affects DENV2 titer. A. Huh7 cells were transfected with a plasmid containing the UGT8 gene and an empty vector control. At 72 hours post-transfection cells were collected, and RNA was extracted and analyzed for UGT8 mRNA expression. Results were normalized to the RPLP0 housekeeping gene. UGT8 expression was increased to 39% greater than the negative control. **B.** 48 hours following transfection, cells were infected DENV2 (MOI = 0.3) for 24 hr. At 24 hpi, viral supernatants were collected and analyzed via plaque assays. Overexpression of UGT8 results in a 35% decrease in viral titer. **C.** Cell viability following plasmid transfection and mock infection was assessed using an Alamar Blue Cell Viability Assay. Fluorescence at 590 nm corresponds to the cells' metabolic activity. The positive control, Triton-X100, is toxic to the cells, and shows decreased fluorescence, indicating decreased metabolic activity. No plasmid treatment significantly affected cell viability. (A-D one-way ANOVA with Dunnett's multiple comparison's test: ns = $p \geq 0.05$ * = $p \leq 0.05$, ** = $p \leq 0.01$, ***= $p \leq 0.001$, **** = $p \leq 0.0001$; results are expressed as mean values with standard deviation indicated by error bars) [Abbreviations: EV, empty vector control plasmid; UGT8, UDP-galactosyltransferase 8 plasmid].

We also developed stable Huh7 clones overexpressing UGT8. However, since we experienced difficulties in validating UGT8 expression, these studies are discussed in detail in the Appendix (Supplemental Figure A.3).

These experiments validated the siRNA knockdown results from St. Clair et al. The addition of overexpression of the UGT8 enzyme demonstrated the opposing phenotype, suggesting that UGT8 may be an antiviral factor in the DENV2 life cycle. Additional experiments were designed to understand the mechanism behind the change in viral titer following knockdown or over-expression of UGT8.

2.2.2 DENV2 infection alters UGT8 expression at peak viral replication (24 hpi)

If UGT8 is antiviral, it was our hypothesis that viral infection may reduce its expression for viral benefit. To appreciate how expression of UGT8 is changed during infection, we infected Huh7 with DENV2 (MOI = 1), and collected cells at time points 0-, 6-, 12- 24-, 48, and 72-hours post-infection. RNA was extracted and qRT-PCR was

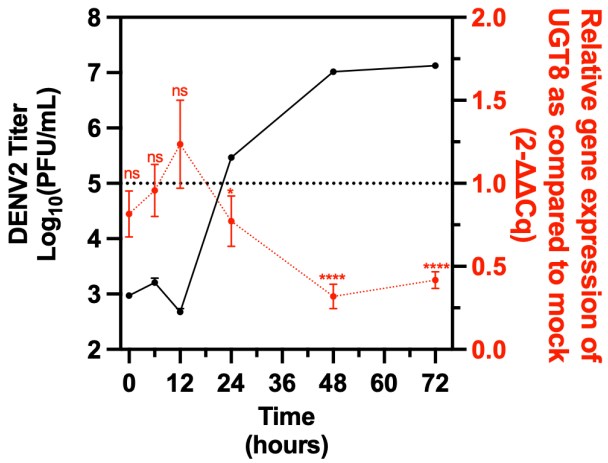

Figure 2.3. DENV2 infection alters UGT8 expression at peak viral replication (24 hpi). UGT8 mRNA expression is temporally decreased during DENV2 infection. Huh7 cells were either mock-infected or DENV2-infected (MOI = 1) and cells were collected in triplicate at 0, 6, 12-, 24-, 48-, and 72-hours post-infection. RNA was extracted and assessed using qRT-PCR. DENV2-infected samples were compared to mock infected samples at matched timepoints. Results are reported as an expression ratio between each timepoint sample and its respective mock-infected timepoint (in red). Statistical comparison performed between the mock and infected values for each time point. Corresponding titers at each time point in the DENV2-infected samples are shown in black. (Student's unpaired T test: ns = $p \geq 0.05$, * $p \leq 0.05$, **** $p \leq 0.0001$).

performed to quantify UGT8 mRNA expression at each time point. Expression was normalized to a cellular housekeeping gene, RPLP0 [171]. This experiment was repeated for a minimum of three replicates and representative data from a single experiment is shown. We found that during DENV2 infection, UGT8 mRNA expression was unchanged at early time points. However, by 24 hpi, UGT8 mRNA expression was decreased by 23%, as compared to mock-infected cells (Figure 2.3). At 48 and 72 hpi, the level of UGT8 expression was further reduced by 68% and 58%, respectively. This data indicated that as infection progresses, mRNA levels of UGT8 continue to decrease, suggesting that infection is correlated with, or potentially causative of, a decrease in UGT8 expression. In addition, the UGT8 enzyme has been shown to be upregulated by the Sox10 transcription factor in basal-like breast cancer, and it is possible that infection could reduce Sox10 expression, leading to reduced UGT8 transcription [163]. The roles of Sox10 have not been reported in viral infections.

2.2.3 DENV2 infection alters GalCer expression on the surface of Huh7 cells

In conjunction with UGT8 expression, we wanted to determine if expression of the product of UGT8, the metabolite, GalCer, was similarly affected by DENV2 infection. We infected Huh7 with DENV2 (MOI = 3) and performed a concurrent mock infection and harvested cells at 24-, 48- and 72 hpi. Cells were washed and stained with a cell viability dye and an anti-GalCer antibody conjugated to AlexFluor488. The MOI of 3 was selected to ensure as many cells as possible would be infected. Additionally, the risk of analyzing dead cells was minimized by exclusion of dead cells from the analysis using the cell viability dye, alleviating this concern. Flow cytometry was performed to determine the expression of GalCer during infection. This experiment was performed once and therefore the data shown represents preliminary data. Fluorescence intensity was normalized to cells stained only with viability stain and not the GalCer antibody and the fluorescence intensity of the DENV2-infected cells was compared to the mock-infected cells. We did not have sufficient cells to analyze at the 24 hpi time point due to cell losses during the staining protocol. We observed that there was a 38% decrease in GalCer expression at 48 hpi relative to mock-infected cells (Figure 2.5A-F). We had a minimum of 25,000 cells for each sample in the 48-hour time point. At 72 hpi, we observed a significant increase in GalCer expression by 91% compared to mock-infected cells, however, the majority of cells were lost in the staining process for the 72 hpi time point, leaving us with only 1,654 and 2,694 cells in the two replicates of DENV2-infected stained with the GalCer antibody, which complicated our analysis (Figure 2.5G-L). The data for the 48 hpi time point is consistent with the decrease in UGT8 mRNA expression observed in 2.2.2, confirming the expected correlation between UGT8 expression and GalCer expression.

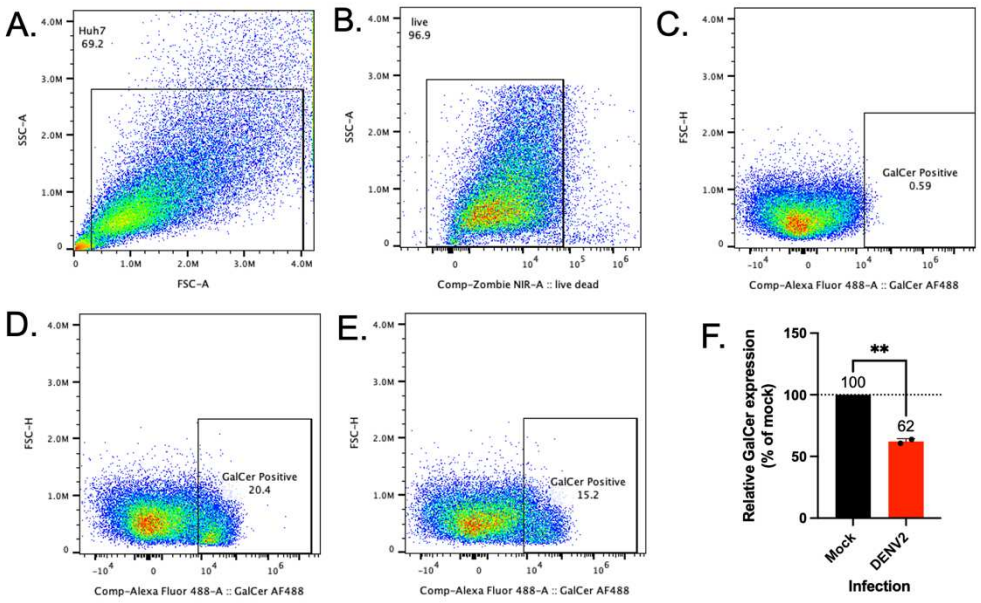

Figure 2.4A-F. **Flow cytometric analysis of GalCer expression in DENV2-infected Huh7 cells at 48 hpi.** **A.** Forward scatter area (FSC-A) versus side scatter area (SSC-A) plot showing gating strategy to exclude debris and select intact cells. **B.** Viability gating using Zombie NIR stain to discriminate live cells (Zombie NIR-negative). **C.** Representative plot of unstained control cells used to set GalCer-negative gate. **D-E.** GalCer expression in mock-infected (**D**) and DENV2-infected (**E**) cells. Numbers in plots indicate percentage of cells within each gate. **F.** Quantification of relative GalCer expression in DENV2-infected cells as compared to mock. Data are presented as mean ± SEM. Student's unpaired T test. ** $p \leq 0.005$

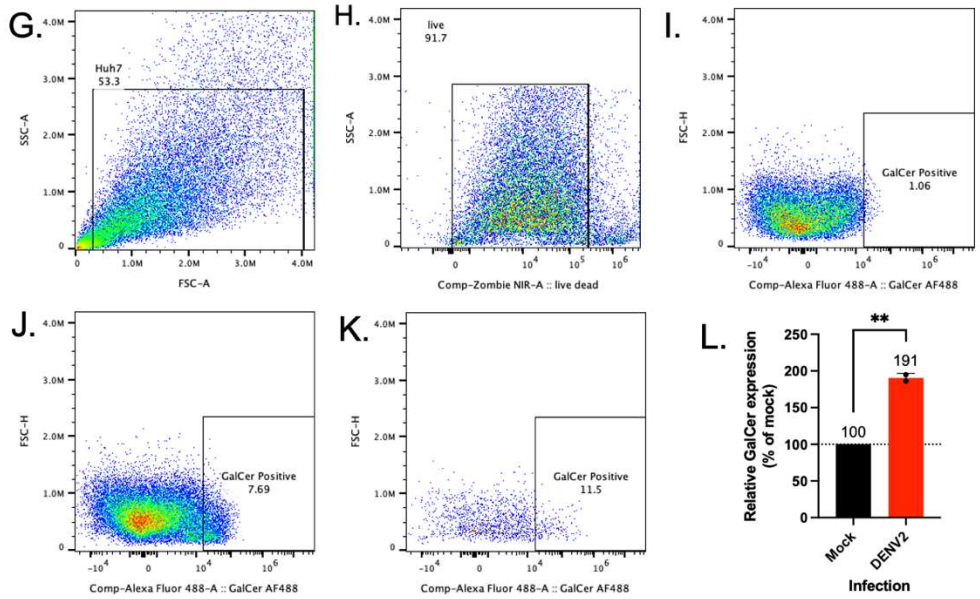

Figure 2.4G-L. **Flow cytometric analysis of GalCer expression in DENV2-infected Huh7 cells at 72 hpi**. **G.** Forward scatter area (FSC-A) versus side scatter area (SSC-A) plot showing gating strategy to exclude debris and select intact cells. **H.** Viability gating using Zombie NIR stain to discriminate live cells (Zombie NIR-negative). **I.** Representative plot of unstained control cells used to set GalCer-negative gate. **J-K.** GalCer expression in mock-infected **J.** and DENV2-infected **K.** cells. Numbers in plots indicate percentage of cells within each gate. **L.** Quantification of relative GalCer expression in DENV2-infected cells as compared to mock. Data are presented as mean ± SEM. Student's unpaired T test. ** $p \leq 0.005$

2.2.4 Altering UGT8 expression affects extracellular DENV2 titer but not intracellular titer

To further investigate the cause of the change in DENV2 titer following modulation of UGT8 expression, we examined intra- and extracellular titers to determine if there was a change in virus assembly and release. We carried out loss of function studies using the UGT8 siRNA followed by infection with DENV2 at MOI 0.3 detailed in section 2.2.1. At 24 hpi, supernatants and cells were collected. The cells were washed, harvested, and subjected to repeated freeze-thaw cycles to lyse the cells. Cellular debris was removed using centrifugation, and the intracellular and extracellular supernatants were titrated on BHK cells. This experiment was repeated for a minimum of three independent biological replicates with three technical replicates and representative data from a single experiment is shown.

The extracellular titer for cells transfected with UGT8 siRNA was significantly increased compared to the negative control siRNA (Figure 2.5A). However, the titer was not significantly different to the control (Figure 2.5B). This indicated that there were higher numbers of infectious virus particles in the extracellular space, despite the fact that there was no difference in the concentration of infectious particles within the cells. When extracellular and intracellular titers were compared, the controls had an approximately 1:1 ratio whereas with UGT8 knockdown there was a 4:3 extracellular to intracellular ratio (Figure 2.5C).

This experiment was repeated with plasmid overexpression and we observed a significant decrease in extracellular titer when UGT8 was over-expressed (Figure 2.5D). However, similar to when UGT8 was knocked down, there was not a significant difference

in intracellular titers (Figure 2.5E). When comparing extracellular and intracellular titers, again the control had a 1:1 ratio, but UGT8 overexpression caused a 1:2 extracellular to intracellular ratio in virus titer (Figure 2.5F). This demonstrates an opposing phenotype to the UGT8 knockdown experiments.

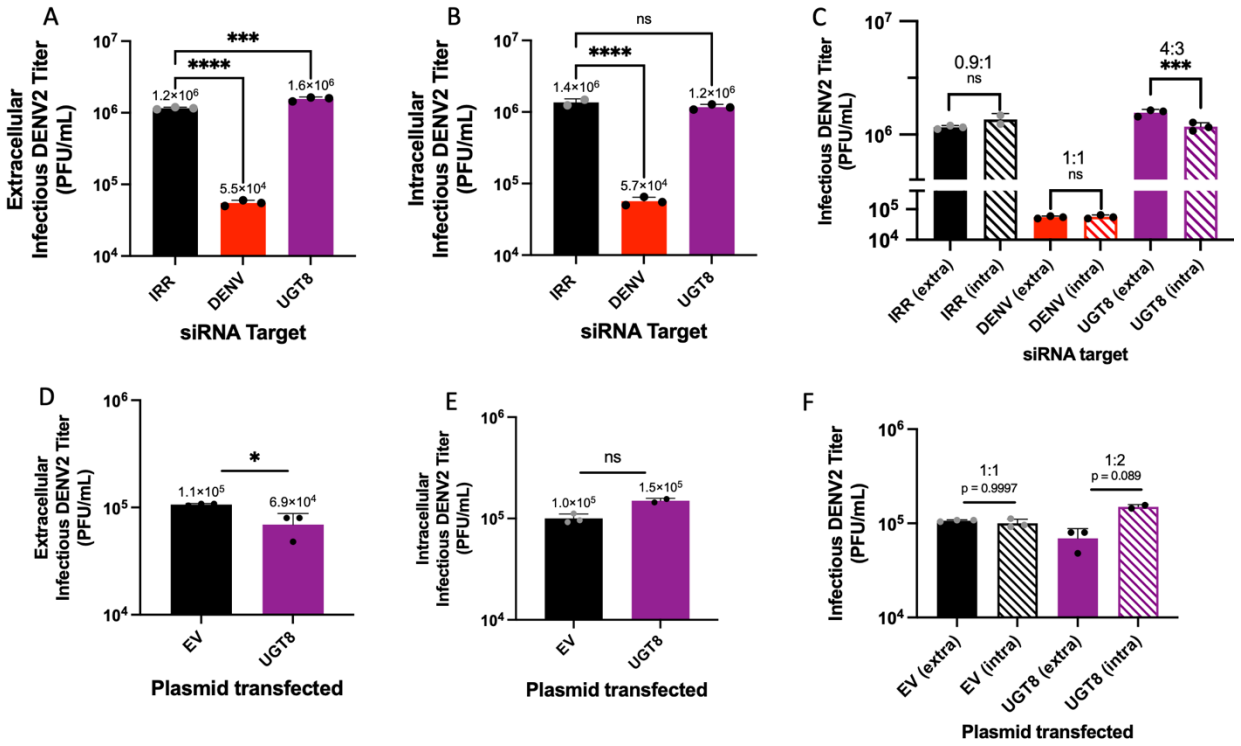

Figure 2.5. Altering UGT8 expression affects extracellular DENV2 titer but not intracellular titer
A. Extracellular and intracellular viral titers following siRNA knockdown detailed in figure 1 were measured using plaque assays. Intracellular virus was harvested from cells using repeated freeze-thaw cycles and centrifugation to remove the cellular debris from the supernatant. There was no significant difference in intracellular titer of UGT8 knockdown cells compared to the negative control. **B**. The extracellular titer of UGT8 knockdown cells was significantly increased by 25%. **C**. The ratio of extracellular to intracellular titer of the negative and positive control was 0.9:1 and 1:1, respectively. For the controls, there was no significant difference between intra- and extracellular titers when compared to each other. The extracellular to intracellular ratio of cells with UGT8 knockdown was 4:3, which was significantly increased relative to the negative control.. **D.** Extracellular and intracellular viral titers following overexpression detailed in figure 2 were measured using plaque assays. Intracellular virus was harvested from cells using repeated freeze-thaw cycles and centrifugation to remove the cellular debris from the supernatant. There was no significant difference in intracellular titer of UGT8 knockdown cells compared to the negative control. **E.** The extracellular titer of UGT8 overexpression cells was significantly decreased by 37%. **F.** The ratio of extracellular to intracellular titer of the control was 1:1 and there was no significant difference between intra- and extracellular titers when compared to each other. The extracellular to intracellular ratio of cells with UGT8 overexpression was 1:2, though not statistically significant. One-way ANOVA with Dunnett's multiple comparison's test: ns = $p \geq 0.05$ * = $p \leq 0.05$, *** = $p \leq 0.001$, **** = $p \leq 0.0001$. Results are expressed as mean values with standard deviation indicated by error bars.

2.2.5 UGT8 knockdown increases the rate of virus release

To understand if UGT8 knockdown affected the rate of virus release, we performed a time course of virus release following UGT8 siRNA knockdown. We collected viral supernatants every 24 hours for 4 days post-infection. This experiment was performed with triplicate samples one time and the data is presented below. We determined that there was a significant increase in the rate of virus release between 24 to 48 hours (Figures 2.6A and 2.6B). Validation of UGT8 knockdown was performed for time points 24, 48, and 72 and showed significant decrease in UGT8 mRNA expression at every time point (Figure 2.6C).

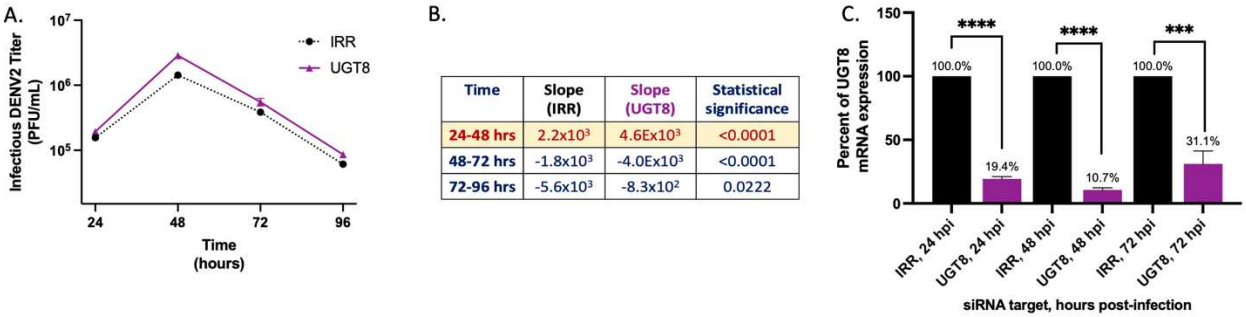

Time	Slope (IRR)	Slope (UGT8)	Statistical significance
24-48 hrs	$2.2x10^3$	$4.6Ex10^3$	<0.0001
48-72 hrs	$-1.8x10^3$	$-4.0Ex10^3$	<0.0001
72-96 hrs	$-5.6x10^3$	$-8.3x10^2$	0.0222

Figure 2.6. UGT8 knockdown increases the rate of virus release A. siRNA knockdown was performed as previously described. At 24 hours post-infection, supernatant was removed, and new media was replaced. 24 hours later, this process was repeated, 24-, 48-, and 72-hours collect four days of viral supernatants and perform plaque assays to evaluate virus release over time. **B.** The rate of DENV2 release was significantly increased for cells with UGT8 knockdown between 24 to 48 hours. **C.** The efficiency of UGT8 siRNA knockdown was measured at 24-, 48-, and 72-hours post-mock infection and was performed concurrently with the rate of release experiment. At all time points, there is a significant decrease in UGT8 mRNA expression, confirming sufficient knockdown. Expression was normalized to cellular housekeeping gene, Rplp0. Expression in UGT8 knockdown cells was compared to expression in cells treated with the negative control siRNA (IRR). C: One-way ANOVA with Dunnett's multiple comparison's test: *** = p≤0.001, **** = p≤0.0001. Results are expressed as mean values with standard deviation indicated by error bars.

2.2.6 DENV2 particles made in cells with UGT8 knockdown exhibit decreased entry

It was our hypothesis that changes to extracellular titer were due to an accumulation of virus in the supernatant caused by a disruption in virus entry. To investigate this, we infected Huh7 cells with 10^7 genome copies of virus harvested from

Huh7 cells transfected with UGT8 siRNA or the negative control (IRR) siRNA. At time points 0, 2-, 4-, 6-, 24-, and 48-hours post-infection, cells were harvested and total RNA was extracted. Quantitative RT-PCR was performed to quantify the number of viral genome copies that had entered cells. These experiments were repeated for a minimum of three independent biological replicates with a minimum of three technical replicates and representative data from a single experiment is shown. We determined that the number of intracellular genome copies in the supernatants from UGT8 knockdown cells was significantly lower compared to the control at 0-, 2-, and 24-hpi (Figure 2.7). The number of genome copies in cells treated with UGT8 knockdown supernatant in the 4- and 6-hpi groups was reduced, but not statistically significant ($p=0.18$ and $p=0.33$, respectively). At 48 hours, the number of genome copies in the two groups were not significantly different ($p=0.74$). This data suggests that entry of virus particles made in cells with UGT8 knockdown have impaired ability to enter wild type Huh7 cells. Furthermore, when virus replication is robust at the 48-hour time point, there is no significant difference between the two groups.

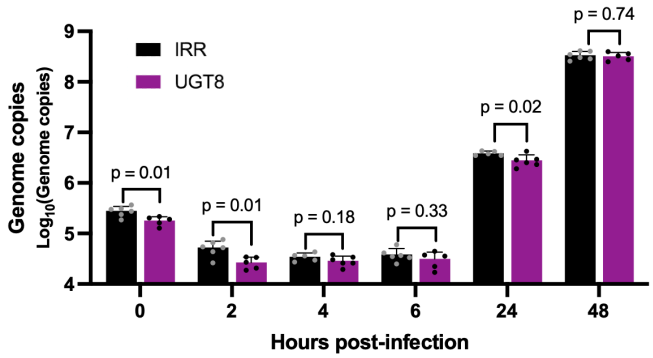

Figure 2.7. DENV2 particles made in cells with UGT8 knockdown exhibit decreased entry
Huh7 cells were infected with equivalent particle numbers (as determined by qRT-PCR) of DENV2 made by cells transfected with UGT8 siRNA or the negative control (IRR) siRNA. At 0, 2, 4, 6, 24, and 48 hours, sextuplicate wells were washed, treated with acid glycine to inactivate any extracellular virus, and cells were collected in TRIzol. RNA was extracted and qRT-PCR was performed to quantify the number of intracellular genomes. This showed that there was a significant difference in the ability of the particles made from cells with UGT8 knockdown to enter new cells. At the early time point of 2 hpi which is used to measure virus entry, there was significantly fewer genome copies in cells infected with virus produced by cells with UGT8 knockdown. At 24 hpi there continues to be significantly fewer genome copies in the cells infected with virus made from cells with UGT8 knockdown. At 48 hpi there is no longer a significant difference between the two groups. Additional statistics are reported in Supplemental Figure 4. (Student's unpaired T test). Results are expressed as mean values with standard deviation indicated by error bars).

2.2.7 DENV2 particles produced in cells with UGT8 knockdown have altered transmission

To determine if the entry and transmission of virus particles released from UGT8 knockdown cells was altered, we carried out a transmission assay in wild type Huh7 cells over an extended time course. We infected each well of 10,000 Huh7 cells with 10^8 genome copies of virus harvested from Huh7 cells transfected with the UGT8 siRNA or the negative control (IRR) siRNA. In this experiment, because we used fluorescence microscopy to quantify the number of infected cells, the amount of virus added is different than in the entry assay in 2.2.5 which detected viral RNA using PCR. Fluorescence microscopy has a different limit of detection than PCR. We optimized similar concentrations of virus to what was used in the entry experiment, including 10^3 to 10^8 genome copies, but we found that viral infection could only be detected at the 24-hour time point when we utilized 10^8 genome copies, meaning that we had to infect with a log

more virus in this experiment. We then fixed cells at 24-, 48-, and 72-hpi and stained them with an antibody against the FV E protein along with a DAPI stain to highlight nuclei (Figure 2.8A). This experiment was repeated for two replicates and representative data from a single experiment is shown. An additional replicate was attempted and the use of the Celigo Image Cytometer (Revvity, product# 200-BFFL-5C) was employed for a higher throughput experiment. However, this experiment failed because the amount of background fluorescence was too great to measure fluorescence with high accuracy and acquire data. We observed that at all time points there were more cells positive for E protein in the cells infected with the virus harvested from the negative control (IRR) versus UGT8 knockdown cells, though it was only statistically significant at 24 and 72 hpi (Figure 2.8B).

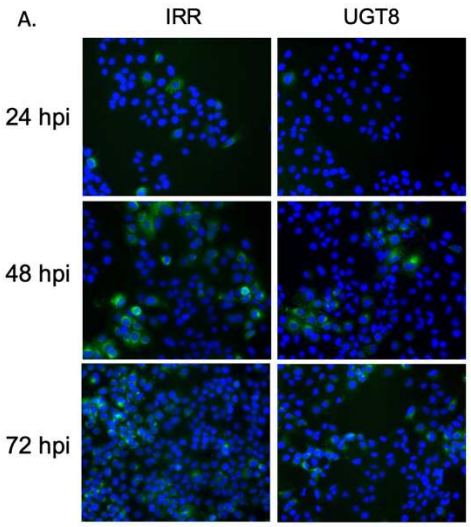

Time	IRR sup	UGT sup
24 hpi	25/324 (7.7%)	5/444 (1.1%)
48 hpi	350/1,160 (30.2%)	285/1,190 (23.9%)
72 hpi	595/1,635 (48.7%)	753/1,979 (38.0%)

Figure 2.8. DENV2 particles produced in cells with UGT8 knockdown have altered transmission. A. Huh7 cells were infected with equivalent particle numbers (as determined by qRT-PCR) of DENV2 made by cells transfected with UGT8 siRNA or the negative control (IRR) siRNA. Every 24 hours, cells were fixed with paraformaldehyde, permeabilized, and stained with pan-flavivirus E protein antibody (4g2, green) and DAPI (blue). At each time point infected and uninfected cells were counted. **B.** At each time point, there are more cells infected in the group treated with IRR supernatant than UGT8 supernatant. At 72 hours, this difference becomes statistically significant. Odds ratio: ns = $p \geq 0.05$ * = $p \leq 0.05$. Results are expressed as mean values with standard deviation indicated by error bars).

2.2.8 Modulation UGT8 expression does not affect genome replication

To appreciate if alterations in UGT8 expression affected DENV2 genome replication, we measured the number of genome copies using quantitative RT-PCR in total cellular RNA obtained from the siRNA knockdown or plasmid overexpression experiment detailed in section 2.2.1. These experiments were performed for minimum of three independent biological replicates with three technical replicates and representative data from a single experiment is shown. There was no significant difference in the number of viral genome copies in cells transfected with UGT8 siRNA when compared to the negative control (IRR) (Figure 2.9A), nor in cells transfected with the UGT8 over-expression plasmid compared to the empty vector control (Figure 2.9B). This confirmed that changes in genome replication were not responsible for the changes in virus titer we observed.

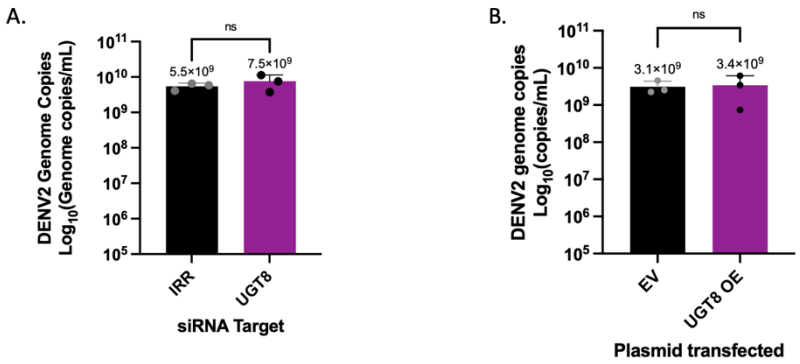

Figure 2.9. Modulation UGT8 expression does not affect genome replication.
A. Huh7 cells were transfected with siRNAs targeting UGT8 and a non-targeting irrelevant (IRR) negative control. 48 hours following transfection, cells were infected DENV2 (MOI = 0.3) for 24 hr. At 24 hpi, cells were collected and RNA was extracted. qRT-PCR was performed to quantify copies of DENV2 genomes. There was no significant difference in genome copy number in cells with UGT8 knockdown when compared to the negative control (IRR). **B**. There was no significant difference in genome copy number in cells with UGT8 overexpression when compared to the negative control (EV). One-way ANOVA with Dunnett's multiple comparison's test. Results are expressed as mean values with standard deviation indicated by error bars : ns = $p \geq 0.05$.

2.2.10 UGT8 loss of function does not affect specific infectivity

To determine if the virus particles being released from UGT8 knockdown cells were less infectious and that was the cause of the accumulation of the particles in the supernatant, we measured their specific infectivity. Following transfection of either siRNA or plasmids and infection with DENV2, viral RNA in the supernatants were quantified to obtain the concentration of genome copies/ml using qRT-PCR. We also titrated the supernatants on BHK cells as detailed in section 2.2.1. These experiments were performed for a minimum of three biological replicates with three technical replicates and representative data from a single experiment is shown. The data indicated that for both knockdown (Figure 2.10A) and overexpression (Figure 2.10B), there was an increase in the particle to PFU ratio, but it was not statistically significant. These data suggest that the changes in titer were not related to changes in infectivity of the virus particles released from UGT8 knockdown cells.

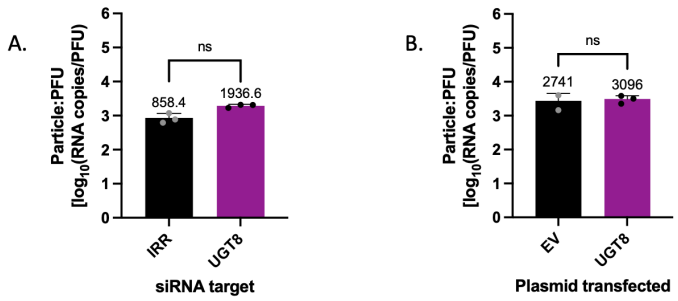

Figure 2.10. Modulating UGT8 expression does not significantly alter specific infectivity of DENV2
A. Huh7 cells were transfected with siRNAs targeting UGT8, a non-targeting irrelevant (IRR) negative control, and a DENV2-specific positive control siRNA. 48 hours following transfection, cells were infected DENV2 (MOI = 0.3) for 24 hr. At 24 hpi, supernatants and cells were collected. Titer was determined using plaque assays and qRT-PCR was performed to quantify copies of DENV2 genomes in the supernatant. These values were compared to generate the ratio of total particles:infectious particles. There was an increase in the particle:PFU ratio in cells with UGT8 knockdown relative to the negative control (IRR), but it was not statistically significant. **B.** This protocol was also performed with overexpression. There was no significant difference between cells with UGT8 overexpression and the negative control (EV). (A-B one-way ANOVA with Dunnett's multiple comparison's test: ns = $p \geq 0.05$. Results are expressed as mean values with standard deviation indicated by error bars).

2.3 Discussion

The roles of UGT8 in viral infection has not previously been reported. Our study aimed to understand the roles of UGT8 and its metabolite, GalCer, in DENV2 infection. Our results suggest that UGT8 plays a role in DENV2 entry into Huh7 cells. When UGT8 expression is reduced, fewer GalCer molecules are produced from ceramides in the ER, resulting in less GalCer that can be trafficked to the plasma membrane. Consequently, we expect that the ER membrane and plasma membranes would have a lower proportion of GalCer. The opposite effect is expected with UGT8 overexpression.

Changes to the GalCer composition to a membrane can have numerous effects. Increasing GalCer can slow the lateral diffusion of molecules within a membrane due to increased hydrogen binding between GalCer and adjacent phospholipids [172], increase the thickness and stiffness of a membrane which reduces the flexibility [173], and increase the formation of lipid rafts [174]. Based on our knowledge of the shapes of lipid molecules, we know that GalCer is a conical lipid with a large polar head group. This is a shape that favors positive membrane curvature [80,81,83]. However, the effects of altering GalCer membrane composition on membrane curvature have not been specifically reported in the literature.

An important consideration in knockdown and overexpression systems is that not every cell will have the intended modulation of expression. It is possible that the cells that are not successfully transfected with either the siRNA or plasmid DNA may dilute the overall phenotype we observe when we infect with DENV2. Therefore, a key future direction would be to study the effects of knockout of UGT8, such as with a CRISPR-Cas9 system to circumvent the above problems. These studies are currently underway in

the Perera laboratory. However, a knockout of UGT8 may alter the expression of other molecules within the cells causing metabolic shifts. These shifts could be examined by assessing the metabolic landscape with LC-MS/MS. In addition to a knockout system, another possibility that could provide valuable insight would be single cell studies, such as single molecule fluorescence resonance energy transfer (smFRET), to measure uptake of virus and resulting phenotypes, though these can be technically challenging.

Entry

In the context of DENV2 infection, these changes in GalCer composition of the ER and plasma membrane could alter the functionality of the viral lipid membrane and the target host cellular membrane, explaining the observed changes in entry. We will discuss changes to each and their potential impact on viral entry individually.

For the virus particles, alterations in lipid membrane composition could alter entry by affecting how the E proteins on the particle interact with host cell attachment molecules. Attachment molecules such as heparan sulfate, DC-SIGN, and heat shock protein 70, among many others, are the first interactions the virus particle has with the cell surface [40,41,47,175]. Changes in membrane fluidity and curvature secondary to alterations in GalCer concentrations may hinder E protein access to host cell attachment molecules, thereby inhibiting the attachment and entry process. GalCer is a lipid with a large polar headgroup (galactose), which favors bending outward (termed positive membrane curvature). If there are increased numbers of GalCer molecules in the viral membrane, the membrane may have specific areas with increased positive curvature, causing the membrane to bend outward. However, if there are decreased quantities of GalCer, the membrane may be relatively more planar or even have a more negative

curvature (which would bend inward). Both of these conformations could affect the viral E proteins ability to assemble into the required icosahedral conformations, which ultimately are required to access attachment molecules. If there are fewer E proteins able to interact with cellular attachment molecules, it could decrease the avidity of the interaction, which could in turn result in a reduction in entry.

For the host cell, the downstream effects of altering membrane composition include altering lipid rafts and how attachment molecules cluster within them, altering membrane fluidity which can affect how attachment molecules move within the membrane, and alterations to the electrostatic charge of the membrane (2.11). Attachment molecules such a DC-SIGN and heparan sulfate often cluster within lipid rafts. It has been reported that disruption of lipid rafts by altering cholesterol composition can reduce DENV infection in vitro [176]. This concept could be applied to changing the GalCer composition of the membrane. As GalCer is a component of lipid rafts, it could affect attachment molecule clustering and availability of molecules for the virus to bind. Decreasing GalCer composition would increase the membrane fluidity while increasing the GalCer composition would decrease it. Increasing the fluidity could potentially aid in the virus locating the attachment molecules for binding. However, if the pattern in which the attachment molecules typically cluster is disrupted, this could limit the benefits of increased mobility. Altering the membrane composition could also affect the electrostatic charge. DENV virions are typically positively charged, and therefore, anionic lipids such as heparan sulfate and phosphatidylserine on the plasma membrane contribute to the negative charge of the host membrane, to facilitate virus binding [177]. If the plasma membrane composition is shifted to have fewer anionic lipids as a result of altering GalCer

composition, it could affect the electrostatic interactions between the virus and the cell and in turn affect binding.

These concepts could explain both the decreased entry of particles made from cells with UGT8 knockdown in 2.2.5, but may also help explain the differences in extracellular titer observed in 2.2.3. When we knocked down UGT8 in 2.2.3, we noticed an increase in extracellular titer, but no difference in intracellular titer. In this assay, the virus added for the initial infection is wildtype, but the cells have a significant reduction in UGT8 expression, a condition that is expected to decrease GalCer in the ER and plasma membranes. This modulation of UGT8 expression, which we hypothesize will change the composition of the plasma membrane, appears to limit the ability of the virus to enter. However, as time progresses, these cells with UGT8 knockdown begin to produce new virus particles. As the virus derives their membrane from the host cell ER membrane, these new particles produced have altered lipid membranes, which in turn further affect their ability to enter uninfected cells. We observed in the entry assay in 2.2.5 that when these virus particles produced by cells with UGT8 knockdown were used to infect wild type Huh7 cells, that their ability to enter was diminished, confirming that both the host and the viral membranes were playing a role in this phenotype.

Fusion

In addition to entry, changes in GalCer composition could affect viral envelope fluidity and the ability of the embedded viral glycoproteins to undergo structural conformations necessary to facilitate fusion with the endosome membrane. Fusion with the host cell membranes require significant curvature and bending, including the

formation of energetically unfavorable intermediate membrane conformations before achieving formation of the fusion pore [80–82].

There are two possibilities to consider in regards to how the structure of the membrane could affect fusion. First, fewer GalCer molecules may decrease the positive curvature of the membrane, which may hinder the ability of the virus particle membrane to protrude towards the endosome membrane during the fusion process (Figure 2.12). Alternatively, decreasing GalCer could make the viral membrane more fluid and flexible, which could affect the formation of the fusion intermediates. Similar to how altering the cholesterol composition of the endosome membrane affects the ability of the virus to fuse, modulation of GalCer in the virus particle membrane may also affect fusion [57,58].

In addition to membrane structure, we must also consider the conformation of the viral E proteins and how the membrane characteristics may impact their ability to rearrange. During endosomal fusion, the reduction in pH results in rearrangement of the E proteins on the virus surface from homodimers which lie flat on the virus surface to homotrimers which extend outward and expose the fusion peptide. This conformational change also increases the proximity of the viral and endosomal membranes t[51]. Changes in the particle membrane composition may impede these structural rearrangements, potentially making fusion more challenging. As mentioned above in the discussion of entry, decreasing GalCer composition would increase the fluidity of the membrane, and vice versa. It is possible that altering membrane fluidity could affect the rearrangement of the E proteins and affect fusion.

Our entry assay in 2.2.5 showed a significant change in the number of genome copies in cells infected with virus particles that were produced from cells with UGT8

knockdown. In this experiment, the 2-, 4, and 6 hpi time points are most relevant for measuring viral entry, as it is early enough that genome replication is not at detectable levels, but the virus has likely been delivered to the late endosome and fused. Entry and fusion have been reported to occur within 15 minutes of infection [48,54]. There was no significant difference between the 2-, 4-, and 6 hpi time points when compared to each other as they represent entry and fusion with only low levels of genome replication (Supplementary Figure 2).

At 24 hpi, significantly fewer genome copies were measured in the cells infected with virus produced by UGT8 knockdown cells, indicating that even after genome replication is detectable, fewer cells are infected due to the reduction in initial entry. However, the 48 hpi group showed no significant difference in genome copies between the control and experimental groups. Once the entry-defective virus has entered cells and begins replicating, newly released viral particles should be equivalent to those released from control-treated cells. The initial amount of virus that entered for either group ranged from 1 genome copy per 2-4 cells, leaving many uninfected cells. As more and more Huh7 cells become infected with wild type virus, the disparity between the two groups decreases.

Release

In addition to affecting the virus particle membrane, the rate of release experiment suggests potential changes to the host cell membrane following modulation of UGT8 expression. UGT8 knockdown is expected to decrease ER and plasma membrane GalCer, potentially reducing membrane rigidity and thickness [136,137]. These changes

to the membrane could make virus release more efficient, by improving the trafficking of secretory vesicles containing virions to facilitate exocytosis. The general secretory pathways of the cell may be altered following modulation of UGT8 expression. It has been shown that lipid rafts may play a key role in the cellular exocytosis pathways and depletion of cholesterol in the cell can result in a reduction in exocytosis pathways [178]. It is possible that either the change in GalCer composition or the downstream effects of this change alter lipid rafts and subsequently affect exocytosis pathways, which will directly impact virus release.

Assembly

Changes to virus assembly were not directly studied in any of our experiments. Changes in assembly could impact extracellular and intracellular titers, but we did not perform an experiment to parse out any changes to assembly following modulation of UGT8 expression. One experiment that could be performed to assess changes in assembly is a single molecule RNA Fluorescence In Situ Hybridization (FISH) to probe for viral RNA and both capsid and E protein within the Golgi of infected cells with UGT8 knockdown or overexpression. Alternatively, an analytical ultracentrifugation approach could be pursued. In this method, we would centrifuge virus fractions and then probe each fraction for capsid, prM, and E structural proteins using Western blots as described in [169]. It is possible that changes in the ER membrane following modulation of UGT8 and GalCer expression could affect the efficiency of assembly. For example, if UGT8 is knocked down, and there is a corresponding decrease in GalCer expression in the ER membrane, a decrease in the membrane thickness and an increase in the fluidity could affect how the replication complexes form or how quickly viral proteins are able to be aggregated.

Specific Infectivity

Specific infectivity, defined as the ratio of plaque forming units (PFU) to the total number of viral genomes, indicates the proportion viral particles that are infectious. The lack of significant difference in specific infectivity between virus particles produced in in Huh7 cells with UGT8 knockdown and over-expression compared to controls in our study may be complicated by the cell type used for the assay. Viral titers for DENV are measured using plaque assays which are carried out in baby hamster kidney cells (BHK), which may have different membrane lipid composition from human liver cells (Huh7) [179]. Therefore, the specific infectivity results may not be representative of the infectivity of the particles to human cells. In addition, it is possible that DENVs released from human cells are optimized for efficient infection of the vector. As human-to-human transmission of DENVs does not naturally occur, it would make sense that the virus released from human cells could be optimized to infect mosquitoes. Work to evaluate infection of mosquito cells and the mosquito vector with virus made from cells with modulation of UGT8 expression is currently underway to evaluate how it could affect virus transmission.

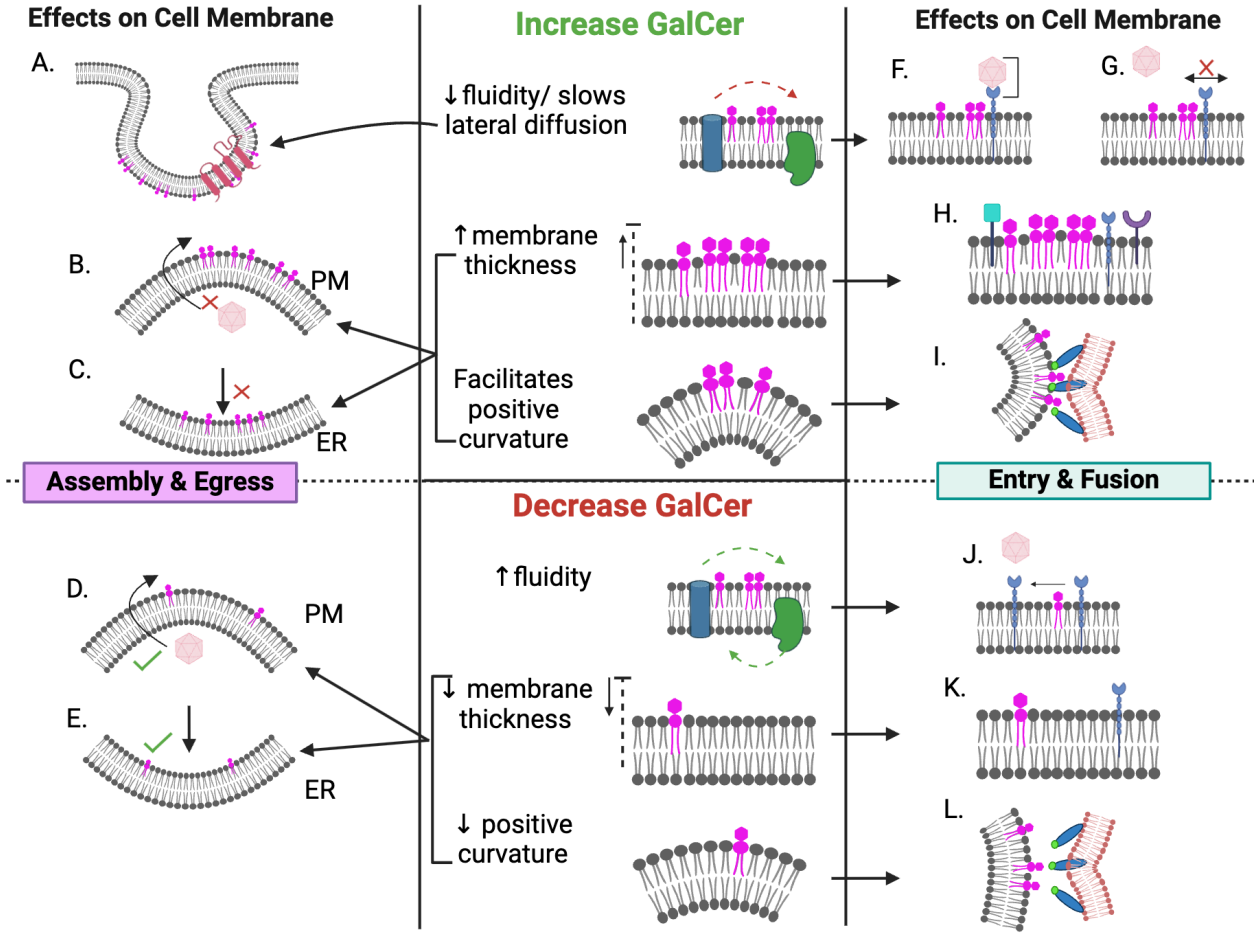

Figure 2.11. A-K. The possible effects of altering GalCer composition on host cell membranes during the DENV2 life cycle.

A-C. Effect of Increased GalCer on Cell Membrane during Assembly and Release. A. Increased GalCer could mean large or more numerous lipid rafts which may concentrate viral proteins in the ER membrane to aid in efficiency of replication complex to facilitate assembly. **B.** Positive curvature induced by increased numbers of GalCer molecules could hinder release, and **C.** may hinder replication complex formation during assembly.

D-E. Effect of Decreased GalCer on Cell Membrane during Assembly and Release. D. Decreased GalCer may cause a decrease in positive membrane curvature, which **D.** may facilitate release, or E. may facilitate formation of replication complexes during assembly.

F-I. Effect of Increased GalCer on Cell Membrane during Entry and Fusion. F. Decreased membrane fluidity may stabilize interaction of attachment molecule and virus. **G.** Decreased lateral diffusion resulting in less movement of the attachment may reduce the chance of the molecule encountering virus. **H.** Lipid rafts can aggregate attachment molecules which may facilitate virus attachment. **I.** Positive membrane curvature may facilitate fusion by bending toward the virus particle.

J-K. Effect of Decreased GalCer on Cell Membrane during Entry and Fusion. J. Increased attachment molecule movement may decrease chance of encountering virus. **K.** Less aggregation of attachment molecules may decrease attachment. **L.** Less positive curvature may make it more difficult to form fusion intermediates.

All figures were made with Biorender.

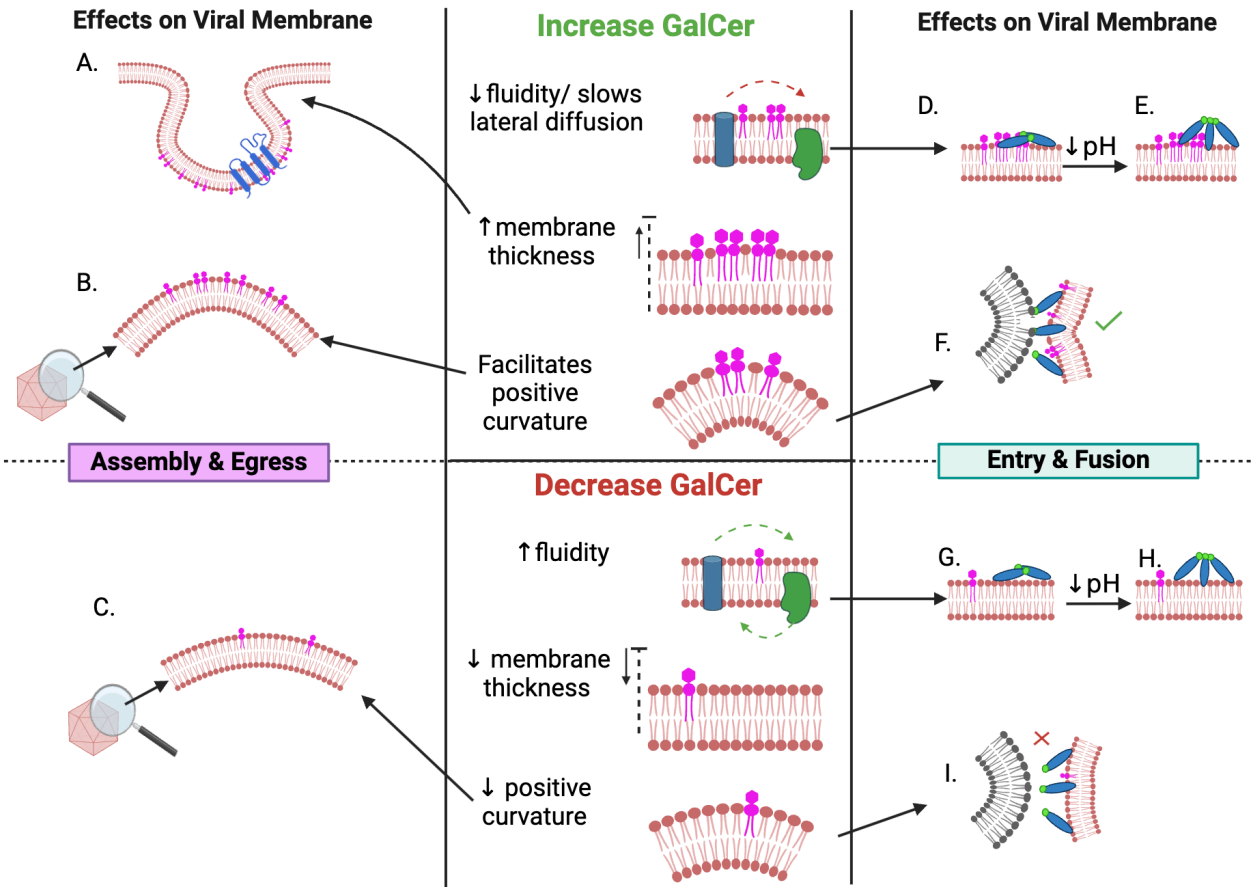

Figure 2.12. A-I. The possible effects of altering GalCer composition on viral membrane during the DENV2 life cycle.

A-B. Effect of Increased GalCer on Viral Membrane during Assembly and Release. A. Increased GalCer could mean large or more numerous lipid rafts which may concentrate viral proteins at a replication complex to facilitate assembly. **B.** Increased positive curvature induced by increased numbers of GalCer molecules could cause subtle alterations in the icosahedral shape of the virion.

C. Effect of Decreased GalCer on Viral Membrane during Assembly and Release. D. Decreased GalCer may cause a decrease in positive membrane curvature that could cause subtle alterations in the icosahedral shape of the virion.

D-F. Effect of Increased GalCer on Viral Membrane during Entry and Fusion. D-E. Decreased membrane fluidity may alter how the E proteins rearrange from flat homodimers on the virus surface to homotrimers extending away from the viral membrane during the reduction in pH that occurs in the endosome during fusion. **F.** Positive membrane curvature may facilitate fusion by bending toward the endosome membrane.

G-I. Effect of Decreased GalCer on Viral Membrane during Entry and Fusion. G-H. Increased membrane fluidity may alter how the E proteins rearrange from flat homodimers on the virus surface to homotrimers extending away from the viral membrane during the reduction in pH that occurs in the endosome during fusion. **I.** Less positive curvature may make it more difficult to form fusion intermediates.

All figures were made with Biorender.

In conclusion, our study provides novel insights on the role of UGT8 and its metabolite GalCer in DENV2 infection in vitro, particularly regarding their roles in virus entry and release. We showed that modulation of UGT8 expression significantly affected entry of DENV2 particles into Huh7 cells, likely related to changes in the viral membrane and/or changes in the host cell membranes. These data showcase the intricate relationships between host cell membrane lipid composition and events in the viral life cycle. Further studies to confirm how modulation GalCer expression in a membrane affects the structure and function of the membrane could provide valuable insight into how it impacts virus assembly, exit, entry and fusion. Expanding the study to include other flaviviruses and cell types would be informative. Specifically, since UGT8 was shown to interact with ZIKV NS4A in a high confidence protein-protein interaction study [180]. Expanding this work into other cell types and Zika virus was begun and is discussed in chapter 4 of this dissertation. While the magnitude of change in entry with modulation of UGT8 expression is relatively moderate, it may be more exacerbated if CRISPR-based UGT8 knockout approaches are used. Additional investigation of the UGT8 hub of the sphingolipid metabolic pathway may ultimately uncover additional targets for future design of therapeutics.

2.4 Materials and Methods

2.4.1 siRNA knockdown and infection:

Huh7 cells were seeded at 40,000 cells per well in a 24 well plate. siRNA transfection with 5μM siRNA was performed the following day with RNAi Max lipofectamine (ThermoFisher). All siRNA experiments included a non-targeting siRNA (irrelevant,

abbreviated IRR) negative control and DENV2-specific positive control (abbreviated DENV2). 48 hours following transfection, cells were infected with DENV2 at an MOI of 0.3. Twenty-four hours post-infection supernatants were harvested and virus in the supernatant tittered via plaque assay on baby hamster kidney (BHK) cells. The siRNAs are SMARTpools designed for the UGT8 transcript (Gene bank ID: 7368)

Horizon Discovery SMARTpool siRNA for UGT8 (catalog # M-010270-02) target sequences:

5' ACACUAAACUCAUAGAAUG 3' (binds nucleotides #67,350-67,368)

5' CGAGAGAGGCCACCAUACA 3' (binds nucleotides #24,653 - 24,671)

5' GAUGCUGUGUACUGACGUA 3' (binds nucleotides #25,235 - 25,253)

5' CAGUCCAAGAUGCGGAAUA 3' (binds nucleotides #24,774 - 24,792)

2.4.2 Plasmid overexpression and infection:

Plasmid purification:

Plasmids were transformed into One Shot Stbl3 Chemically Competent E. coli (ThermoFisher, catalog #C737303). They were grown on LB agar plates with carbemecillin (1µg/mL). Individual colonies were selected and grown for 8 hours at 37°C shaking at 250 RPM in LB media with carbemecillin (1µg/mL). These cultures were then added to 250 mL of in LB media with carbemecillin (1µg/mL) to generate large scale cultures and grown overnight at 37°C shaking at 250 RPM. Cells were then harvested by centrifugation at 5,000xg for 15 minutes at 4°C. Supernatant was discarded and the

EndoFree Plasmid Maxi Kit (Qiagen, catalog #12362) was used to extract and clean the plasmids.

Plasmid transfection: Huh7 cells were seeded at 110,000 cells per well in a 24 well plate. Transfection with 500 ng of plasmid per well was performed the following day utilizing the Lipofectamine 3000 kit (ThermoFisher, catalog# L3000008) as per kit instructions. Briefly, one tube was prepared with 25 µl of Gibco OptiMEM I Reduced Serum Medium (ThermoFisher, catalog #31985062) and 0.75 µl of Lipofectamine 3000. A second tube was prepared with 25 µl of Gibco OptiMEM I Reduced Serum Medium, 500 ng of plasmid DNA, and 1 µl P3000 reagent. The contents of the second tube were added to the first tube, mixed well, and incubated at room temperature for 10-15 minutes as per kit instructions. During this incubation period, the media on the cells was replaced with fresh media with 2% serum. 50 µl of this mixture was added to one well. The quantity of Lipofectamine used for transfection of A549 cells was increased to 1.5 µl as per manufacturer recommendations. Forty-eight hours following transfection, cells were infected with DENV2 at an MOI of 0.3. At 24 hours post-infection supernatants were harvested and plaque assays were performed on BHK cells.

Plasmids:

Human UGT8 cDNA ORF clone (SinoBiological, catalog# HG20264-UT)

Empty vector plasmid pCMV3-untagged vector (SinoBiological, catalog #CV011)

2.4.3 Alamar Blue Cell Viability assay:

Cell viability was assessed using a resazurin-based assay (Resazurin sodium salt, powder, BioReagent, suitable for cell culture (Sigma Aldrich Cat# R7017-5G)). A stock solution of Resazurin was made at by dissolving 1.382 g in 200 mL of H2O (50X stock). For the working solution, the 50X stock solution was diluted 1:50 (1X) and then one part of the working solution was added to 9ml of DMEM with 2% FBS. 200ml of this 1:10 diluted solution was added to each well. For siRNA experiments, 40,000 cells per well were plated in a 24 well plate and for plasmid overexpression experiments 110,000 cells per well were plated in a 24 well plate. Following siRNA or plasmid transfection and mock infection, at 24 hours post-infection media was removed from cells and replaced with the resazurin/DMEM solution and cells were incubated for 1-3 hours at 37°C and 5% CO2. Fluorescence output was measured using Biotek Synergy HTX Mµlti-Mode plate reader (Agilent) with excitation at 560nm and emission at 590 nm.

2.4.4 Confirmation of UGT8 mRNA knockdown or overexpression in Huh7 cells

Cells were seeded and transfected as described in the siRNA knockdown or plasmid overexpression methods, mock-infected with 1XPBS, and cells were collected in TRIzol (ThermoFisher) for RNA extraction. For mRNA expression, RNA was extracted, and qRT-PCR was performed to determine the percent of knockdown of the UGT8 mRNA relative to cells treated with the negative control siRNA or empty vector plasmid. A one-step qRT-PCR kit (SYBR III Kit, Agilent) was used and samples were run on a LightCycler 96 real-time PCR machine (Roche). In each well, we added 5 µl of Sybr 2x Master Mix, 3.4 µl of DEPC water, 0.5 µl of 20µM forward primer, 0.5 µl of 20µM reverse primer, 0.5 µl of

reverse transcriptase, and 0.1 µl Dithiothreitol (DTT), with 2.5 µl of RNA diluted in DEPC water to a concentration of 5 ng/µl. The total volume of the reaction was 12.5 µl. The cycling parameters were: 20 mins at 50˚C for reverse transcription, then 5 mins at 95˚C followed by 45 two-step cycles of 95˚C for 5 seconds and 60˚C for 60 seconds. Ct values from all samples were normalized to Ribosomal Protein Lateral Stalk Subunit P0 (RPLP0) using the delta delta ct method described in [181].

Primer sequences:

UGT8 forward primer (5' to 3'): ATTCAGCGCACAAACACAGG (binds nucleotides # 519-538)
UGT8 reverse primer (3' to 5'): CCTTCGCTATCCCAACAGCA (binds nucleotides # 24,554-24,573)

Rplp0 forward primer (5' to 3'): AGATGCAGCAGATCCGCAT
Rplp0 reverse primer (3' to 5'): GGATGGCCTTGCGCA

2.4.5 Quantification of UGT8 mRNA expression over a time course of DENV2 infection

Huh7 cells were seeded at 200,000 cells per well in a 6 well plate. The next day, cells were mock-infected or infected with DENV2 at an MOI of 3. At 24 hours post-infection, cells were collected in TRIzol. RNA extraction was completed and qRT-PCR was performed. The protocol and primers utilized in section 2.4.4 above was employed and Ct values from all samples were normalized to Ribosomal Protein Lateral Stalk Subunit P0 (RPLP0) using the delta delta ct method described in [181].

2.4.6 Quantification of intracellular and extracellular virus titer in Huh7 cells

Following either siRNA or plasmid transfection and DENV2 infection with an MOI of 0.3, as detailed in 2.4.1 and 2.4.2, supernatants and cells were collected at 24 hpi. Supernatants were titered via plaque assay to determine the quantity of infectious virus released. All cells in each well were collected and resuspended in equal volume of media as the supernatants that were collected (500ml). We did not count the cells in each well due to the number of samples involved. The cells were lysed using three freeze-thaw cycles, wherein cells were placed at -80 C for 10 minutes, then placed at room temperature until completely thawed, for a total of three cycles. Cells were centrifuged at 4,000 RPM (1,300 x g) for 5 minutes on a table top microfuge to pellet the cell debris, and soluble cytoplasmic extracts were transferred to a new tube. The infectious virus in the cytoplasmic extracts were quantified via plaque assay. The ratio of extracellular to intracellular titer was determined by expressing each titer value in plaque forming units/mL and then dividing the extracellular titer by the intracellular titer value.

2.4.7 Quantification of virus entry into Huh7 cells

100,000 Huh7 cells per well were seeded in a 24 well plate and infected with 10^7 genome copies per well of either virus made from cells transfected with the UGT8 siRNA or the negative control IRR siRNA. We first quantified the number of genome copies/mL in supernatants collected from a previous siRNA knockdown experiment. We then calculated the amount of volume needed to achieve 10^7 genome copies and added media to a final volume of 100 µl, scaling up by multiplying both values by the number of wells to be infected. The final number of genome copies to be used in the experiment was

optimized via preliminary experiments that used 10^5, 10^6, 10^7, and 10^8 genome copies to infect Huh7 cells, harvesting cells at 0- and 4 hpi, extracting RNA, and using qRT-PCR to quantify genome copies/mL. We found that 10^8 genome copies were too great, as it overwhelmed the cells and gave us similar numbers of genome copies at both 0- and 4 hpi. 10^7 genome copies gave us the most consistent data across the three replicates when compared to 10^5 and 10^6. We elected to move forward with 10^7. Media was removed from the cells, and virus inoculum was incubated onto the cells at 4°C on a rocker for 1 hour. Virus was then removed from all wells and cells were washed with ice cold 1XPBS. For the 0 hpi time point, virus was removed, cells were washed with ice cold 1XPBS. Cells were then treated with acid glycine for 1 minute to aid in inactivation of extracellular virus which was prepared as described in [182,183]. The cells were washed a second time with ice cold 1XPBS and then collected in TRIzol. For all cells except those belonging to the 0 hpi time point, DMEM with 2% FBS was added after the 1hr incubation at 4°C and cells were placed at 37°C. At 2-, 4-, 6-, 24-, and 48 hpi, media was harvested, cells were washed, treated with acid glycine, washed a second time, and then collected in TRIzol, similar to the 0 hpi time point. RNA was extracted from the cells and analyzed via quantitative RT-PCR to determine the number of genome copies/mL.

Quantitative RT-PCR was carried out using the QIAGEN Quantitect kit as described in Butrapet et al, 2006 [184]. Briefly, the cycle run on the LightCycler 96 real-time PCR machine (Roche) includes a 20-minute 50°C reverse transcription step, followed by a 5-minute 95°C hold, and then 50 cycles of a 15 second 95°C denaturation and 75 second 57°C annealing/extension step. Each well contained 6.75 µl of DEPC water, 2.5 µl QIAGEN Virus NR Master Mix 5x, 0.5 µl of the 20µM forward primer, 0.5 µl

of the 20μM reverse primer, 0.25 μl of the FAM probe, and μl QIAGEN Quantitect Virus RT Mix, 100x for a total volume of 10 μl. 2.5 ul of RNA standardized to 10 ng/μl was added to each well for a total RNA concentration of 25 ng per well. The primers listed below are specific to the 3' non-coding region of DENV2 and the probe is universal for all DENV serotypes. A standard curve including 10^2 to 10^7 genome copies/mL was plated in duplicate on each plate. Standards were generously donated by Claire Huang. They were generated by her lab by in vitro transcription of viral RNA from a plasmid containing the primer/probe-target DENV2 cDNA fragment. The concentration was quantified and serially diluted to generate a standard curve.

Primer and probe sequences [184]:

DENV genome forward primer (3' to 5', binds at nucleotide 10578 in the DENV2 16681 genome): AAG GAC TAG AGG TTA GAG GAG ACC C

DENV genome reverse primer (5' to 3', binds at nucleotide 10687 in the DENV2 16681 genome): GGC GTT CTG TGC CTG GAA TGA TG

DENV FAM-probe (binds at nucleotide 10616 in the DENV2 16681 genome): AAC AGC ATA TTG ACG CTG GGA AAG ACC

2.4.8 In vitro transmission of virus harvested from UGT8 knockdown cells

10,000 Huh7 cells were seeded in a 96 well plate. Each well was infected with a serial dilution of virus, ranging from 10^5 to 10^8 viral genome copies from supernatants made from cells transfected with UGT8 siRNA or the negative control IRR siRNA. At 24-, 48-, and 72 hpi, media was removed, cells were washed with 1XPBS and fixed with 4% paraformaldehyde diluted in 1XPBS for 20 minutes at room temperature on a rocker. Then cells were washed 3 times with 1XPBS for 5 minutes on the rocker and permeabilized for

20 minutes at room temperature with a 0.5% Triton X-100/1% bovine serum albumin (BSA, Gold Biotechnology) solution in 1XPBS. Cells were then blocked overnight on the rocker at 4°C in a 0.01% Triton X-100/1% BSA solution in 1x PBS. Cells were stained with Mouse Anti-Flavivirus E protein (D1-4G2-4-15 (4G2)) (Abcam cat.no: AB286196-200UG) diluted 1:1,000 in a 0.01% Triton X-100/1% bovine serum albumin solution in 1XPBS for one hour on the rocker at room temperature, Goat anti-mouse AlexaFluor 488 diluted 1:500 in a 0.01% Triton X-100/1% bovine serum albumin solution in 1XPBS for one hour on the rocker at room temperature, and DAPI diluted 1:2,000 in in a 0.01% Triton X-100/1% bovine serum albumin solution in 1XPBS for 20 seconds. Between stains cells were washed 3 times for 10 minutes in 1XPBS. Cells were imaged and photographed on the Echo microscope Revolve R4 model (Bico Company).

2.4.9 Specific Infectivity (Particle:PFU ratio) of virus harvested from UGT8 knockdown cells

Following either siRNA or plasmid transfection and DENV2 infection at MOI of 0.3 in Huh7 as detailed in 2.4.1 and 2.4.2, 250 µl of supernatant was collected for titration via plaque assay on BHK cells. In addition, 250 µl of supernatant was collected in TRIzol-LS (ThermoFisher) to extract viral RNA. qRT-PCR was performed using the QIAGEN kit detailed in 2.4.7 to quantify the number of viral genomes in the supernatant. The volume of RNA added was 2.5 µl, the concentration was not standardized. The ratio of the number of genomes to the number of plaque forming units per mL (specific infectivity) was then calculated.

2.4.10 Quantification of DENV2 genomes

RNA was extracted from cells either treated with siRNA against UGT8 or cells over-expressing UGT8 and collected in TRIzol to determine intracellular genome copies or from supernatant collected in TRIzol-LS (ThermoFisher) to determine supernatant genome copies. Quantitative RT-PCR using the QIAGEN Quantitect kit as described as described in Butrapet et al, 2006 and detailed in section 2.4.7 [184].

2.4.12. Flow cytometry to detect changes in GalCer expression during infection

200,000 Huh7 cells were seeded per well in 24 well plates. The following day, cells were infected with DENV2 (MOI of 1) or mock-infected. At 24-, 48-, and 72 hpi cells were trypsinized and harvested and 4 wells were pooled per sample to achieve a minimum of 10^6 cells per sample. Cells were transferred to a 96 well V-bottom plate and centrifuged at 500xg for 5 minutes at 4°C. The supernatant was discarded and cells were washed in 1XPBS, centrifuged at 500xg for 5 minutes at 4°C, and the supernatant discarded. All wells of the plate except those designated as the unstained control wells were stained with 100 µl of a 1:200 dilution of Zombie NIR cell viability stain (Sony Biotechnology, catalog # 2715525) in 1XPBS. Cells were incubated for 15 minutes in the dark at room temperature. The plate was then centrifuged at 500xg for 5 minutes at 4°C and the supernatant discarded. For all wells except those designated for unstained control and no antibody control, 100 µl of a 1:200 dilution of Anti-Galactocerebroside Antibody, clone mGalC, Alexa Fluor™488 Conjugate (Millipore Sigma, catalog #MAB342A4) to stain the surface of the cells. The cells were incubated in the dark for 30 minutes at 4°C. The plate was then centrifuged at 500xg for 5 minutes at 4°C and the supernatant discarded. Cells

were resuspended in 150 µl of FACS buffer (PBS with 2% fetal bovine serum and 0.05% sodium azide) and centrifuged at 500xg for 5 minutes at 4°C. The supernatant was discarded and cells were resuspended in permabilization buffer (ThermoFisher catalog # 88-8824-00). Flow cytometry was performed on the Cytek Aurora 4 laser flow cytometer and data was acquired using SpectoFlo software. Data was then unmixed and analyzed using the FlowJo application.

The first time this experiment was performed, Anti-Galactocerebroside Antibody, clone mGalC, Alexa Fluor™488 Conjugate (Millipore Sigma, catalog #MAB342A4) was used to stain cells. However, it became evident that the Huh7 cells exhibit intense autofluorescence at a similar wavelength, complicating analysis of the experiment. The second attempt at this experiment Anti-Galactocerebroside Antibody, clone mGalC, Alexa Fluor™647 Conjugate (Millipore Sigma, catalog # MAB342-AF647) was used, however, there were such significant cell losses during the staining process that the efficacy of the stain was difficult to evaluate.

2.4.12 Statistical analysis

The statistical analyses used are noted in the figure legends. When applicable results are expressed as mean values with standard deviation. Statistical significance was determined using one way ANOVA with Dunnett's multiple comparisons test or Student's unpaired T tests using the GraphPad Prism software (GraphPad software, La Jolla, California, USA).

Chapter 3: The role of Galactocerebrosidase in DENV2 Infection

3.1 Introduction

Galactocerebrosidase (also called galactoceramidase, GALC) is a lysosomal enzyme that recycles galactosylceramides and other galactolipids via hydrolysis. This breakdown process for galactosylceramide begins in the acidic conditions of the lysosome where GALC severs the glycosidic bond, separating the galactose from the ceramide (Fig 1A) [185]. The ceramides are further broken down into a sphingoid base and a fatty acid. From here, sphingoid bases can be made into many different new molecules: they can be phosphorylated to form sphingosine-1-phosphatase (S1P), they can be further degraded in the ER into phosphotidylethanolamine and ethanolamine, or they can be re-used in the salvage pathway and be made into new ceramides in the ER by ceramide synthases. The fatty acids can be trafficked to the mitochondria for beta-oxidation to produce energy, be incorporated into glycerolipids, or may be recycled and made into new ceramides through the salvage pathway.

GALC is expressed ubiquitously by cells at variable levels, but is most highly expressed in nervous tissues. As galactosylceramide is one of the principal components of myelin, GALC is responsible for normal turnover and recycling of galactosylceramides. This maintains myelin health and ensures smooth and efficient nerve conduction, allowing for coordinated movement as a result [167,186,187]. Galactosylceramides are also found in cell membranes, often as parts of glycosphingolipid-enriched microdomains (GEMs, also called lipid rafts). GEMs are involved in a variety of roles in the cell, including regulation of signal transduction, receptor activation, host-pathogen and cell-cell

interactions, membrane permeability, and intracellular lipid and protein trafficking [99,131,132,134].

When the GALC enzyme is dysfunctional, normal breakdown of GalCer is disrupted, resulting in devastating medical diseases. Krabbe disease (KD), also called Globoid Cell Leukodystrophy, is a heritable disorder that presents in young children caused by a loss of function mutation in the GALC gene that results in demyelination [186]. Symptomatic patients have <10% of normal GALC activity, and a different enzyme, acid ceramidase, breaks down GalCer, which results in formation of a toxic metabolite called psychosine (also called galactosphingosine) [186,188,189]. Acid ceramidase deacylates GalCer, removing the fatty acid to form psychosine. Psychosine will progressively accumulate in the lysosome over time, compounding the toxicity. The toxic effects can cause the lysosome membrane to lose its structural integrity, resulting in oxidative stress [190].

Oxidative stress can result in hydrolysis of sphingomyelins within membranes to produce ceramides [191,192]. For example, it can activate c-Jun N-terminal kinase (JNK) signaling, which stimulates phosphorylation and subsequent activation of neutral sphingomyelinase 1, leading to increases in ceramide levels [192]. Cellular stress can also upregulate ceramide formation via the de novo synthesis pathway, wherein activation of serine palmitoyltransferase and ceramide synthases generate new ceramides [193]. These ceramides can have many functions, but importantly, these signaling cascades can result in apoptosis to remove cells affected by toxic metabolites. This chain of events demonstrates the important role of GALC in regulating cellular homeostasis and highlights the far-reaching consequences of its dysfunction on cellular health and lipid metabolism.

While GALC has been extensively studied in neurodegenerative diseases, currently there are no publications regarding its role in viral infections. In this study, we aimed to understand the role of GALC in viral infection. Given what we had learned from the work presented in Chapter 2 about the opposing reaction of UGT8 which forms GalCer, we anticipated that GALC might have the opposite effect (to UGT8) on viral titer. Supporting this idea was the preliminary data from the siRNA knockdown screen performed by St. Clair et al (discussed in detail in Chapter 2) which showed a significant decrease in DENV2 titer following knockdown of GALC. The preliminary studies presented in this chapter establish that modulation of the expression of GALC affects the DENV2 virus life cycle and appears to affect virus assembly. While the specific role of GALC in DENV2 begs further exploration, these studies provide a foundation upon which we can build future studies.

3.2 Results

3.2.1 Modulation of GALC expression affects DENV2 titer

Based on the preliminary data that showed a decrease in DENV2 following siRNA knockdown of GALC, we hypothesized that GALC played a pro-viral role in DENV2 infection. To validate the results from St Clair et al, we performed an siRNA knockdown of GALC using pooled siRNAs (Dharmacon) to target the GALC gene in Huh7 cells. A non-targeting irrelevant siRNA (IRR) was employed as a negative control and an siRNA targeting the DENV2 genome was employed as a positive control. Forty-eight hours following transfection, cells were infected with DENV2 at an MOI of 0.3. Twenty-four hours post-infection (hpi) supernatants were collected and titrated using baby hamster kidney

(BHK) cells. Following siRNA knockdown, we observed that GALC mRNA expression was significantly reduced by 67% (Figure 3.1B). We observed that following GALC loss of function there was a 3.2-fold increase in DENV2 titer relative to the IRR control (Figure 3.1C). This data was opposite from the preliminary data obtained in the siRNA knockdown screen as described in St. Clair et al, however, the knockdown experiments were repeated for a minimum of three independent replicates and the increase in titer was observed each time. None of the siRNA treatments were cytotoxic (Figure 3.1D). These findings were conserved when we repeated this experimental procedure using ZIKV, however, the magnitude of change in titer was greater with a 5-fold increase compared to the negative control (Supplemental figure A.8).

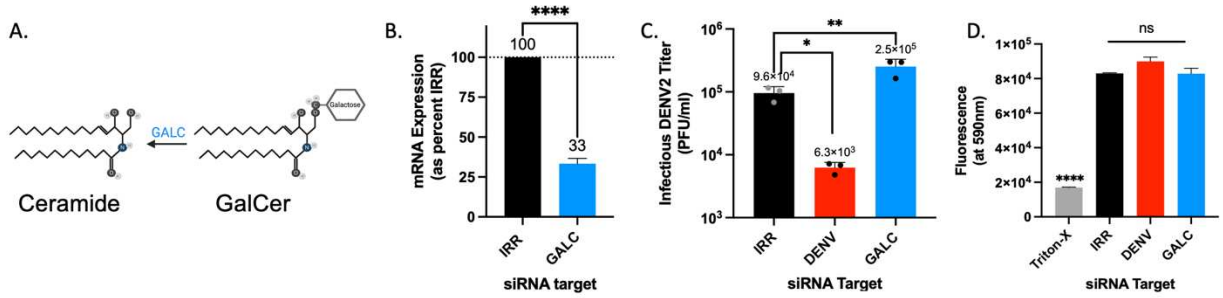

Figure 3.1. A. GALC recycles galactosylceramide by breaking it down into a fatty acid and a sphingosine molecule in the lysosome. **B.** Huh7 cells were transfected with siRNAs targeting GALC, a negative control siRNA (irrelevant siRNA, IRR), or a DENV2-specific positive control siRNA (DENV). At 48 hours post-transfection, cells were mock infected. At 24 hour post-mock infection, they were collected and RNA was extracted and analyzed for GALC mRNA expression. Results were normalized to the RPLP0 housekeeping gene. GALC knockdown resulted in a 67% decrease in GALC mRNA expression. **C.** Huh7 cells were transfected with siRNAs targeting GALC, a non-targeting irrelevant (IRR) negative control, and a DENV2-specific positive control siRNA. 48 hours following transfection, cells were infected DENV2 (MOI = 0.3) for 24 hr. At 24 hpi, viral supernatants were collected and analyzed via plaque assays. siRNA knockdown of GALC shows a 3.2-fold increase in DENV2 titer relative to the IRR control. **D.** Cell viability following siRNA transfection and mock infection was assessed using an Alamar Blue Cell Viability Assay. Fluorescence at 590 nm corresponds to the cells' metabolic activity. The positive control, Triton-X100, is toxic to the cells, and shows decreased fluorescence, indicating decreased metabolic activity. No siRNA treatment significantly affected cell viability. (B-D one-way ANOVA with Dunnett's multiple comparison's test: ns = $p \geq 0.05$ * = $p \leq 0.05$, ** = $p \leq 0.01$, **** = $p \leq 0.0001$; results are expressed as mean values with standard deviation indicated by error bars) [Abbreviations: IRR, irrelevant, non-targeting siRNA; DENV, DENV2-specific siRNA; GALC, galactocerebrosidase].

With these data, we wanted to understand if the effect on titer was sustained beyond peak replication at 24 hours. We repeated the knockdown and overexpression experiments and collected supernatants at 48 hours. The titer at 48 hpi following GALC knockdown was slightly increased, but not statistically significant (Figure 2A). The titer following GALC overexpression was not significantly different compared to the negative control (Figure 3.2B).

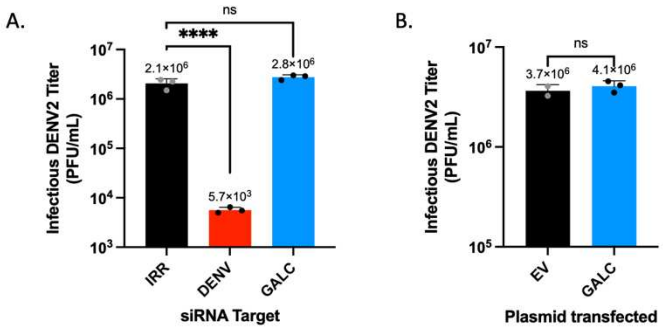

Figure 3.2A. Huh7 cells were transfected with siRNAs targeting GALC and a negative control siRNA (irrelevant siRNA, IRR), or a DENV2-specific positive control siRNA (DENV). At 48 hours post-transfection, cells were infected with DENV2 at an MOI of 0.3 At 48 hpi, supernatants were collected and titrated on BHK cells. There was no significant difference in titer in cells with GALC knockdown relative to the negative control. **B.** Huh7 cells were transfected with a plasmid containing the GALC gene or an empty vector control. At 48 hours post-transfection, cells were infected DENV2 (MOI = 0.3). At 48 hpi, viral supernatants were collected and titrated on BHK cells. There was no significant difference in titer in cells with GALC overexpression. (A-B one-way ANOVA with Dunnett's multiple comparison's test: ns = $p \geq 0.05$; **** = $p \leq 0.0001$; results are expressed as mean values with standard deviation indicated by error bars) [Abbreviations: IRR, irrelevant, non-targeting siRNA; DENV, DENV2-specific siRNA; EV, empty vector control plasmid; GALC, galactocerebrosidase].

Concurrently with the loss of function experiments we performed transient overexpression of GALC by transfecting in a plasmid containing the GALC gene. An empty vector plasmid (EV) was used as a negative control. Overexpression was confirmed using qRT-PCR which showed a significant increase in GALC mRNA expression which was 399% of the GALC expression in the negative control (Figure 3.3A). With transient overexpression, we observed a 2-fold decrease in viral titer at 24 hpi (Figure 3.3B). There were no significant cytotoxic effects of the plasmids (Figure 3.3C).

The 24 hpi knockdown results were incongruous with the preliminary data, however, the opposing phenotypes we observed between our knockdown and overexpression data is compelling and supports the validity of the results. The temporally limited nature of the changes in titer also suggests that the effects of modulation GALC expression may be stronger earlier in infection, as represented by the 24 hpi time point, or may be overwhelmed as the infection progresses. From here, we wanted to understand the specific steps of the virus life cycle altered to produce the phenotypes above.

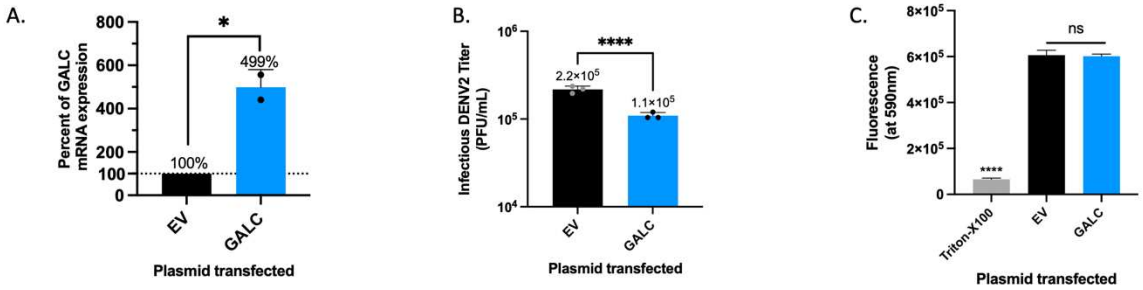

Figure 3.3. A. Huh7 cells were transfected with a plasmid containing the GALC gene or an empty vector control. At 48 hours post-transfection, cells were mock infected. At 24 hour post-mock infection, cells were washed and collected in TRIzol, and RNA was extracted. qRT-PCR was performed to assess GALC mRNA expression. Results were normalized to the RPLP0 housekeeping gene. Overexpression resulted in a 399% increase in GALC mRNA expression **B.** To assess changes in viral titer, 48 hours following transfection, cells were infected DENV2 (MOI = 0.3) for 24 hr. At 24 hpi, viral supernatants were collected and analyzed via plaque assays. Overexpression of UGT8 results in a 2-fold decrease in viral titer. **D.** Cell viability following plasmid transfection and mock infection was assessed using an Alamar Blue Cell Viability Assay. Fluorescence at 590 nm corresponds to the cells' metabolic activity. The positive control, Triton-X100, is toxic to the cells, and shows decreased fluorescence, indicating decreased metabolic activity. No plasmid treatment significantly affected cell viability. (A-D one-way ANOVA with Dunnett's multiple comparison's test: ns = $p \geq 0.05$ * = $p \leq 0.05$, **** = $p \leq 0.0001$; results are expressed as mean values with standard deviation indicated by error bars) [Abbreviations: EV, empty vector control plasmid; GALC, galactocerebrosidase plasmid].

3.2.2 Reducing GALC expression increases extracellular and intracellular DENV2 titer

To delve deeper into why DENV2 titer was altered following modulation of GALC expression, we examined intra- and extracellular titers to determine if there were changes in virus assembly and release. We repeated the loss of function studies using the GALC siRNA following by infection with DENV2 at MOI 0.3 as detailed in section 3.2.1. At 24 hpi, supernatants and cells were collected. The cells were washed and subjected to

repeated freeze-thaw cycles to lyse the cells. Cell extracts were centrifuged to remove any cellular debris and plaque assays were performed with the intracellular cell extracts and extracellular supernatants. The extracellular titer for cells treated with GALC siRNA was significantly increased compared to the negative control siRNA (Figure 3.4A). The intracellular titer was also observed to be significantly increased compared to the control (Figure 3.4B). These data suggest that increased extracellular virus may be due to an increase in the production of virus inside the cell. Increased intracellular titer could be due to increased genome replication and/or increased virus assembly, or an increased efficiency in maturation making them more infectious than the particles produced in control cells. In addition, the ratio of extracellular to intracellular infectious viral titer was increased to 1.4 : 1.0 for the GALC knockdown samples in comparison to 0.9:1 for the negative control, suggesting release and/or entry may additionally be implicated (Figure 3.4C). To parse out what may be the driving force(s) behind these titer increases, we pursued experiments that would inform us about changes in genome replication and specific infectivity following modulation of GALC expression.

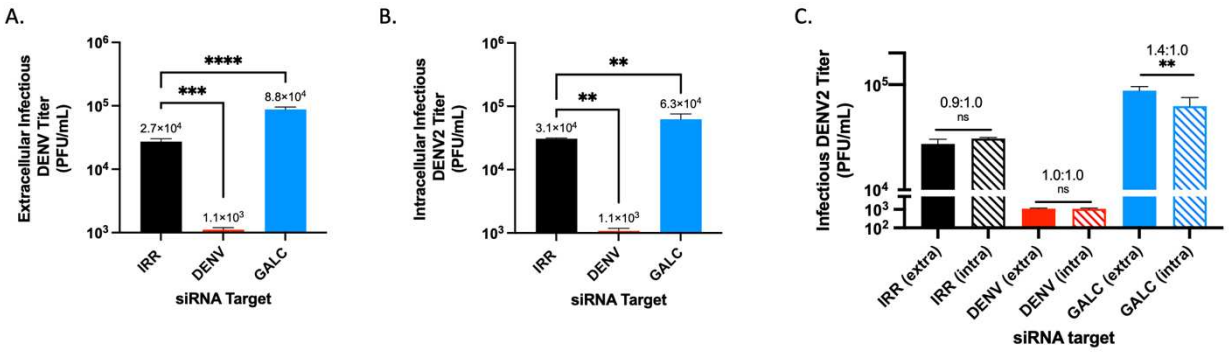

Figure 3.4 A. Extracellular and intracellular viral titers following siRNA knockdown detailed in figure 1 were measured using plaque assays. Intracellular virus was harvested from cells using repeated freeze-thaw cycles and centrifugation to remove the cellular debris from the supernatant. The extracellular titer following siRNA knockdown of GALC shows a 3.2-fold increase in DENV2 titer relative to the IRR control. **B**. The intracellular titer following GALC knockdown shows a 2-fold increase in the DENV2 titer relative to the IRR control. **C**. The ratio of extracellular to intracellular titer of the negative and positive control was 0.9:1 and 1:1, respectively. For the controls, there was no significant difference between intra- and extracellular titers when compared to each other. The extracellular to intracellular ratio of cells with GALC knockdown was 1.4:1, which was increased relative to the negative control. Dunnett's multiple comparison's test: ns = $p \geq 0.05$, *** = $p \leq 0.001$, **** = $p \leq 0.0001$ (A-C one-way ANOVA with Dunnett's multiple comparison's test: ns = $p \geq 0.05$, ** = $p \leq 0.01$, ***= $p \leq 0.001$, **** = $p \leq 0.0001$; results are expressed as mean values with standard deviation indicated by error bars) [Abbreviations: IRR, irrelevant, non-targeting siRNA; DENV, DENV2-specific siRNA; GALC, galactocerebrosidase].

3.2.3 Modulation GALC expression does not affect DENV2 genome replication

To determine if modulation of GALC expression affects DENV2 genome replication, we measured the number of genome copies using quantitative RT-PCR in total cellular RNA obtained from the siRNA knockdown or plasmid overexpression experiments detailed in section 3.2.1. There was no significant change in the number of viral genome copies in cells transfected with GALC siRNA when compared to the negative control (Figure 3.5A), nor in cells transfected with the GALC over-expression plasmid compared to the empty vector control (Figure 3.5B). These data suggest that genome replication is not the cause of the increase in intracellular and extracellular titer.

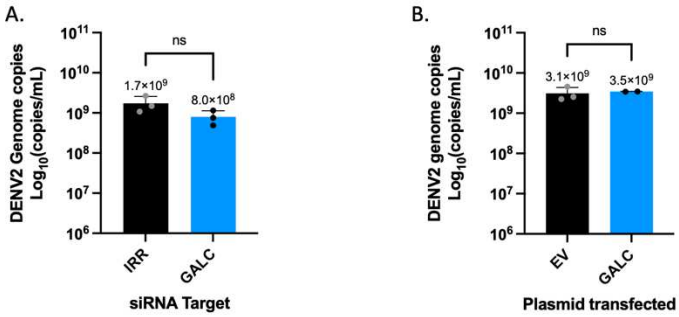

Figure 3.5 A. Huh7 cells were transfected with siRNAs targeting GALC or a non-targeting irrelevant (IRR) negative control. 48 hours following transfection, cells were infected DENV2 (MOI = 0.3) for 24 hr. At 24 hpi, cells were collected and RNA was extracted. qRT-PCR was performed to quantify copies of DENV2 genomes. There was no significant difference in genome copy number in cells with UGT8 knockdown when compared to the negative control (IRR). **B**. Huh7 cells were transfected with a plasmid containing the GALC gene or an empty vector control. At 48 hours post-transfection, cells were infected DENV2 (MOI = 0.3) for 24 hr. At 24 hpi, cells were collected and RNA was extracted. qRT-PCR was performed to quantify copies of DENV2 genomes. There was no significant difference in genome copy number in cells with GALC overexpression when compared to the negative control (EV). A-B One-way ANOVA with Dunnett's multiple comparison's test. Results are expressed as mean values with standard deviation indicated by error bars : ns = $p \geq 0.05$. [Abbreviations: IRR, irrelevant, non-targeting siRNA; DENV, DENV2-specific siRNA; EV, empty vector control plasmid; GALC, galactocerebrosidase].

3.2.4 Modulation GALC expression does not affect DENV2 specific infectivity

We then aimed to learn if the specific infectivity of the virus particles being produced was increased following modulation of GALC expression. After transfection of either siRNA or plasmids (as described in 3.2.1) and infection with DENV2, viral RNA in the supernatants was extracted and the concentration of genome copies/ml was determined using qRT-PCR. We also titrated the supernatants on BHKs as detailed in section 3.2.1. We observed that there was no significant difference in the specific infectivity of virus released from cells with either GALC knockdown or overexpression (Figure 3.6). These data suggest that the changes in titer were not related to changes in infectivity.

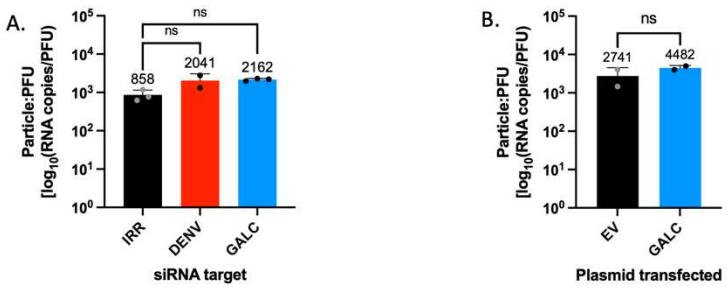

Figure 3.6A. Huh7 cells were transfected with siRNAs targeting GALC, a non-targeting irrelevant (IRR) negative control, and a DENV2-specific positive control siRNA. 48 hours following transfection, cells were infected DENV2 (MOI = 0.3) for 24 hr. At 24 hpi, supernatants and cells were collected. Titer was determined using plaque assays and qRT-PCR was performed to quantify copies of DENV2 genomes in the supernatant. These values were compared to generate the ratio of total particles:infectious particles. There was an increase in the particle:PFU ratio in cells with UGT8 knockdown relative to the negative control (IRR), but it was not statistically significant. **B.** Huh7 cells were transfected with a plasmid containing the GALC gene or an empty vector control. At 48 hours post-transfection, cells were infected DENV2 (MOI = 0.3) for 24 hr. At 24 hpi, cells were collected and RNA was extracted. qRT-PCR was performed to quantify copies of DENV2 genomes. There was no significant difference in genome copy number in cells with GALC overexpression when compared to the negative control (A-B one-way ANOVA with Dunnett's multiple comparison's test: ns = $p \geq 0.05$. Results are expressed as mean values with standard deviation indicated by error bars). [Abbreviations: IRR, irrelevant, non-targeting siRNA; DENV, DENV2-specific siRNA; EV, empty vector control plasmid; GALC, galactocerebrosidase].

3.3 Discussion

The role of GALC in viral infection has not been thoroughly investigated and our studies aimed to provide an introductory understanding of its role in DENV2 infection. Our findings revealed a significant increase in DENV2 titer following GALC knockdown in Huh7 cells, which was in contrast to the previous data from St Clair et al. This intriguing results challenged the notion that GALC and UGT8 play contrasting roles in DENV2 infection, highlighting the complexity of the sphingolipid metabolic pathway [194,195]. GALC resides in the lysosome, a distinct cellular compartment from the ER where galactose is added to ceramide by UGT8. The observed increase in titer (section 3.2.2) was not related to changes in genome replication or virus particle infectivity, suggesting there may be alterations in virus assembly.

Reduced GALC activity can result in the conversion of galactosylceramides into psychosine, a toxic metabolite. Psychosine accumulation in the lysosome can result in

ceramide upregulation. In oligodendrocytes, this process has been reported to occur within a few days of GALC knockdown in vitro [196]. In that study, approximately 25% of their oligodendrocyte cells did not survive GALC knockdown. In our study, it is important to note that we did not see any difference in cytotoxicity in our cells with GALC knockdown (Fig 1D), so it is possible that Huh7 cells may be more resistant to the toxic effects. That study utilized a lentivirus-mediated knockdown system and observed a qualitative decrease in GALC expression using Western blot analysis, though they did not quantify the level of knockdown. It is possible that they achieved a greater level of GALC knockdown, contributing to more severe toxic effects than what we observed. While the timeframe to accumulation of psychosine has not been confirmed in Huh7 cells, a similar timeline is possible, and this should be validated in future studies.

A study from Leier et al showed that ceramides were significantly enriched and recruited to viral replication complexes in Zika virus infected Huh7 cells [95]. Although our study focused on DENV2, it is possible that these findings are similar if not conserved in related flaviviruses. This finding has not been reported in DENV2 infected human cells in vitro, however, ceramide upregulation has been demonstrated in DENV2-infected mosquito cells and in mosquito midguts following an infectious DENV2 blood meal using liquid chromatography-tandem mass spectrometry (LC-MS/MS), and in clinical samples from humans infected with DENVs using reversed-phase high performance liquid chromatography [197–199]. These findings suggest that ceramide upregulation may happen in DENV2-infected Huh7 cells in vitro, but confirmation is needed in future studies.

Ceramide upregulation following GALC knockdown may be beneficial for virus assembly by supporting the formation of replication complexes in the ER or by increasing the efficiency of virus assembly. For instance, ceramides are lipids that promote negative membrane curvature which could facilitate the formation of the replication complexes in the ER membrane where assembly occurs [200]. This concept is further supported by the observation that NS4B, a nonstructural protein involved in replication complex formation, has been shown to be associated with ceramides in the ER membrane by superresolution microscopy [95]. In addition, ceramides are an important component of lipid rafts. In the ER membrane, lipid rafts may help to concentrate high numbers of structural proteins E and prM to increase the efficiency of virus assembly [201]. Changes in assembly could explain the increase in intracellular and extracellular DENV2 titers observed in 3.2.2. To validate this hypothesis, ceramide levels in GALC knockdown cells should be evaluated using an LC-MS/MS approach.

The question of why the ratio of extracellular to intracellular viral titer is increased in GALC knockdown cells remains unexplained. Increases in virus assembly alone may not be the only driver of this change. Increasing ceramide levels may provide the cell more substrates for synthesis of complex sphingolipids, including glycolipids like galactosylceramide, which could potentially alter the plasma membrane composition. Changes in the plasma membrane composition could in turn affect virus entry and egress. Additional studies, similar to those conducted for UGT8 in Chapter 2, are necessary to determine if GALC impacts virus assembly, release or entry and these are important future directions for this work.

3.4 Materials and Methods

Please see the following methods in Chapter 2, section 2.4:

- siRNA knockdown and infection
  Horizon Discovery SMARTpool siRNA for GALC (catalog #M-011038-01) target sequences:
    5' CUGGCAACGCCGAGCGAAA 3'
    5' GAGAAUUAUUUCCGAGGAU 3'
    5' GAAAGGAGGAAGCUACGUA 3'
    5' GAUUAUCUCUUUAAGCCGA 3'

- Plasmid overexpression and infection
  Plasmids:
    Human, GALC cDNA ORF Clone, untagged (SinoBiological, catalog #HG13681-UT)
    Empty vector plasmid pCMV3-untagged vector (SinoBiological, catalog #CV011)

- Alamar Blue Cell Viability assay
- Confirmation of UGT8 mRNA knockdown or overexpression in Huh7 cells
- Quantification of intracellular and extracellular virus titer in Huh7 cells
- Specific Infectivity (Particle:PFU ratio)
- Quantification of DENV2 genomes
- Statistical analysis

Chapter 4: The role of UGT8 in ZIKV Infection

4.1 Introduction

In Chapter 2, UDP-galactosyl transferase 8 (UGT8) was shown to affect the ability of DENV2 to enter liver cells in vitro. In this chapter, we aimed to explore if this phenotype was conserved in other flaviviruses (FVs). While neurological manifestations of DENVs are reported in about 5% of cases, a related FV, Zika virus (ZIKV), is primarily neurotropic [202]. The rationale for selecting Zika virus in our study was two-fold: first, ZIKV is a related FV that primarily affects the nervous system where UGT8 expression is most abundant, and second, UGT8 was shown to interact with ZIKV NS4A protein in a high confidence protein-protein interaction study, suggesting UGT8 could play a role in ZIKV infection [180].

We first wanted to compare ZIKV infection of Huh7 cells to our study performed with DENV2 in Huh7 cells. We hypothesized that the role of UGT8 could be conserved in ZIKV infection of Huh7 cells. We also were curious if we could see a more pronounced phenotype in a cell line with higher UGT8 expression. Neuroblastoma cells offered the perfect balance: they have been shown to be highly permissive for ZIKV, proving to be an excellent in vitro model for studying ZIKV, while still displaying moderate UGT8 expression [203,204]. In this chapter, we present our preliminary studies to identify the role of UGT8 in ZIKV infection of both liver and neuroblastoma cell lines.

4.2 Results

4.2.1 ZIKV infection altered UGT8 expression late in infection (72 hpi)

To investigate the role of UGT8 in ZIKV infection of Huh7 cells we first looked at how expression may be changed over time. We infected Huh7 cells with ZIKV strain PRVABC59 (MOI of 1) and collected cells at time points 0-, 6-, 12- 24-, 48, and 72-hours

post-infection. We extracted RNA and qRT-PCR was performed to quantify UGT8 mRNA expression at each time point. Expression was normalized to a cellular housekeeping gene, RPLP0 [171]. During ZIKV infection, UGT8 expression is not significantly altered until 72 hpi, where it is decreased by 30% as compared to mock-infected cells. This indicated that UGT8 expression is not significantly affected by ZIKV infection of Huh7 cells until the cells begin to recover at 72 hpi (Figure 4.1). This differed from the phenotype we observed in DENV2 infection of Huh7 cells where UGT8 expression was significantly decreased from 24 hpi and onwards.

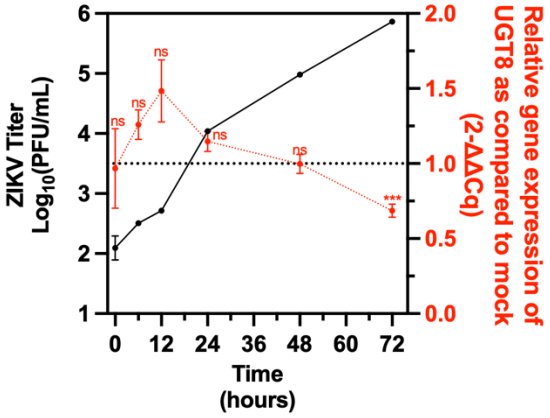

Figure 4.1. ZIKV infection altered UGT8 expression late in infection (72 hpi)
Huh7 cells were either mock-infected or ZIKV-infected (MOI = 1) and cells were collected in triplicate at 0, 6, 12-, 24-, 48-, and 72-hours post-infection. RNA was extracted and assessed using qRT-PCR. ZIKV-infected samples were compared to mock infected samples at matched timepoints. Results are reported as an expression ratio between each timepoint sample and its respective mock-infected timepoint (in red). Statistical comparison performed between the mock and infected values for each time point. Corresponding titers at each time point in the ZIKV-infected samples are shown in black. UGT8 expression is significantly decreased at 72 hpi. There is no significant change to UGT8 expression from 0 to 48 hpi. (Student's unpaired T test: ns = $p \geq 0.05$, *** $p \leq 0.001$).

4.2.2 ZIKV infection alters GalCer expression on the surface of Huh7 cells

Similar to what was described in Chapter 2 section 2.2.3, we investigated the expression of the product of UGT8, GalCer, during infection of Huh7 cells with ZIKV. We infected Huh7 with ZIKV (MOI = 3) and performed a concurrent mock infection and harvested cells at 48- and 72 hpi. Cells were washed and stained with a cell viability dye and an anti-GalCer antibody conjugated to AlexFluor488. Flow cytometry was performed to determine the

expression of GalCer during infection. Fluorescence intensity was normalized to cells stained only with viability stain and not the GalCer antibody and the fluorescence intensity of the DENV2-infected cells was compared to the mock-infected cells. We did not observe a significant change in GalCer expression at 48 hpi (Figure 4.2A- F). However, at 72 hpi, we observed a 23% reduction in GalCer expression (Figure 4.2G-L). These results correlated with the decrease in UGT8 mRNA expression that we observed at 72 hpi.

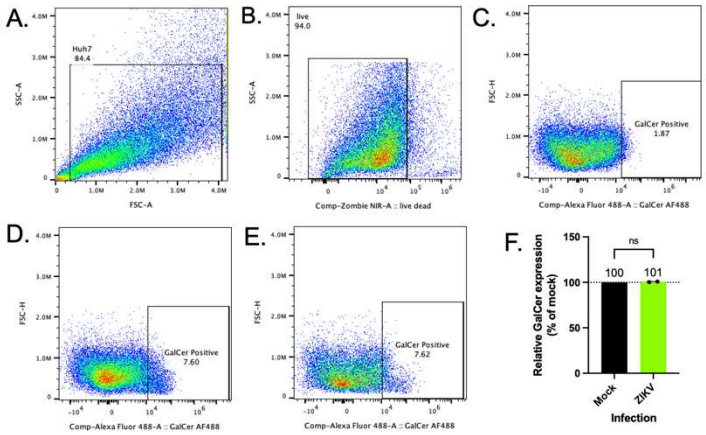

Figure 4.2. Flow cytometric analysis of GalCer expression in ZIKV-infected Huh7 cells at 48 hpi.
A. Forward scatter area (FSC-A) versus side scatter area (SSC-A) plot showing gating strategy to exclude debris and select intact cells. **B.** Viability gating using Zombie NIR stain to discriminate live cells (Zombie NIR-negative). **C.** Representative plot of unstained control cells used to set GalCer-negative gate. **D-E.** GalCer expression in mock-infected (**D**) and ZIKV-infected (**E**) cells. Numbers in plots indicate percentage of cells within each gate. **F.** Quantification of relative GalCer expression in ZIKV-infected cells as compared to mock showed no significant difference. Data are presented as mean ± SEM. Student's unpaired T test. ns = $p \geq 0.05$.

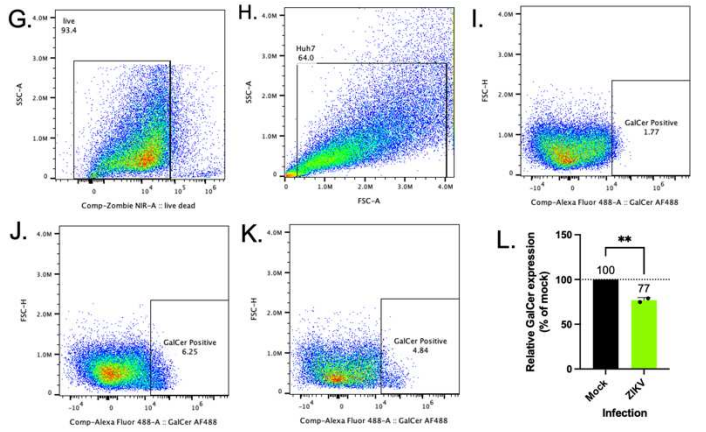

Figure 4.2G-L. Flow cytometric analysis of GalCer expression in ZIKV-infected Huh7 cells at 72 hpi.
G. Forward scatter area (FSC-A) versus side scatter area (SSC-A) plot showing gating strategy to exclude debris and select intact cells. **H.** Viability gating using Zombie NIR stain to discriminate live cells (Zombie NIR-negative). **I.** Representative plot of unstained control cells used to set GalCer-negative gate. **J-K.** GalCer expression in mock-infected **J.** and DENV2-infected **K.** cells. Numbers in plots indicate percentage of cells within each gate. **L.** Quantification of relative GalCer expression in DENV2-infected cells as compared to mock. Data are presented as mean ± SEM. Student's unpaired T test. ** $p \leq 0.005$.

4.2.3 Modulating UGT8 expression affected ZIKV titer in Huh7 cells

To understand the role of UGT8 in ZIKV infection we performed loss of function studies similar to those performed with DENV2 in Chapter 2. Briefly, we used an siRNA pool against UGT8, a negative control siRNA (IRR) with no homology to human genes, and a siRNA targeting the ZIKV genome as a positive control [169,170]. Forty-eight hours following siRNA transfection cells were infected with ZIKV PRVABC59 (MOI of 0.3) and at 24 hpi supernatants were collected and titered on Vero CCL-81 cells. We observed a 5-fold increase in ZIKV titer following UGT8 knockdown (Figure 4.3A).

Concurrently with loss of function experiments we performed transient overexpression of UGT8 via transfection of a plasmid containing the UGT8 gene. An empty vector plasmid (EV) was used as a negative control. With overexpression we observed a minor but significant 0.79-fold decrease in ZIKV titer (Figure 4.3B) Confirmation of UGT8 mRNA knockdown and overexpression was performed previously and the data was presented in Chapter 2 section 2.2.1. Confirmation of protein knockdown was attempted but was unsuccessful and is discussed in the Appendix. These two experiments show a similar trend to what we showed with DENV2 infection of Huh7 cells.

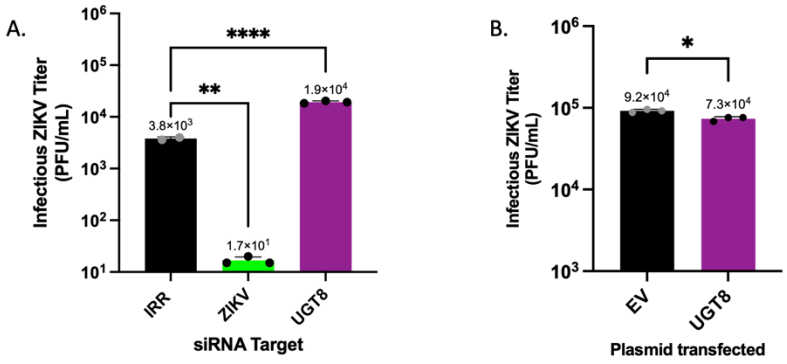

Figure 4.3. Modulating UGT8 expression affected ZIKV titer in Huh7 cells **A.** Huh7 cells were transfected with siRNAs targeting UGT8, a non-targeting irrelevant (IRR) negative control, and a ZIKV-specific positive control siRNA. 48 hours following transfection, cells were infected ZIKV (MOI = 0.3) for 24 hr. At 24 hpi, supernatants and cells were collected. Titer was determined using plaque assays on Vero cells. UGT8 knockdown results in a significant increase in ZIKV titer. **B.** Huh7 cells were transfected with a plasmid containing the UGT8 gene and an empty vector control**.** 48 hours following transfection, cells were infected ZIKV (MOI = 0.3) for 24 hr. At 24 hpi, supernatants and cells were collected. Titer was determined using plaque assays on Vero cells. UGT8 overexpression results in a small but significant decrease in ZIKV titer. (A-B one-way ANOVA with Dunnett's multiple comparison's test: * = p≤0.05, ** = p≤0.01, **** = p≤0.0001; results are expressed as mean values with standard deviation indicated by error bars).

4.2.4 Modulating UGT8 expression affected ZIKV titer in neuroblastoma (SH-SY5Y) cells

To understand how UGT8 might affect infection in a cell line of the central nervous system, we repeated the loss of function experiment detailed in 4.2.2 with human neuroblastoma cells (SH-SY5Y cells). We first determined the transfection efficiency by transfecting the IRR negative control siRNA and the pool of UGT8 siRNAs. Forty-eight hours after transfection, cells were mock-infected or ZIKV-infected. At 24 hpi, infected supernatants were collected and titrated on Vero CCL-81 cells, and mock-infected cells were harvested for mRNA knockdown confirmation. RNA was extracted from mock-infected SH-SY5Y cells and qRT-PCR was performed and results were normalized to the RPLP0 housekeeping gene. We observed a 15% decrease in UGT8 expression following siRNA transfection (Figure 4.4A). We observed that despite this small reduction in UGT8 mRNA expression, the ZIKV titer was significantly increased 1.7-fold from the negative control (Figure 4.4B). siRNA treatments

were not cytotoxic (Figure 4.4C). This suggested that UGT8 may play a similar role in neuroblastoma cells as in liver cells.

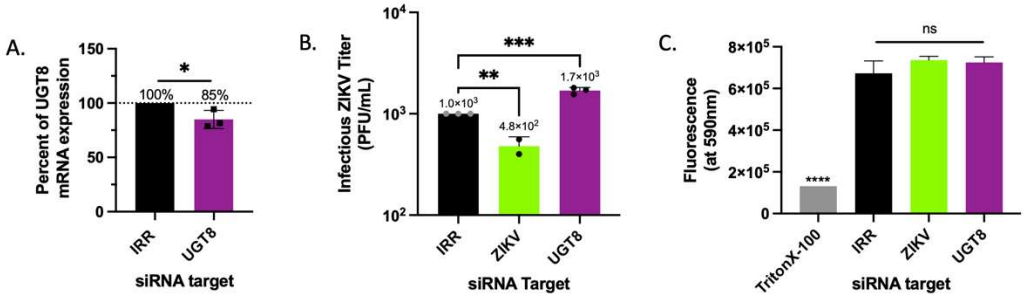

Figure 4.4. Modulating UGT8 expression affected ZIKV titer in neuroblastoma (SH-SY5Y) cells. A. SH-SY5Y cells were transfected with siRNAs targeting UGT8, a negative control irrelevant siRNA (IRR), or a positive control siRNA specific to the Zika virus used for infection (ZIKV). Cells were mock infected and collected 24 hours post-transfection to confirm mRNA knockdown. qRT-PCR was performed and results were normalized to the RPLP0 housekeeping gene. There was a 15% decrease in UGT8 expression following siRNA knockdown. **B.** 48 hours following transfection, cells were infected with ZIKV (MOI = 0.3) for 24 hr. At 24 hpi, viral supernatants were collected and analyzed via plaque assays. Viral titer was significantly increased 1.7-fold increase following UGT8 knockdown. **C.** Cell viability following siRNA transfection and mock infection was assessed using an Alamar Blue Cell Viability Assay. Fluorescence at 590 nm corresponds to the cells' metabolic activity. The positive control, Triton-X100, is toxic to the cells, and shows decreased fluorescence, indicating decreased metabolic activity. No siRNA treatment significantly affected cell viability. (A-C one-way ANOVA with Dunnett's multiple comparison's test: ns = $p \geq 0.05$ * = $p \leq 0.05$, ** = $p \leq 0.01$, *** = $p \leq 0.001$; results are expressed as mean values with standard deviation indicated by error bars) [Abbreviations: IRR, irrelevant, non-targeting siRNA; ZIKV, ZIKV-specific siRNA; UGT8, UDP-galactosyltransferase 8].

4.3 Discussion

Our studies reveal that modulation of UGT8 expression in both liver and neuroblastoma cells has a significant effect on the extracellular ZIKV titer, mirroring our observations for DENV2 in Chapter 2. To elucidate the mechanisms behind these changes in titer, we plan to conduct similar studies to those performed in Chapter 2 with DENV2. Given that entry, fusion, and release were potentially altered during modulation of UGT8 expression during DENV2 infection, those studies are key future directions for this work to determine if the mechanisms are similar in ZIKV.

The UGT8 knockdown in neuroblastoma cells produced a phenotype similar to what we observed in Huh7 cells. However, the relatively low level of mRNA knockdown raises the question of how a more efficient knockdown might alter viral titer. To address this,

studies are currently underway using a CRISPR-Cas9 knockout system followed by infection to improve upon these results.

Interestingly, the mRNA expression of UGT8 during ZIKV infection of Huh7 cells differed from that seen in DENV2 infection. In ZIKV we observed no significant change until 72 hpi, whereas infection with DENV2 led to a progressive decrease from 24 to 72 hpi. This suggests that ZIKV infection may not directly affect UGT8 mRNA expression. The reduction at 72 hpi could be related to the recovery efforts of the cell or cellular exhaustion. Because host cell membranes undergo significant alterations and rearrangements during infection, ceramides might be preferentially shuttled into other metabolic pathways that support membrane rebuilding and stabilization. It is possible that GalCer is less critical for these processes compared to other sphingolipids, so the cell is not producing as much UGT8 mRNA due to decreased need. Future studies include evaluating UGT8 mRNA expression during infection of neuroblastoma cells to understand if these results are conserved.

4.4 Materials and Methods

4.4.1 Quantification of UGT8 mRNA expression over a time course of ZIKV infection

These methods are described in Chapter 2 section 2.4.5. The only modification was that infection was performed with ZIKV PRVABC59 instead of DENV2.

4.4.2 Flow cytometry to detect changes in GalCer expression during infection

These methods are described in Chapter 2 section 2.4.12. The only modification was that infection was performed with ZIKV PRVABC59 instead of DENV2.

4.4.3 siRNA knockdown and infection

These methods are described in Chapter 2 section 2.4.1. For these experiments performed in Huh7 cells, the only modification was that infection was performed with ZIKV PRVABC59 instead of DENV2. The same protocol was then employed for SH-SY5Y cells with ZIKV.

4.4.4 Plasmid overexpression and infection

These methods are described in Chapter 2 section 2.4.2. The only modification was that infection was performed with ZIKV PRVABC59 instead of DENV2.

4.4.5 Confirmation of UGT8 mRNA knockdown or overexpression in SH-SY5Y cells

These methods are described in Chapter 2 section 2.4.4. The only modification was that SH-SY5Y cells were used in the place of Huh7.

Chapter 5: Conclusions and Future Directions

Flaviviruses (FVs) remain one of the most significant global viral health threats without a widely available vaccine or anti-viral medications. FVs are highly dependent on host cell lipids and membranes. Lipids play important roles in FV pathogenesis that we are only just beginning to understand. Sphingolipids, a specialized lipid class that plays a myriad of roles in both signaling and membrane structure, are starting to be recognized as powerful regulators of homeostasis and keepers of the cell barriers.

In this dissertation, we explored how galactosylceramides, synthesized by UGT8 in the ER and degraded by GALC in the lysosome, affect the DENV2 and ZIKV virus life cycles in vitro. We primarily used a human liver cell line, Huh7, as the liver is a primary site of pathology in DENV2 infection. We demonstrated how modulation of UGT8 and GALC expression, and thereby GalCer expression, impacts the various stages of the virus life cycle.

5.1.1 The role of UDP-galactosyltransferase 8 in DENV2 infection of Huh7 cells

Summary

In chapter 2 we focused on the role of UDP-galactosyltransferase 8 (UGT8) during DENV2 infection of Huh7 cells and discovered it played a role in entry and release of virus particles. We discovered that the level of UGT8 expression was progressively decreased between 24 to 72 hours post-infection. This finding was correlated with our observation that expression of GalCer on the cell surface was reduced at 48 hpi. To our knowledge, UGT8 is the only enzyme that can produce GalCer, and thus it makes sense that with

less UGT8 expression there is less GalCer expression. We further discovered that when UGT8 expression was decreased using an siRNA knockdown approach that extracellular virus titer increased, though intracellular titer was not affected. Overexpression of UGT8 revealed an opposing phenotype. This led us to investigate if virus had a defect in entry, forcing virus to remain in the extracellular space, elevating the titer. We showed that virus particles made in cells with UGT8 knockdown did not enter wild type cells as readily as virus made in cells transfected with the negative control siRNA. Evaluation of virus transmission showed that fewer cells were infected at each time point by virus made from cells with UGT8 knockdown relative to the control. These two experiments confirmed that the virus particles were significantly altered following loss of UGT8 function. In addition to the virus being altered, there were other data that indicated that the cells might also be affected following modulation of UGT8 expression. We noted an increase in the rate of virus release in cells with UGT8 knockdown, suggesting that alterations in GalCer composition of the plasma membrane may facilitate more efficient viral egress.

Future directions

To complete our study, understanding the global changes in the lipidomic landscape of Huh7 cells in response to knockdown and overexpression would help us to fully characterize the phenotype. By performing liquid chromatography tandem mass spectrometry (LC-MS/MS) to quantify the metabolic landscape of both mock/infected Huh7 and also Huh7 cells with knockdown and overexpression of UGT8, it would help us to explain the mechanisms behind the changes in release and entry we see in the cells.

In addition, evaluation of the virus particles by electron microscopy to look for structural changes that affect entry and/or fusion would be valuable.

One of the virus life cycle stages we did not specifically investigate was fusion of the virus particle to the endosome membrane. Researchers have used liposomes as surrogates for the endosomal membrane and have created different compositions of membranes to use to study how a related FV, Tick-borne encephalitis virus, undergoes fusion [205]. Experiments to test the ability of different virus particles we generated for the entry and transmission experiments to fuse could provide valuable insight into which part of the entry process is affected. From our data, it is not clear if it is the attachment and endocytosis of the particles, fusion with the endosomal membrane, or a combination thereof that is affected when we modulate UGT8 expression.

A major challenge with this study was the relatively low magnitude of the changes we observed across all experiments. Liver cells have relatively low levels of UGT8 expression which tempers the magnitude of change we see when we manipulate UGT8 gene expression. Studies are currently underway to develop of CRISPR-Cas9 knockout of UGT8 in liver cells in hopes that it may produce a more pronounced phenotype. However, in addition to that, it would be interesting to explore the effects of UGT8 in cell lines that have more abundant expression. Some of this work was begun in neuroblastoma cells in chapter 4, but expanding to cells like oligodendrocytes, a myelinating cell type that has some of the highest expression of UGT8, could be rewarding.

5.1.2 The role of galactocerebrosidase in DENV2 infection of Huh7 cells

Summary

In chapter 3 we approached the role of GalCer from a different angle by studying the enzyme that degrades it, galactocerebrosidase (GALC). GALC functions in the lysosome to break GalCer down into galactose and ceramide. The gene has been extensively studied in developmental neurodegenerative diseases but has never been reported in viral infections. We observed that when we modulated the expression of GALC using siRNA knockdown it caused an increase in extracellular titer and the opposing phenotype with overexpression. This was fascinating as we had hypothesized that GALC might have the opposite effect to UGT8 on titer as they perform the reciprocal reactions from each other. We then looked at differences in intracellular and extracellular titer following GALC knockdown and observed an increase in both. This finding, in conjunction with the lack of effect on genome replication and specific infectivity of the virus particles, led us to believe that assembly may be occurring with greater efficiency.

This was a unique finding that we attributed to possible changes in ceramide levels within the cells. With GALC knockdown, there is formation of the toxic metabolite psychosine in the lysosome, which can result in oxidative stress. Oxidating stress within the cell can prompt upregulation of ceramides. Ceramides have been demonstrated to be enriched and recruited to viral replication sites in ZIKV infection of Huh7 cells, and there is compelling evidence to suggest that there may be a similar effect in DENV2 infection though it has not been confirmed in Huh7 cells [95,197–199].

Future directions

To complete the work in this chapter, mechanistic studies similar to those performed for UGT8 in chapter 2 would deepen our knowledge of how GALC affects the virus life cycle. Specifically looking at if release is altered and if that is contributing to the increase in extracellular titer would be beneficial. Similar to chapter 2, it would be useful to understand the metabolic landscape by following these studies with LC-MS/MS of both mock/infected Huh7 and also Huh7 cells with knockdown and overexpression of GALC. Confirmation of both the landscape during infection and also the downstream effects of modulating GALC expression would inform us of the metabolic drivers behind the changes we observed. Furthermore, to investigate if altering ceramide levels within the cell increases the efficiency of assembly, we could employ the use of compartment-specific sphingomyelinase and ceramidase plasmids that can modulate the expression of ceramide in specific cellular organelles [206].

5.1.3 The role of UDP-galactosyltransferase 8 in ZIKV infection

Summary

The goal of the preliminary work presented in this chapter was to understand if the changes we observed with UGT8 in DENV2 were conserved in ZIKV in Huh7 cells. We demonstrated that while the decrease in titer following knockdown and the increase in titer following overexpression were the same, the expression of UGT8 and GalCer during infection differed. In contrast to DENV2 infection which resulted in a progressive decrease in UGT8 expression between 24-72 hours, in ZIKV there was no significant change until 72 hours where there was a small reduction in UGT8 expression. This suggested that

ZIKV may not directly impact UGT8 expression. It was intriguing to see that changes in GalCer expression measured using flow cytometry mirrored the changes in expression of UGT8 mRNA, with no change at 48 hpi and a small reduction at 72 hpi. Furthermore, this suggests that decreases in UGT8 expression precipitate a decrease in the product, GalCer, in the plasma membrane. At the end of this study, we began to explore the role of UGT8 in neuroblastoma cells, which have a much higher level of UGT8 expression than Huh7 cells. Despite achieving a modest level of knockdown efficiency, we observed an increase in ZIKV titer following knockdown. This indicates that with greater knockdown efficiency, the phenotype may be greater in magnitude, warranting further study.

Future directions

The neuroblastoma cells are a key resource for this project that we should continue to explore. Studies are currently underway to develop a CRISPR-Cas9 UGT8 knockout system that we could deploy in this cell line. If the knockout of UGT8 is not lethal to the neuroblastoma cells, the ability to study the role of UGT8 in ZIKV infection in this system could be informative. It would also be helpful to understand how UGT8 and GalCer expression may change during ZIKV infection of the neuroblastoma cells. As described in the future directions for chapter 2, it would also be worthwhile to study to effects of UGT8 modulation in other cells lines with high UGT8 expression, such as oligodendrocytes. Oligodendrocytes are also permissive to ZIKV, and because they are a cell that produces myelin, they have even greater expression of both UGT8 and GalCer (which is a major component of myelin).

5.2 Concluding remarks

The intricate relationship between FVs and UGT8 and GALC, enzymes that perform the synthesis and degradation of galactosylceramides, was a central theme of this dissertation work. Our findings demonstrate that even subtle alterations to UGT8 and GALC expression can have significant effects on the flavivirus life cycle in vitro. This underscores the critical role of galactosylceramides in flavivirus infection.

References:

1. Pereira MR. Global rise in dengue transmission—2023. American Journal of Transplantation. 2024 Mar 1;24(3):318–9.

2. Dengue - Global situation [Internet]. [cited 2024 Dec 23]. Available from: https://www.who.int/emergencies/disease-outbreak-news/item/2024-DON518

3. Vector-borne diseases [Internet]. [cited 2024 Oct 2]. Available from: https://www.who.int/news-room/fact-sheets/detail/vector-borne-diseases

4. Economic Burden of Mosquito-Borne Diseases in Low- and Middle-Income Countries: Protocol for a Systematic Review - PMC [Internet]. [cited 2024 Oct 2]. Available from: https://www.ncbi.nlm.nih.gov/pmc/articles/PMC10750235/

5. Dengue and severe dengue [Internet]. [cited 2024 Oct 2]. Available from: https://www.who.int/news-room/fact-sheets/detail/dengue-and-severe-dengue

6. Vector-borne diseases [Internet]. [cited 2025 Jan 16]. Available from: https://www.who.int/news-room/fact-sheets/detail/vector-borne-diseases

7. The global economic burden of dengue: a systematic analysis - The Lancet Infectious Diseases [Internet]. [cited 2024 Oct 2]. Available from: https://www.thelancet.com/journals/laninf/article/PIIS1473-3099(16)00146-8/abstract

8. Bhatt S, Gething PW, Brady OJ, Messina JP, Farlow AW, Moyes CL, Drake JM, Brownstein JS, Hoen AG, Sankoh O, Myers MF, George DB, Jaenisch T, Wint GRW, Simmons CP, Scott TW, Farrar JJ, Hay SI. The global distribution and burden of dengue. Nature. 2013 Apr 25;496(7446):504–7.

9. Schaefer TJ, Panda PK, Wolford RW. Dengue Fever. In: StatPearls [Internet]. Treasure Island (FL): StatPearls Publishing; 2024 [cited 2024 Oct 3]. Available from: http://www.ncbi.nlm.nih.gov/books/NBK430732/

10. Messina JP, Brady OJ, Scott TW, Zou C, Pigott DM, Duda KA, Bhatt S, Katzelnick L, Howes RE, Battle KE, Simmons CP, Hay SI. Global spread of dengue virus types: mapping the 70 year history. Trends Microbiol. 2014 Mar;22(3):138–46.

11. Halstead S. Recent advances in understanding dengue. F1000Res. 2019;8:F1000 Faculty Rev-1279.

12. Brady OJ, Gething PW, Bhatt S, Messina JP, Brownstein JS, Hoen AG, Moyes CL, Farlow AW, Scott TW, Hay SI. Refining the global spatial limits of dengue virus transmission by evidence-based consensus. PLoS Negl Trop Dis. 2012;6(8):e1760.

13. Muller DA, Depelsenaire ACI, Young PR. Clinical and Laboratory Diagnosis of Dengue Virus Infection. The Journal of Infectious Diseases. 2017 Mar 1;215(suppl_2):S89–95.

14. Narayan R, Tripathi S. Intrinsic ADE: The Dark Side of Antibody Dependent Enhancement During Dengue Infection. Front Cell Infect Microbiol. 2020;10:580096.

15. Dr M, Sw M, Rs B. Dengue Vaccines: The Promise and Pitfalls of Antibody-Mediated Protection. Cell host & microbe [Internet]. 2021 Jan 13 [cited 2024 Oct 4];29(1). Available from: https://pubmed.ncbi.nlm.nih.gov/33444553/

16. Halstead SB. Dengue Antibody-Dependent Enhancement: Knowns and Unknowns. Microbiol Spectr. 2014 Dec;2(6).

17. Pintado Silva J, Fernandez-Sesma A. Challenges on the development of a dengue vaccine: a comprehensive review of the state of the art. J Gen Virol. 2023 Mar 1;104(3):001831.

18. Thomas SJ. Is new dengue vaccine efficacy data a relief or cause for concern? npj Vaccines. 2023 Apr 15;8(1):1–6.

19. Thomas SJ, Yoon IK. A review of Dengvaxia®: development to deployment. Hum Vaccin Immunother. 2019 Oct 7;15(10):2295–314.

20. Kallás EG, Cintra MAT, Moreira JA, Patiño EG, Braga PE, Tenório JCV, Infante V, Palacios R, de Lacerda MVG, Batista Pereira D, da Fonseca AJ, Gurgel RQ, Coelho ICB, Fontes CJF, Marques ETA, Romero GAS, Teixeira MM, Siqueira AM, Barral AMP, Boaventura VS, Ramos F, Elias Júnior E, Cassio de Moraes J, Covas DT, Kalil J, Precioso AR, Whitehead SS, Esteves-Jaramillo A, Shekar T, Lee JJ, Macey J, Kelner SG, Coller BAG, Boulos FC, Nogueira ML. Live, Attenuated, Tetravalent Butantan-Dengue Vaccine in Children and Adults. N Engl J Med. 2024 Feb 1;390(5):397–408.

21. Rivera L, Biswal S, Sáez-Llorens X, Reynales H, López-Medina E, Borja-Tabora C, Bravo L, Sirivichayakul C, Kosalaraksa P, Martinez Vargas L, Yu D, Watanaveeradej V, Espinoza F, Dietze R, Fernando L, Wickramasinghe P, Duarte MoreiraJr E, Fernando AD, Gunasekera D, Luz K, Venâncioda Cunha R, Rauscher

M, Zent O, Liu M, Hoffman E, LeFevre I, Tricou V, Wallace D, Alera M, Borkowski A. Three-year Efficacy and Safety of Takeda's Dengue Vaccine Candidate (TAK-003). Clin Infect Dis. 2021 Oct 4;75(1):107–17.

22. WHO prequalifies new dengue vaccine [Internet]. [cited 2025 Jan 15]. Available from: https://www.who.int/news/item/15-05-2024-who-prequalifies-new-dengue-vaccine

23. Chang C, Ortiz K, Ansari A, Gershwin ME. The Zika outbreak of the 21st century. J Autoimmun. 2016 Apr;68:1–13.

24. Zika virus [Internet]. [cited 2025 Jan 1]. Available from: https://www.who.int/news-room/fact-sheets/detail/zika-virus

25. Zika - PAHO/WHO | Pan American Health Organization [Internet]. 2024 [cited 2025 Jan 1]. Available from: https://www.paho.org/en/topics/zika

26. Zika virus disease outbreak 2015-2016 [Internet]. [cited 2025 Jan 1]. Available from: https://www.who.int/emergencies/situations/zika-virus-outbreak

27. Zika epidemiology update - February 2022 [Internet]. [cited 2025 Jan 1]. Available from: https://www.who.int/publications/m/item/zika-epidemiology-update---february-2022

28. Gubler DJ, Vasilakis N, Musso D. History and Emergence of Zika Virus. J Infect Dis. 2017 Dec 15;216(Suppl 10):S860–7.

29. Ai JW, Zhang Y, Zhang W. Zika virus outbreak: ‘a perfect storm’. Emerg Microbes Infect. 2016 Mar;5(3):e21.

30. Halani S, Tombindo PE, O’Reilly R, Miranda RN, Erdman LK, Whitehead C, Bielecki JM, Ramsay L, Ximenes R, Boyle J, Krueger C, Willmott S, Morris SK, Murphy KE, Sander B. Clinical manifestations and health outcomes associated with Zika virus infections in adults: A systematic review. PLOS Neglected Tropical Diseases. 2021 Jul 12;15(7):e0009516.

31. The Epidemic of Zika Virus–Related Microcephaly in Brazil: Detection, Control, Etiology, and Future Scenarios - PMC [Internet]. [cited 2025 Jan 1]. Available from: https://pmc.ncbi.nlm.nih.gov/articles/PMC4816003/

32. Oliveira WK de, França GVA de, Carmo EH, Duncan BB, Kuchenbecker R de S, Schmidt MI. Infection-related microcephaly after the 2015 and 2016 Zika virus outbreaks in Brazil: a surveillance-based analysis. The Lancet. 2017 Aug 26;390(10097):861–70.

33. Voermans JJC, Pas, SD, van der Linden A, GeurtsvanKessel C, Koopmans M, van der Eijk A, Reusken CBEM. Whole-Blood Testing for Diagnosis of Acute Zika Virus Infections in Routine Diagnostic Setting. Emerg Infect Dis. 2019 Jul;25(7):1394–6.

34. Fujimura K, Guise AJ, Nakayama T, Schlaffner CN, Meziani A, Kumar M, Cheng L, Vaughan DJ, Kodani A, Van Haren S, Parker K, Levy O, Durbin AF, Bosch I, Gehrke L, Steen H, Mochida GH, Steen JA. Integrative systems biology

characterizes immune-mediated neurodevelopmental changes in murine Zika virus microcephaly. iScience. 2023 May 19;26(7):106909.

35. Davies AJ, Lleixà C, Siles AM, Gourlay DS, Berridge G, Dejnirattisai W, Ramírez-Santana C, Anaya JM, Falconar AK, Romero-Vivas CM, Osorio L, Parra B, Screaton GR, Mongkolsapaya J, Fischer R, Pardo CA, Halstead SK, Willison HJ, Querol L, Rinaldi S. Guillain-Barré Syndrome Following Zika Virus Infection Is Associated With a Diverse Spectrum of Peripheral Nerve Reactive Antibodies. Neurol Neuroimmunol Neuroinflamm. 2022 Nov 21;10(1):e200047.

36. Kusunoki S, Kaida K ichi. Antibodies against ganglioside complexes in Guillain-Barré syndrome and related disorders. Journal of Neurochemistry. 2011;116(5):828–32.

37. Guillain–Barré syndrome [Internet]. [cited 2025 Jan 1]. Available from: https://www.who.int/news-room/fact-sheets/detail/guillain-barré-syndrome

38. Perera R, Kuhn RJ. Host Metabolism and its Contribution in Flavivirus Biogenesis. In: Arboviruses: Molecular Biology, Evolution and Control [Internet]. Caister Academic Press; 2016 [cited 2024 Oct 3]. p. 45–60. Available from: https://www.caister.com/arbo

39. Messina JP, Brady OJ, Scott TW, Zou C, Pigott DM, Duda KA, Bhatt S, Katzelnick L, Howes RE, Battle KE, Simmons CP, Hay SI. Global spread of dengue virus types: mapping the 70 year history. Trends in Microbiology. 2014 Mar 1;22(3):138–46.

40. Laureti M, Narayanan D, Rodriguez-Andres J, Fazakerley JK, Kedzierski L. Flavivirus Receptors: Diversity, Identity, and Cell Entry. Front Immunol. 2018 Sep 26;9:2180.

41. Perera-Lecoin M, Meertens L, Carnec X, Amara A. Flavivirus Entry Receptors: An Update. Viruses. 2013 Dec 30;6(1):69–88.

42. Smit JM, Moesker B, Rodenhuis-Zybert I, Wilschut J. Flavivirus Cell Entry and Membrane Fusion. Viruses. 2011 Feb 22;3(2):160–71.

43. Balsitis SJ, Coloma J, Castro G, Alava A, Flores D, McKerrow JH, Beatty PR, Harris E. Tropism of dengue virus in mice and humans defined by viral nonstructural protein 3-specific immunostaining. Am J Trop Med Hyg. 2009 Mar;80(3):416–24.

44. Jessie K, Fong MY, Devi S, Lam SK, Wong KT. Localization of dengue virus in naturally infected human tissues, by immunohistochemistry and in situ hybridization. J Infect Dis. 2004 Apr 15;189(8):1411–8.

45. Miner JJ, Diamond MS. Zika virus pathogenesis and tissue tropism. Cell Host Microbe. 2017 Feb 8;21(2):134–42.

46. Tajik S, Farahani AV, Ardekani OS, Seyedi S, Tayebi Z, Kami M, Aghaei F, Hosseini TM, Nia MMK, Soheili R, Letafati A. Zika virus tropism and pathogenesis: understanding clinical impacts and transmission dynamics. Virol J. 2024 Oct 29;21:271.

47. Cruz-Oliveira C, Freire JM, Conceição TM, Higa LM, Castanho MARB, Da Poian AT. Receptors and routes of dengue virus entry into the host cells. FEMS Microbiology Reviews. 2015 Mar 1;39(2):155–70.

48. Schaar HM van der, Rust MJ, Chen C, Ende-Metselaar H van der, Wilschut J, Zhuang X, Smit JM. Dissecting the Cell Entry Pathway of Dengue Virus by Single-Particle Tracking in Living Cells. PLOS Pathogens. 2008 Dec 19;4(12):e1000244.

49. Chu JJH, Ng ML. Infectious entry of West Nile virus occurs through a clathrin-mediated endocytic pathway. J Virol. 2004 Oct;78(19):10543–55.

50. Fritz R, Stiasny K, Heinz FX. Identification of specific histidines as pH sensors in flavivirus membrane fusion. J Cell Biol. 2008 Oct 20;183(2):353–61.

51. Kaufmann B, Rossmann MG. Molecular mechanisms involved in the early steps of flavivirus cell entry. Microbes Infect. 2011 Jan;13(1):1–9.

52. Pierson TC, Kielian M. Flaviviruses: Braking the entering. Curr Opin Virol. 2013 Feb;3(1):3–12.

53. Guirakhoo F, Bolin RA, Roehrig JT. The Murray Valley encephalitis virus prM protein confers acid resistance to virus particles and alters the expression of epitopes within the R2 domain of E glycoprotein. Virology. 1992 Dec 1;191(2):921–31.

54. Krishnan MN, Sukumaran B, Pal U, Agaisse H, Murray JL, Hodge TW, Fikrig E. Rab 5 Is Required for the Cellular Entry of Dengue and West Nile Viruses. J Virol. 2007 May;81(9):4881–5.

55. Pattanakitsakul S nga, Poungsawai J, Kanlaya R, Sinchaikul S, Chen ST, Thongboonkerd V. Association of Alix with late endosomal lysobisphosphatidic acid is important for dengue virus infection in human endothelial cells. J Proteome Res. 2010 Sep 3;9(9):4640–8.

56. Stiasny K, Koessl C, Heinz FX. Involvement of Lipids in Different Steps of the Flavivirus Fusion Mechanism. J Virol. 2003 Jul;77(14):7856–62.

57. Moesker B, Rodenhuis-Zybert IA, Meijerhof T, Wilschut J, Smit JM. Characterization of the functional requirements of West Nile virus membrane fusion. Journal of General Virology. 2010;91(2):389–93.

58. Umashankar M, Sánchez-San Martín C, Liao M, Reilly B, Guo A, Taylor G, Kielian M. Differential Cholesterol Binding by Class II Fusion Proteins Determines Membrane Fusion Properties. J Virol. 2008 Sep;82(18):9245–53.

59. Lescar J, Soh S, Lee LT, Vasudevan SG, Kang C, Lim SP. The Dengue Virus Replication Complex: From RNA Replication to Protein-Protein Interactions to Evasion of Innate Immunity. In: Hilgenfeld R, Vasudevan SG, editors. Dengue and Zika: Control and Antiviral Treatment Strategies [Internet]. Singapore: Springer; 2018 [cited 2025 Jan 7]. p. 115–29. Available from: https://doi.org/10.1007/978-981-10-8727-1_9

60. Rossignol ED, Peters KN, Connor JH, Bullitt E. Zika Virus Induced Cellular Remodeling. Cell Microbiol. 2017 Aug;19(8):10.1111/cmi.12740.

61. Arakawa M, Morita E. Flavivirus Replication Organelle Biogenesis in the Endoplasmic Reticulum: Comparison with Other Single-Stranded Positive-Sense RNA Viruses. Int J Mol Sci. 2019 May 11;20(9):2336.

62. Welsch S, Miller S, Romero-Brey I, Merz A, Bleck CKE, Walther P, Fuller SD, Antony C, Krijnse-Locker J, Bartenschlager R. Composition and Three-Dimensional Architecture of the Dengue Virus Replication and Assembly Sites. Cell Host Microbe. 2009 Apr 23;5(4):365–75.

63. Mackenzie JM, Jones MK, Young PR. Immunolocalization of the Dengue Virus Nonstructural Glycoprotein NS1 Suggests a Role in Viral RNA Replication. Virology. 1996 Jun 1;220(1):232–40.

64. Edeling MA, Diamond MS, Fremont DH. Structural basis of Flavivirus NS1 assembly and antibody recognition. Proceedings of the National Academy of Sciences. 2014 Mar 18;111(11):4285–90.

65. Pan Q, Jiao H, Zhang W, Chen Q, Zhang G, Yu J, Zhao W, Hu H. The step-by-step assembly mechanism of secreted flavivirus NS1 tetramer and hexamer captured at atomic resolution. Science Advances. 2024 May;10(18):eadm8275.

66. Puerta-Guardo H, Glasner DR, Espinosa DA, Biering SB, Patana M, Ratnasiri K, Wang C, Beatty PR, Harris E. Flavivirus NS1 Triggers Tissue-Specific Vascular

Endothelial Dysfunction Reflecting Disease Tropism. Cell Rep. 2019 Feb 5;26(6):1598-1613.e8.

67. Leung JY, Pijlman GP, Kondratieva N, Hyde J, Mackenzie JM, Khromykh AA. Role of Nonstructural Protein NS2A in Flavivirus Assembly. J Virol. 2008 May;82(10):4731–41.

68. Wu J, Bera AK, Kuhn RJ, Smith JL. Structure of the Flavivirus Helicase: Implications for Catalytic Activity, Protein Interactions, and Proteolytic Processing. J Virol. 2005 Aug;79(16):10268–77.

69. Zou J, Xie X, Wang QY, Dong H, Lee MY, Kang C, Yuan Z, Shi PY. Characterization of Dengue Virus NS4A and NS4B Protein Interaction. Journal of Virology. 2015 Mar 10;89(7):3455–70.

70. Renner M, Dejnirattisai W, Carrique L, Martin IS, Karia D, Ilca SL, Ho SF, Kotecha A, Keown JR, Mongkolsapaya J, Screaton GR, Grimes JM. Flavivirus maturation leads to the formation of an occupied lipid pocket in the surface glycoproteins. Nat Commun. 2021 Feb 23;12(1):1238.

71. Plevka P, Battisti AJ, Sheng J, Rossmann MG. Mechanism for maturation-related reorganization of flavivirus glycoproteins. J Struct Biol. 2014 Jan;185(1):27–31.

72. van Meer G, Voelker DR, Feigenson GW. Membrane lipids: where they are and how they behave. Nat Rev Mol Cell Biol. 2008 Feb;9(2):112–24.

73. Marsh D. Lateral Pressure Profile, Spontaneous Curvature Frustration, and the Incorporation and Conformation of Proteins in Membranes. Biophys J. 2007 Dec 1;93(11):3884–99.

74. Girard M, Bereau T. Regulating Lipid Composition Rationalizes Acyl Tail Saturation Homeostasis in Ectotherms. Biophys J. 2020 Sep 1;119(5):892–9.

75. Pomorski T, Menon AK. Lipid flippases and their biological functions. Cell Mol Life Sci. 2006 Nov 13;63(24):2908–21.

76. Varki A, Cummings RD, Esko JD, Freeze HH, Stanley P, Bertozzi CR, Hart GW, Etzler ME, editors. Essentials of Glycobiology [Internet]. 2nd ed. Cold Spring Harbor (NY): Cold Spring Harbor Laboratory Press; 2009 [cited 2024 Dec 30]. Available from: http://www.ncbi.nlm.nih.gov/books/NBK1908/

77. Quinville BM, Deschenes NM, Ryckman AE, Walia JS. A Comprehensive Review: Sphingolipid Metabolism and Implications of Disruption in Sphingolipid Homeostasis. Int J Mol Sci. 2021 May 28;22(11):5793.

78. Yesylevskyy SO, Rivel T, Ramseyer C. The influence of curvature on the properties of the plasma membrane. Insights from atomistic molecular dynamics simulations. Sci Rep. 2017 Nov 22;7(1):16078.

79. Cha HJ, He C, Zhao H, Dong Y, An IS, An S. Intercellular and intracellular functions of ceramides and their metabolites in skin (Review). International Journal of Molecular Medicine. 2016 Jul 1;38(1):16–22.

80. Chernomordik LV, Kozlov MM. Mechanics of membrane fusion. Nat Struct Mol Biol. 2008 Jul;15(7):675–83.

81. Melikyan GB. Driving a wedge between viral lipids blocks infection. Proc Natl Acad Sci U S A. 2010 Oct 5;107(40):17069–70.

82. Espósito DLA, Nguyen JB, DeWitt DC, Rhoades E, Modis Y. Physico-chemical requirements and kinetics of membrane fusion of flavivirus-like particles. J Gen Virol. 2015 Jul;96(Pt 7):1702–11.

83. Holopainen JM, Angelova MI, Kinnunen PK. Vectorial budding of vesicles by asymmetrical enzymatic formation of ceramide in giant liposomes. Biophys J. 2000 Feb;78(2):830–8.

84. Perera R, Kuhn RJ. Host Metabolism and its Contribution in Flavivirus Biogenesis. In: Arboviruses: Molecular Biology, Evolution and Control [Internet]. Caister Academic Press; 2016 [cited 2024 Dec 8]. p. 45–60. Available from: https://www.caister.com/arbo

85. Junjhon J, Pennington JG, Edwards TJ, Perera R, Lanman J, Kuhn RJ. Ultrastructural characterization and three-dimensional architecture of replication sites in dengue virus-infected mosquito cells. J Virol. 2014 May;88(9):4687–97.

86. Aktepe TE, Pham H, Mackenzie JM. Differential utilisation of ceramide during replication of the flaviviruses West Nile and dengue virus. Virology. 2015 Oct;484:241–50.

87. Chotiwan N, Andre BG, Sanchez-Vargas I, Islam MN, Grabowski JM, Hopf-Jannasch A, Gough E, Nakayasu E, Blair CD, Belisle JT, Hill CA, Kuhn RJ, Perera R. Dynamic remodeling of lipids coincides with dengue virus replication in the midgut of Aedes aegypti mosquitoes. PLOS Pathogens. 2018 Feb 15;14(2):e1006853.

88. Gould SB. Membranes and evolution. Curr Biol. 2018 Apr 23;28(8):R381–5.

89. Casares D, Escribá PV, Rosselló CA. Membrane Lipid Composition: Effect on Membrane and Organelle Structure, Function and Compartmentalization and Therapeutic Avenues. International Journal of Molecular Sciences. 2019 May 1;20(9):2167.

90. Liao Z, Cimakasky LM, Hampton R, Nguyen DH, Hildreth JE. Lipid rafts and HIV pathogenesis: host membrane cholesterol is required for infection by HIV type 1. AIDS Res Hum Retroviruses. 2001 Jul 20;17(11):1009–19.

91. Olsen BN, Schlesinger PH, Ory DS, Baker NA. 25-Hydroxycholesterol Increases the Availability of Cholesterol in Phospholipid Membranes. Biophys J. 2011 Feb 16;100(4):948–56.

92. Rattay S, Hufbauer M, Hoboth P, Sztacho M, Akgül B. Viruses and phospholipids: Friends and foes during infection. Journal of Medical Virology. 2023;95(3):e28658.

93. Li C, Deng YQ, Wang S, Ma F, Aliyari R, Huang XY, Zhang NN, Watanabe M, Dong HL, Liu P, Li XF, Ye Q, Tian M, Hong S, Fan J, Zhao H, Li L, Vishlaghi N, Buth JE, Au C, Liu Y, Lu N, Du P, Qin FXF, Zhang B, Gong D, Dai X, Sun R, Novitch BG,

Xu Z, Qin CF, Cheng G. 25-Hydroxycholesterol Protects Host against Zika Virus Infection and Its Associated Microcephaly in a Mouse Model. Immunity. 2017 Mar 21;46(3):446–56.

94. Zha X, Pierini LM, Leopold PL, Skiba PJ, Tabas I, Maxfield FR. Sphingomyelinase Treatment Induces ATP-independent Endocytosis. J Cell Biol. 1998 Jan 12;140(1):39–47.

95. Leier HC, Weinstein JB, Kyle JE, Lee JY, Bramer LM, Stratton KG, Kempthorne D, Navratil AR, Tafesse EG, Hornemann T, Messer WB, Dennis EA, Metz TO, Barklis E, Tafesse FG. A global lipid map defines a network essential for Zika virus replication. Nat Commun. 2020 Jul 21;11(1):3652.

96. Jacquemyn J, Cascalho A, Goodchild RE. The ins and outs of endoplasmic reticulum-controlled lipid biosynthesis. EMBO Rep. 2017 Nov;18(11):1905–21.

97. van Meer G, de Kroon AIPM. Lipid map of the mammalian cell. Journal of Cell Science. 2011 Jan 1;124(1):5–8.

98. Morita E, Suzuki Y. Membrane-Associated Flavivirus Replication Complex—Its Organization and Regulation. Viruses. 2021 Jun 3;13(6):1060.

99. Ripa I, Andreu S, López-Guerrero JA, Bello-Morales R. Membrane Rafts: Portals for Viral Entry. Front Microbiol [Internet]. 2021 Feb 4 [cited 2024 Oct 6];12. Available from: https://www.frontiersin.org/journals/microbiology/articles/10.3389/fmicb.2021.631274/full

100. Stancevic B, Kolesnick R. CERAMIDE-RICH PLATFORMS IN TRANSMEMBRANE SIGNALING. FEBS Lett. 2010 May 3;584(9):1728–40.

101. Nurminen TA, Holopainen JM, Zhao H, Kinnunen PKJ. Observation of Topical Catalysis by Sphingomyelinase Coupled To Microspheres. J Am Chem Soc. 2002 Oct 1;124(41):12129–34.

102. Martín-Acebes MA, Merino-Ramos T, Blázquez AB, Casas J, Escribano-Romero E, Sobrino F, Saiz JC. The Composition of West Nile Virus Lipid Envelope Unveils a Role of Sphingolipid Metabolism in Flavivirus Biogenesis. J Virol. 2014 Oct;88(20):12041–54.

103. Diaz-Rohrer B, Levental KR, Levental I. Rafting through traffic: Membrane domains in cellular logistics. Biochimica et Biophysica Acta (BBA) - Biomembranes. 2014 Dec 1;1838(12):3003–13.

104. Yau WL, Peters MBA, Sorin M, Rönfeldt S, Pulkkinen LIA, Carlson LA, Överby AK, Lundmark R. The flavivirus protein NS4B recruits the cis-Golgi protein ACBD3 to modify ER-Golgi trafficking for virion release [Internet]. bioRxiv; 2024 [cited 2025 Jan 19]. p. 2024.04.03.587877. Available from: https://www.biorxiv.org/content/10.1101/2024.04.03.587877v1

105. van Meer G, Lisman Q. Sphingolipid transport: rafts and translocators. J Biol Chem. 2002 Jul 19;277(29):25855–8.

106. van Meer G, Holthuis JC. Sphingolipid transport in eukaryotic cells. Biochim Biophys Acta. 2000 Jun 26;1486(1):145–70.

107. Koichi K, Michiya F, Makoto N. Lipid components of two different regions of an intestinal epithelial cell membrane of mouse. Biochimica et Biophysica Acta (BBA) - Lipids and Lipid Metabolism. 1974 Nov 18;369(2):222–33.

108. Patton JL, Lester RL. The phosphoinositol sphingolipids of Saccharomyces cerevisiae are highly localized in the plasma membrane. Journal of Bacteriology. 1991 May;173(10):3101–8.

109. Schulze RJ, Schott MB, Casey CA, Tuma PL, McNiven MA. The cell biology of the hepatocyte: A membrane trafficking machine. Journal of Cell Biology. 2019 Jun 14;218(7):2096–112.

110. Reza S, Ugorski M, Suchański J. Glucosylceramide and galactosylceramide, small glycosphingolipids with significant impact on health and disease. Glycobiology. 2021 Dec 18;31(11):1416–34.

111. Avota E, Bodem J, Chithelen J, Mandasari P, Beyersdorf N, Schneider-Schaulies J. The Manifold Roles of Sphingolipids in Viral Infections. Front Physiol [Internet]. 2021 Sep 29 [cited 2025 Feb 4];12. Available from: https://www.frontiersin.org/journals/physiology/articles/10.3389/fphys.2021.715527/full

112. Canals D, Hannun YA. Biological function, topology, and quantification of plasma membrane Ceramide. Advances in Biological Regulation. 2024 Jan 1;91:101009.

113. Gault C, Obeid L, Hannun Y. An overview of sphingolipid metabolism: from synthesis to breakdown. Adv Exp Med Biol. 2010;688:1–23.

114. Kitatani K, Idkowiak-Baldys J, Hannun YA. The sphingolipid salvage pathway in ceramide metabolism and signaling. Cell Signal. 2008 Jun;20(6):1010–8.

115. Bartke N, Hannun YA. Bioactive sphingolipids: metabolism and function. J Lipid Res. 2009 Apr;50(Suppl):S91–6.

116. Quinville BM, Deschenes NM, Ryckman AE, Walia JS. A Comprehensive Review: Sphingolipid Metabolism and Implications of Disruption in Sphingolipid Homeostasis. International Journal of Molecular Sciences. 2021 Jan;22(11):5793.

117. Canals D, Hannun YA. Biological function, topology, and quantification of plasma membrane Ceramide. Adv Biol Regul. 2024 Jan;91:101009.

118. Dutagaci B, Becker-Baldus J, Faraldo-Gómez JD, Glaubitz C. Ceramide–lipid interactions studied by MD simulations and solid-state NMR. Biochimica et Biophysica Acta (BBA) - Biomembranes. 2014 Oct 1;1838(10):2511–9.

119. Pullmannová P, Staňková K, Pospíšilová M, Školová B, Zbytovská J, Vávrová K. Effects of sphingomyelin/ceramide ratio on the permeability and microstructure of model stratum corneum lipid membranes. Biochimica et Biophysica Acta (BBA) - Biomembranes. 2014 Aug 1;1838(8):2115–26.

120. Alonso A, Goñi FM. The Physical Properties of Ceramides in Membranes. Annu Rev Biophys. 2018 May 20;47(1):633–54.

121. Pewzner-Jung Y, Ben-Dor S, Futerman AH. When Do Lasses (Longevity Assurance Genes) Become CerS (Ceramide Synthases)?: INSIGHTS INTO THE

REGULATION OF CERAMIDE SYNTHESIS *. Journal of Biological Chemistry. 2006 Sep 1;281(35):25001–5.

122. Haimovitz-Friedman A, Kolesnick RN, Fuks Z. Ceramide signaling in apoptosis. British Medical Bulletin. 1997 Jan 1;53(3):539–53.

123. Schulze H, Sandhoff K. Lysosomal Lipid Storage Diseases. Cold Spring Harb Perspect Biol. 2011 Jun;3(6):a004804.

124. Hanada K, Kumagai K, Yasuda S, Miura Y, Kawano M, Fukasawa M, Nishijima M. Molecular machinery for non-vesicular trafficking of ceramide. Nature. 2003 Dec 18;426(6968):803–9.

125. Tafesse FG, Huitema K, Hermansson M, Poel S van der, Dikkenberg J van den, Uphoff A, Somerharju P, Holthuis JCM. Both Sphingomyelin Synthases SMS1 and SMS2 Are Required for Sphingomyelin Homeostasis and Growth in Human HeLa Cells *. Journal of Biological Chemistry. 2007 Jun 15;282(24):17537–47.

126. Utermöhlen O, Herz J, Schramm M, Krönke M. Fusogenicity of membranes: the impact of acid sphingomyelinase on innate immune responses. Immunobiology. 2008;213(3–4):307–14.

127. Tettamanti G, Bassi R, Viani P, Riboni L. Salvage pathways in glycosphingolipid metabolism. Biochimie. 2003 Mar 1;85(3):423–37.

128. Sphingolipid Catabolism | Encyclopedia MDPI [Internet]. [cited 2025 Feb 22]. Available from: https://encyclopedia.pub/entry/20892

129. Sphingolipid Advice [Internet]. [cited 2025 Feb 25]. Available from: https://www.caymanchem.com/news/sphingolipid-advice

130. Beckmann N, Becker KA. Ceramide and Related Molecules in Viral Infections. International Journal of Molecular Sciences. 2021 Jan;22(11):5676.

131. Hanafusa K, Hotta T, Iwabuchi K. Glycolipids: Linchpins in the Organization and Function of Membrane Microdomains. Front Cell Dev Biol [Internet]. 2020 Oct 29 [cited 2024 Dec 30];8. Available from: https://www.frontiersin.org/journals/cell-and-developmental-biology/articles/10.3389/fcell.2020.589799/full

132. Zhang T, de Waard AA, Wuhrer M, Spaapen RM. The Role of Glycosphingolipids in Immune Cell Functions. Front Immunol. 2019 Jan 29;10:90.

133. Chazal N, Gerlier D. Virus Entry, Assembly, Budding, and Membrane Rafts. Microbiol Mol Biol Rev. 2003 Jun;67(2):226–37.

134. Blanchette CD, Lin WC, Ratto TV, Longo ML. Galactosylceramide Domain Microstructure: Impact of Cholesterol and Nucleation/Growth Conditions. Biophysical Journal. 2006 Jun 15;90(12):4466–78.

135. Garcia-Ruiz C, Morales A, Fernández-Checa JC. Glycosphingolipids and cell death: One aim, many ways. Apoptosis. 2015 May;20(5):607–20.

136. Bieberich E. Sphingolipids and lipid rafts: Novel concepts and methods of analysis. Chemistry and Physics of Lipids. 2018 Nov 1;216:114–31.

137. BLITTERSWIJK WJ van, LUIT AH van der, VELDMAN RJ, VERHEIJ M, BORST J. Ceramide: second messenger or modulator of membrane structure and dynamics? Biochemical Journal. 2003 Jan 15;369(2):199–211.

138. Chiricozzi E. Plasma membrane glycosphingolipid signaling: a turning point. Glycoconj J. 2022;39(1):99–105.

139. Grassi S, Giussani P, Mauri L, Prioni S, Sonnino S, Prinetti A. Lipid rafts and neurodegeneration: structural and functional roles in physiologic aging and neurodegenerative diseases: Thematic Review Series: Biology of Lipid Rafts. Journal of Lipid Research. 2020 May 1;61(5):636–54.

140. Varki A. Sialic acids in human health and disease. Trends Mol Med. 2008 Aug;14(8):351–60.

141. Bosio A, Binczek E, Le Beau MM, Fernald AA, Stoffel W. The Human Gene CGT Encoding the UDP-Galactose Ceramide Galactosyl Transferase (Cerebroside Synthase): Cloning, Characterization, and Assignment to Human Chromosome 4, Band q26. Genomics. 1996 May 15;34(1):69–75.

142. Sandhoff K, Kolter T. Topology of glycosphingolipid degradation. Trends in Cell Biology. 1996 Mar 1;6(3):98–103.

143. Iacono D, Koga S, Peng H, Manavalan A, Daiker J, Castanedes-Casey M, Martin NB, Herdt AR, Gelb MH, Dickson DW, Lee CW. Galactosylceramidase deficiency and pathological abnormalities in cerebral white matter of Krabbe disease. Neurobiology of Disease. 2022 Nov 1;174:105862.

144. Ostergaard JR. Juvenile neuronal ceroid lipofuscinosis (Batten disease): current insights. Degener Neurol Neuromuscul Dis. 2016 Aug 1;6:73–83.

145. Harouse JM, Bhat S, Spitalnik SL, Laughlin M, Stefano K, Silberberg DH, Gonzalez-Scarano F. Inhibition of Entry of HIV-1 in Neural Cell Lines by Antibodies Against Galactosyl Ceramide. Science. 1991 Jul 19;253(5017):320–3.

146. Planes R, Bahraoui E. HIV and SIV Envelope Glycoproteins Interact with Glycolipids and Lipids. International Journal of Molecular Sciences. 2023 Jan;24(14):11730.

147. Cook DG, Fantini J, Spitalnik SL, Gonzalez-Scarano F. Binding of Human Immunodeficiency Virus Type I (HIV-1) Gp120 to Galactosylceramide (GalCer): Relationship to the V3 Loop. Virology. 1994 Jun 1;201(2):206–14.

148. Faroux-Corlay B, Greiner J, Terreux R, Cabrol-Bass D, Aubertin AM, Vierling P, Fantini J. Amphiphilic Anionic Analogues of Galactosylceramide: Synthesis, Anti-HIV-1 Activity, and gp120 Binding. J Med Chem. 2001 Jun 1;44(13):2188–203.

149. Villard R, Hammache D, Delapierre G, Fotiadu F, Buono G, Fantini J. Asymmetric Synthesis of Water-Soluble Analogues of Galactosylceramide, an HIV-1 Receptor: New Tools to Study Virus–Glycolipid Interactions. ChemBioChem. 2002;3(6):517–25.

150. Takahashi T, Suzuki T. Role of sulfatide in normal and pathological cells and tissues. Journal of Lipid Research. 2012 Aug 1;53(8):1437–50.

151. Delézay O, Hammache D, Fantini J, Yahi N. SPC3, a V3 loop-derived synthetic peptide inhibitor of HIV-1 infection, binds to cell surface glycosphingolipids. Biochemistry. 1996 Dec 10;35(49):15663–71.

152. Takahashi T, Murakami K, Nagakura M, Kishita H, Watanabe S, Honke K, Ogura K, Tai T, Kawasaki K, Miyamoto D, Hidari KIPJ, Guo CT, Suzuki Y, Suzuki T. Sulfatide is required for efficient replication of influenza A virus. J Virol. 2008 Jun;82(12):5940–50.

153. UGT8 protein expression summary - The Human Protein Atlas [Internet]. [cited 2025 Jan 21]. Available from: https://www.proteinatlas.org/ENSG00000174607-UGT8

154. Meech R, Mubarokah N, Shivasami A, Rogers A, Nair PC, Hu DG, McKinnon RA, Mackenzie PI. A Novel Function for UDP Glycosyltransferase 8: Galactosidation of Bile Acids. Molecular Pharmacology. 2015 Mar 1;87(3):442–50.

155. Mackenzie PI, Walter Bock K, Burchell B, Guillemette C, Ikushiro S ichi, Iyanagi T, Miners JO, Owens IS, Nebert DW. Nomenclature update for the mammalian UDP glycosyltransferase (UGT) gene superfamily. Pharmacogenetics and Genomics. 2005 Oct;15(10):677.

156. Meech R, Mubarokah N, Shivasami A, Rogers A, Nair PC, Hu DG, McKinnon RA, Mackenzie PI. A Novel Function for UDP Glycosyltransferase 8: Galactosidation of Bile Acids. Molecular Pharmacology. 2015 Mar 1;87(3):442–50.

157. Kubo A, Arai Y, Nagashima S, Yoshikawa T. Alteration of sugar donor specificities of plant glycosyltransferases by a single point mutation. Archives of Biochemistry and Biophysics. 2004 Sep 15;429(2):198–203.

158. Pillot T, Ouzzine M, Fournelgigleux S, Lafaurie C, Tebbi D, Treat S, Radominska A, Lester R, Siest G, Magdalou J. Determination of the Human Liver UDP-Glucuronosyltransferase 2B4 Domains Involved in the Binding of UDP-Glucuronic Acid Using Photoaffinity Labeling of Fusion Proteins. Biochemical and Biophysical Research Communications. 1993 Dec 15;197(2):785–91.

159. Saran C, Fu D, Ho H, Klein A, Fallon JK, Honkakoski P, Brouwer KLR. A novel differentiated HuH-7 cell model to examine bile acid metabolism, transport and cholestatic hepatotoxicity. Sci Rep. 2022 Aug 22;12(1):14333.

160. Gillard BK, Rodriguez PJ, Fields DW, Raya JL, Lagor WR, Rosales C, Courtney HS, Gotto AM, Pownall HJ. Streptococcal Serum Opacity Factor promotes Cholesterol Ester Metabolism and Bile Acid Secretion In Vitro and In Vivo. Biochim Biophys Acta. 2016 Mar;1861(3):196–204.

161. Dooner HK, Nelson OE. Controlling element-induced alterations in UDPglucose:flavonoid glucosyltransferase, the enzyme specified by the bronze locus in maize. Proceedings of the National Academy of Sciences. 1977 Dec;74(12):5623–7.

162. Meech R, Hu DG, McKinnon RA, Mubarokah SN, Haines AZ, Nair PC, Rowland A, Mackenzie PI. The UDP-Glycosyltransferase (UGT) Superfamily: New Members,

New Functions, and Novel Paradigms. Physiological Reviews. 2019 Apr;99(2):1153–222.

163. Cao Q, Chen X, Wu X, Liao R, Huang P, Tan Y, Wang L, Ren G, Huang J, Dong C. Inhibition of UGT8 suppresses basal-like breast cancer progression by attenuating sulfatide–αVβ5 axis. J Exp Med. 2018 Jun 4;215(6):1679–92.

164. Dzięgiel P, Owczarek T, Plażuk E, Gomułkiewicz A, Majchrzak M, Podhorska-Okołów M, Driouch K, Lidereau R, Ugorski M. Ceramide galactosyltransferase (UGT8) is a molecular marker of breast cancer malignancy and lung metastases. Br J Cancer. 2010 Aug;103(4):524–31.

165. Beier UH, Görögh T. Implications of galactocerebrosidase and galactosylcerebroside metabolism in cancer cells. International Journal of Cancer. 2005;115(1):6–10.

166. Bosio A, Binczek E, Haupt WF, Stoffel W. Composition and Biophysical Properties of Myelin Lipid Define the Neurological Defects in Galactocerebroside- and Sulfatide-Deficient Mice. Journal of Neurochemistry. 1998 Jan;70(1):308–15.

167. Zaccariotto E, Cachón-González MB, Wang B, Lim S, Hirth B, Park H, Fezoui M, Sardi SP, Mason P, Barker RH, Cox TM. A novel brain-penetrant oral UGT8 inhibitor decreases in vivo galactosphingolipid biosynthesis in murine Krabbe disease. Biomedicine & Pharmacotherapy. 2022 May 1;149:112808.

168. St. Clair L. Reframing viral infections as acute metabolic disorders: Dengue viruses and their dependency on host metabolic pathways. Colorado State University; 2022.

169. Gullberg RC, Steel JJ, Pujari V, Rovnak J, Crick DC, Perera R. Stearoly-CoA desaturase 1 differentiates early and advanced dengue virus infections and determines virus particle infectivity. PLoS Pathog. 2018 Aug 17;14(8):e1007261.

170. Heaton NS, Perera R, Berger KL, Khadka S, LaCount DJ, Kuhn RJ, Randall G. Dengue virus nonstructural protein 3 redistributes fatty acid synthase to sites of viral replication and increases cellular fatty acid synthesis. Proc Natl Acad Sci U S A. 2010 Oct 5;107(40):17345–50.

171. Nazet U, Schröder A, Grässel S, Muschter D, Proff P, Kirschneck C. Housekeeping gene validation for RT-qPCR studies on synovial fibroblasts derived from healthy and osteoarthritic patients with focus on mechanical loading. PLoS One. 2019 Dec 6;14(12):e0225790.

172. Hall A, Róg T, Vattulainen I. Effect of galactosylceramide on the dynamics of cholesterol-rich lipid membranes. J Phys Chem B. 2011 Dec 15;115(49):14424–34.

173. Saeedimasine M, Montanino A, Kleiven S, Villa A. Role of lipid composition on the structural and mechanical features of axonal membranes: a molecular simulation study. Sci Rep. 2019 May 29;9(1):8000.

174. Blanchette CD, Lin WC, Ratto TV, Longo ML. Galactosylceramide Domain Microstructure: Impact of Cholesterol and Nucleation/Growth Conditions. Biophys J. 2006 Jun 15;90(12):4466–78.

175. Oliveira LG, Peron JPS. Viral receptors for flaviviruses: Not only gatekeepers. Journal of Leukocyte Biology. 2019;106(3):695–701.

176. Lee CJ, Lin HR, Liao CL, Lin YL. Cholesterol Effectively Blocks Entry of Flavivirus. J Virol. 2008 Jul;82(13):6470–80.

177. Mazzon M, Mercer J. Lipid interactions during virus entry and infection. Cell Microbiol. 2014 Sep;16(10):1493–502.

178. Salaün C, James DJ, Chamberlain LH. Lipid Rafts and the Regulation of Exocytosis. Traffic. 2004 Apr;5(4):255–64.

179. Alvarez M, Rodriguez-Roche R, Bernardo Lì, Morier L, Guzman MG. Improved Dengue Virus Plaque Formation on BHK21 and LLCMK2 Cells: Evaluation of Some Factors.

180. Shah PS, Link N, Jang GM, Sharp PP, Zhu T, Swaney DL, Johnson JR, Von Dollen J, Ramage HR, Satkamp L, Newton B, Aguirre S, Hüttenhain R, Petit MJ, Baum T, Everitt A, Laufman O, Tassetto M, Shales M, Stevenson E, Iglesias GN, Shokat L, Tripathi S, Balasubramaniam V, Webb LG, Willsey AJ, Garcia-Sastre A, Pollard KS, Cherry S, Gamarnik AV, Marazzi I, Taunton J, Fernandez-Sesma A, Bellen HJ, Andino R, Krogan NJ. Comparative flavivirus-host protein interaction

mapping reveals mechanisms of dengue and Zika virus pathogenesis. Cell. 2018 Dec 13;175(7):1931-1945.e18.

181. Livak KJ, Schmittgen TD. Analysis of Relative Gene Expression Data Using Real-Time Quantitative PCR and the 2−ΔΔCT Method. Methods. 2001 Dec 1;25(4):402–8.

182. Long D, Cohen GH, Muggeridge MI, Eisenberg RJ. Cysteine mutants of herpes simplex virus type 1 glycoprotein D exhibit temperature-sensitive properties in structure and function. J Virol. 1990 Nov;64(11):5542–52.

183. Cai W, Person S, DebRoy C, Gu B. Functional regions and structural features of the gB glycoprotein of herpes simplex virus type 1: An analysis of linker insertion mutants. Journal of Molecular Biology. 1988 Jun 5;201(3):575–88.

184. Butrapet S, Kinney RM, Huang CYH. Determining genetic stabilities of chimeric dengue vaccine candidates based on dengue 2 PDK-53 virus by sequencing and quantitative TaqMAMA. Journal of Virological Methods. 2006 Jan 1;131(1):1–9.

185. Pralhada Rao R, Vaidyanathan N, Rengasamy M, Mammen Oommen A, Somaiya N, Jagannath MR. Sphingolipid Metabolic Pathway: An Overview of Major Roles Played in Human Diseases. J Lipids. 2013;2013:178910.

186. Iacono D, Koga S, Peng H, Manavalan A, Daiker J, Castanedes-Casey M, Martin NB, Herdt AR, Gelb MH, Dickson DW, Lee CW. Galactosylceramidase deficiency and pathological abnormalities in cerebral white matter of Krabbe disease. Neurobiol Dis. 2022 Nov;174:105862.

187. Deane JE, Graham SC, Kim NN, Stein PE, McNair R, Cachón-González MB, Cox TM, Read RJ. Insights into Krabbe disease from structures of galactocerebrosidase. Proc Natl Acad Sci U S A. 2011 Sep 13;108(37):15169–73.

188. Wenger DA, Rafi MA, Luzi P. Molecular genetics of Krabbe disease (globoid cell leukodystrophy): diagnostic and clinical implications. Hum Mutat. 1997;10(4):268–79.

189. Li Y, Xu Y, Benitez BA, Nagree MS, Dearborn JT, Jiang X, Guzman MA, Woloszynek JC, Giaramita A, Yip BK, Elsbernd J, Babcock MC, Lo M, Fowler SC, Wozniak DF, Vogler CA, Medin JA, Crawford BE, Sands MS. Genetic ablation of acid ceramidase in Krabbe disease confirms the psychosine hypothesis and identifies a new therapeutic target. Proceedings of the National Academy of Sciences. 2019 Oct;116(40):20097–103.

190. Reza S, Ugorski M, Suchański J. Glucosylceramide and galactosylceramide, small glycosphingolipids with significant impact on health and disease. Glycobiology. 2021 May 31;31(11):1416–34.

191. Nikolova-Karakashian MN, Rozenova KA. Ceramide in Stress Response. Sphingolipids as Signaling and Regulatory Molecules. 2010 Dec 24;688:86–108.

192. Yabu T, Shiba H, Shibasaki Y, Nakanishi T, Imamura S, Touhata K, Yamashita M. Stress-induced ceramide generation and apoptosis via the phosphorylation and activation of nSMase1 by JNK signaling. Cell Death Differ. 2015 Feb;22(2):258–73.

193. Nikolova-Karakashian MN, Rozenova KA. Ceramide in Stress Response. Sphingolipids as Signaling and Regulatory Molecules. 2010 Dec 24;688:86–108.

194. Snider JM, Luberto C, Hannun YA. Approaches for probing and evaluating mammalian sphingolipid metabolism. Anal Biochem. 2019 Jun 15;575:70–86.

195. Bartke N, Hannun YA. Bioactive sphingolipids: metabolism and function. J Lipid Res. 2009 Apr;50(Suppl):S91–6.

196. Won JS, Kim J, Paintlia MK, Singh I, Singh AK. Role of Endogenous Psychosine Accumulation in Oligodendrocytes Differentiation and Survival: Implication for Krabbe Disease. Brain Res. 2013 May 1;1508:44–52.

197. Perera R, Riley C, Isaac G, Hopf-Jannasch AS, Moore RJ, Weitz KW, Pasa-Tolic L, Metz TO, Adamec J, Kuhn RJ. Dengue Virus Infection Perturbs Lipid Homeostasis in Infected Mosquito Cells. PLoS Pathog. 2012 Mar 22;8(3):e1002584.

198. Elliott K, Caicedo PA, Haunerland NH, Lowenberger C. Profiling lipidomic changes in dengue-resistant and dengue-susceptible strains of Colombian Aedes aegypti after dengue virus challenge. PLoS Negl Trop Dis. 2023 Oct 17;17(10):e0011676.

199. Jeanpierre AR, Mariappan V, Green SR, Mutheneni SR, P S, Pillai AB. Plasma levels of Ceramides and their association with Hematocrit and Thrombocytopenia in Severe and Non-severe dengue [Internet]. bioRxiv; 2022 [cited 2025 Jan 30]. p. 2022.06.22.497160. Available from: https://www.biorxiv.org/content/10.1101/2022.06.22.497160v1

200. Beckmann N, Becker KA. Ceramide and Related Molecules in Viral Infections. Int J Mol Sci. 2021 May 26;22(11):5676.

201. Avota E, Bodem J, Chithelen J, Mandasari P, Beyersdorf N, Schneider-Schaulies J. The Manifold Roles of Sphingolipids in Viral Infections. Front Physiol [Internet]. 2021 Sep 29 [cited 2025 Feb 4];12. Available from: https://www.frontiersin.org/journals/physiology/articles/10.3389/fphys.2021.715527/full

202. Fong SL, Wong KT, Tan CT. Dengue virus infection and neurological manifestations: an update. Brain. 2024 Mar 1;147(3):830–8.

203. Sánchez-San Martín C, Li T, Bouquet J, Streithorst J, Yu G, Paranjpe A, Chiu CY. Differentiation enhances Zika virus infection of neuronal brain cells. Sci Rep. 2018 Sep 28;8(1):14543.

204. Cell line - UGT8 - The Human Protein Atlas [Internet]. [cited 2025 Feb 6]. Available from: https://www.proteinatlas.org/ENSG00000174607-UGT8/cell+line

205. Corver J, Ortiz A, Allison SL, Schalich J, Heinz FX, Wilschut J. Membrane Fusion Activity of Tick-Borne Encephalitis Virus and Recombinant Subviral Particles in a Liposomal Model System. Virology. 2000 Mar 30;269(1):37–46.

206. Sakamoto W, Canals D, Salamone S, Allopenna J, Clarke CJ, Snider J, Obeid LM, Hannun YA. Probing compartment-specific sphingolipids with targeted bacterial sphingomyelinases and ceramidases. J Lipid Res. 2019 Nov;60(11):1841–50.

Appendix

A.1 Generation of stable Huh7 clonal cell lines:

Methods:

Huh7 cells were seeded at $2.4x10^6$ cells per 10 cm dish. The following day, cells were transfected with 10 µg of plasmid DNA (see section 2.4.2 for information on plasmids) using the Lipofectamine 3000 kit (ThermoFisher, catalog# L3000008) as per manufacturer recommendations for HepG2 cells scaled for 10 cm dishes. Briefly, one tube was prepared with 500 µl of Gibco OptiMEM I Reduced Serum Medium (ThermoFisher, catalog #31985062) and 22 µl of Lipofectamine 3000. A second tube was prepared with 500 µl of Gibco OptiMEM I Reduced Serum Medium, 10 µg of plasmid DNA, and 28 µl P3000 reagent. The contents of the second tube were added to the first tube, mixed well, and incubated at room temperature for 10-15 minutes as per kit instructions. During this incubation period, the media on the cells was replaced with fresh media containing 2% serum. Forty-eight hours after transfection, the media was replaced with fresh media containing Gibco™ Hygromycin B (50 mg/mL) (ThermoFisher, catalog #10687010) at a concentration of 400 µg/mL. Media was refreshed every 3-4 days. Starting at 10 days after starting Hygromycin selection, colonies were selected using cloning cylinders and transferred to a 96 well plate. Additional colonies continued to be selected in the weeks that followed. Clonal cells lines were gradually expanded and frozen in liquid nitrogen for future use.

A.2 Infection of clonal cell lines and assessment of cell viability (Supplemental Figure A.3)

To determine how consistent expression of UGT8 affected DENV2 infection, cells were seeded at 400,000 cells per well in a 6 well plate. The following day cells were infected with DENV2 (MOI of 0.3) and supernatants were collected at 24 hpi. Viral supernatants were titered on BHK cells as described in section 2.2.1. Concurrently, cells were mock-infected and an Alamar Blue Cell Viability assay was performed as detailed in 2.4.3.

A.3 Western blot to evaluate for UGT8 protein expression

Confirmation of UGT8 protein expression levels were desired to validate the effects of siRNA knockdown, plasmid overexpression, and to determine success of the development of clonal cell lines.

Methods:

Cell harvest and lysis: Multiple approaches were attempted to optimize harvesting protocols. We first tried fractionating our protein extract. We began by trypsinizing cells, counting cells to collect equivalent cell numbers across all samples, and collecting cells in 0.5% NP40 buffer in 1XPBS. Cells were incubated for 20 minutes on ice in 0.5% NP40 in 1xPBS buffer. Cells were centrifuged at 1,500xg for 5 minutes to pellet nuclear material and then the supernatants (cytoplasmic extracts) were transferred to a new Eppendorf tube. Cytoplasmic extracts were then centrifuged at top speed (20,000xg) for 5 minutes to collect the 20K pellet. Supernatants were transferred to a new Eppendorf tube (cytoplasmic fraction).

To prepare each fraction for analysis, additional processing steps were taken. The nuclear fraction received 2.5x the volume of the pellet of digitoninC (e.g., if the pellet is approximately 10 µl, then 25 µl of digitonin C was added) and was incubated on ice for

60 minutes. The nuclear extract was then centrifuged at 20,000xg for 15 minutes and the supernatant was transferred to a fresh Eppendorf tube. This processing step eliminated chromatin and DNA which can increase sample viscosity resulting in difficulties with pipetting the sample into the wells on the gel. The 20K pellet was resuspended in 15 µl of RIPA buffer (ThermoFisher, catalog #89901). Then, protein concentrations were quantified using a Pierce BCA Protein Assay kit (ThermoFisher, catalog #23225). Concentrations of proteins loaded onto the gel were standardized for each fraction: 25 µg of protein was loaded for the cytoplasmic fraction, 15 µg was loaded for the nuclear fraction, and 10 µg was loaded for the 20K fraction. These numbers were optimized by running a gel with 30 µg, 25 µg, 20 µg, 15 µg, 10 µg, and 5 µg of cytoplasmic protein extracts and probing with Anti-beta Actin antibody (Abcam, catalog# 8226) to determine the optimal concentration of protein to load to achieve good visualization of the actin band. Antibody staining and concentrations are detailed below in the section on antibody optimization. The concentrations for the nuclear and 20K pellets were based on the maximum amount of protein that could be added to achieve a 10 µl volume of sample when combined with 4x loading buffer.

We also tried to perform Western blots using whole protein lysates prepared in RIPA buffer. For this protocol, we trypsinized cells and counted them to collect equivalent cell numbers across all samples, and then collected cells in RIPA buffer. This method of protein lysate preparation resulted in samples that were extremely viscous, making gel loading very difficult. At times these protein samples would float out of the wells of the gel and into the central chamber of the gel running apparatus leaving very little sample in the well.

Types of gels: We began by using NuPAGE™ Bis-Tris Mini Protein Gels, 4–12%, 1.0–1.5 mm (ThermoFisher, catalog #NP0321BOX) and NuPAGE™ MOPS SDS Running Buffer (20X) (ThermoFisher, catalog #NP000102) with 500 µl of NuPage antioxidant (ThermoFisher, catalog #NP0005) added to the central chamber of the gel running apparatus. These gels were very consistent in how they performed, protein samples ran in a straight line through the gel at constant speed, but were cost-prohibitive.

We also attempted to use homemade tris-glycine gels. We made these by preparing two mixtures: a resolving gel mixture and a stacking gel mixture. The resolving gel was composed of 30% acrylamide/Bis solution 29:1 (0.5 * X, where X is the gel percentage to give you a volume in mL, e.g. if a 10% gel is desired, 5 mL of acrylamide is used), 3.75 mL of 1.5 M Tris-HCL pH 8.8, 150 µl of 10% SDS, milliQ water (0.5 * X where X is the gel percentage to give you a volume in mL), 75 µl ammonium persulfate, and 7.5 µl Tetramethylethylenediamine (TEMED, ThermoFisher, catalog #17919). This mixture is added between the two glass plates secured in the gel making apparatus. 2 mL of isopropanol is added on top and the gel is allowed to solidify for 30-45 minutes. Then the stacking gel is prepared: 1.7 mL of 30% acrylamide/Bis solution 29:1, 2.5 mL Tris-HCl pH 6.8, 100 µl of 10% SDS, 5.6 mL of milliQ water, 100 µl of ammonium persulfate, and 10 µl of TEMED. The isopropanol is removed and the stacking gel mixture is added between the two plates and the comb to form the wells is added. These homemade gels were variable in quality, were fragile and ripped easily, and we had variable results with lanes running at constant speeds across the gel.

Sample preparation and gel running conditions: Varying volumes of prestained protein ladder were attempted, with the 2-3 µl of Blue Stain protein ladder (11-245 kb) (Gold Bio, catalog #P007-500) yielding the best success. Using 2-3 µl allowed clear visualization of the ladder without disrupting visualization of the bands from the samples from having too high of intensity. Regardless of the lysis buffer used, all samples were prepared to a total volume of 10-15 µl. Generally, NuPAGE™ LDS Sample Buffer 4x (ThermoFisher, catalog #NP0008) was used for the precast NuPage gels and 4x Laemmli buffer was used for the homemade tris-glycine gels. 4x Laemmli buffer was made by combining 250 mM Tris-HCl pH 6.8, 8% SDS w/v, 0.02% v/v Bromophenol blue, 40% v/v glycerol, and 20% v/v/ mercaptoethanol. However, both loading buffers were attempted in each type of gel and both worked in either type of gel. The gels were run at 150 volts at constant voltage for 60-75 minutes until the dye front approached the bottom of the gel. The gel running apparatus was placed on ice while running to prevent the gels and buffers from becoming too hot.

Blotting procedure: First, the power source was turned off and the gel was removed from the running apparatus. Then the gel was carefully removed from between the two plates and placed in transfer buffer to keep it wet. The Nitrocellulose membrane paper (0.22 micron, BioRad, catalog #1620112) was placed in transfer buffer with two sheets of filter paper of the same size along with the two sponges. The items were arranged in order of sponge, filter paper, gel, membrane, filter paper, sponge, and locked in place, ensuring the membrane side was facing the red side of the apparatus. The transfer was performed in the membrane transfer apparatus containing transfer buffer and an ice pack in the 4°C

fridge for 90 minutes at 150 mA at constant Amps. Then the membrane was removed from the apparatus and blocked in 5% non-fat powdered milk diluted in tris-buffered saline (TBST) for 20 minutes. TBST is made by combining 20 mM Tris and 150 mM NaCl in milliQ water, adjusting the ph to 7.6 with HCl, then adding 0.1% Tween 20. The blocking solution was removed and the gel was briefly rinsed with TBST prior to antibody staining.

Antibody staining: Two UGT8 antibodies were used during the optimization process. The first was UGT8 polyclonal antibody (ThermoFisher, catalog # PA5-103177). At first, we had some success with detecting this antibody when using it at concentrations of 1:50 and 1:100 when using the precast NuPage gels, however, results were not repeatable. Dilutions that were tried included 1:50, 1:100, 1:250, and 1:500. Primary antibody staining was performed overnight at 4°C regardless of the concentration of antibody used. Given the lack of repeatability, the second antibody that was used was Anti-UGT8 rabbit polyclonal antibody (ProteinTech, catalog #17982-1-AP). Success was never achieved with the second antibody and it resulted in abundant non-specific staining. Dilutions that were tried included 1:100, 1:250, 1:500, and 1:1,000. Following application of the primary antibody, the antibody solution was removed and the membrane was washed three time for 10-15 minutes in TBST prior to application of the secondary antibody.

Secondary antibodies used included AlexaFluor 647 and AlexaFluor 488 at a dilution of 1:500. Both secondary antibodies were successful when used to detect actin. Success with either UGT8 antibody was variable. Following application of both the primary and secondary antibodies for detection of UGT8 protein, the membrane was imaged (see section below on membrane imaging). Only once images had been obtained

was the membrane probed with the actin antibody diluted to 1:2,000 in TBST as per manufacturer's recommendations to serve as a loading control (Abcam, catalog# 8226). Depending on which secondary antibody was used for the UGT8 antibody, the opposite secondary was used for actin (e.g. if AlexaFluor 647 was used for UGT8, then AlexaFluor 488 was used for the actin antibody).

Membrane imaging: Membranes were imaged using the ChemiDoc Imaging System (BioRad) using the Blot/UV/Stain tray recommended by BioRad for fluorescent imaging.

Results: Two representative Western blot images are shown.

Figure A.4A. The gel has fractionated samples of cells transfected with IRR siRNA or UGT8 siRNA in an attempt to show UGT8 protein knockdown run on a NuPAGE™ Bis-Tris Mini Protein Gels, 4–12% using NuPAGE™ LDS Sample Buffer 4x with 3 µl of Blue Stain protein ladder (11-245 kb) loaded on either end of the gel. The protein concentrations of each fraction were as follows: 25 µg of protein for the cytoplasmic fraction, 15 µg was for the nuclear fraction, and 5 µg for the 20K fraction. The membrane was cut into two pieces so that the UGT8 protein which is 61 kDa would be on the top segment of the membrane and actin which is 42 kDa would be on the lower segment of the membrane. The top segment of the membrane was stained with UGT8 polyclonal antibody (ThermoFisher, catalog # PA5-103177) followed by AlexaFluor 647. The lower segment of the membrane was stained with Anti-beta Actin antibody (Abcam, catalog# 8226) and AlexaFluor 647. The two segments of the membrane were imaged together using the ChemiDoc Imaging System. There is a strong signal for the actin loading control

band for the nuclear and cytoplasmic fractions but only a faint actin band for the 20K fraction, suggesting insufficient protein concentrations for those samples. For all fractions there is no clear detection of UGT8.

Figure A.4B. The gel has whole cell lysates collected in RIPA buffer of the Huh7 clonal cells lines. Due to space constraints, only one empty vector control was run on the gel (EV 3). Each lane has 20 µg of protein and 3 µl of Blue Stain protein ladder (11-245 kb) loaded on either end of the gel. The membrane was first stained with Anti-UGT8 rabbit polyclonal antibody (ProteinTech, catalog #17982-1-AP) followed by AlexaFluor 647. The membrane was imaged using the ChemiDoc Imaging System. The membrane was then stained with Anti-beta Actin antibody (Abcam, catalog# 8226) and AlexaFluor 488 and imaged a second time. The actin band is clear for all samples, though the 5th UGT8 clone on the far right had difficulties during gel loading due to high sample viscosity. There are multiple bands that appeared during the UGT8 staining but none of them correspond to the correct size (61 kDa) and likely represent non-specific staining.

A.4 Immunofluorescence assay to evaluate for UGT8 protein expression

Methods:

Given the difficulties with optimization of Western blots for UGT8 protein detection, an immunofluorescence-based approach was attempted. 40,000 Huh7 cells were seeded on coverslips in a 12 well plate in media with 10% FBS. The following day, cells were transfected with either the UGT8 siRNA or the IRR siRNA as detailed in 2.4.1. After 48 hours, cells were mock-infected and then 24 hours later the media was removed, wells

were washed with 1XPBS, and then fixed with 500 µl 4% paraformaldehyde per well. Fixation was allowed to occur for 20 minutes on the rocker at room temperature. To mitigate background fluorescence from unquenched aldehydes, following fixation the paraformaldehyde was removed and 500 µl of a quenching solution (500 mL 1XPBS with 30 mM glycine) was added and allowed to incubate for 5 minutes on the rocker at room temperature. Cells were then washed three times for 5 minutes at room temperature on the rocker in 1XPBS. To permeabilize cells for intracellular staining, 500 µl of a permeabilizing solution (0.1% Triton X-100/1% bovine serum albumin in 1XPBS) was added and allowed to incubate for 15 minutes on the rocker at room temperature. Cells were then blocked overnight at 4°C on the rocker in a blocking solution composed of 0.01% Triton X-100/1% BSA solution in 1x PBS.

The following day coverslips were incubated for 1 hour at 37°C in 40 µl 1:250 dilution of the UGT8 polyclonal antibody (ThermoFisher, catalog # PA5-103177) in the blocking solution. Following primary antibody staining, coverslips were washed three times for 10 minutes in the blocking solution (0.01% Triton X-100/1% BSA solution in 1x PBS). Coverslips were then stained with the secondary antibody, Goat anti-Rabbit AlexaFluor 647 (ThermoFisher, catalog #A-21245) at a dilution of 1:500 in the blocking solution for 1 hour at 37°C. coverslips were washed once for 10 minutes in the blocking solution. Coverslips were then stained with DAPI stain diluted 1:2,000 in blocking buffer for 20 seconds at room temperature and washing three times in blocking solution for 10 minutes per wash. Coverslips were then glued to glass slides using FluorSave Reagent (Millipore Sigma, catalog #345789) and stored in a slide box at 4°C until they were imaged.

Coverslips were imaged with the ZEISS Confocal LSM 900. Cells were first identified by locating nuclei which were stained with DAPI and the software was used to draw a circle around each cell. The software then quantified and reported the relative fluorescence of both DAPI, corresponding to the nuclei, and AlexaFluor 647, corresponding to UGT8 expression per cell. From each group, either IRR or UGT8 siRNA treated, 100 cells were analyzed for relative fluorescence. This data was put into an excel sheet and the average of the relative fluorescence of AlexaFluor 647 across all cells for each treatment group was obtained.

Results: Supplemental figure A.5

Three representative images from either group (IRR or UGT8 siRNA) from the ZEISS Confocal LSM 900 software interface are shown. In these images, the selection line around each cell is visible as is the reported fluorescence data per cell. In figure A.5B, relative fluorescence intensity of cells transfected with UGT8 siRNA is 24% lower than cells transfected with IRR siRNA. This was a considerably lower knockdown efficiency than what was observed in 2.2.1 where mRNA knockdown was 81% lower in UGT8 knockdown cells when compared to the negative control. Given our difficulties with using the UGT8 antibody in Western blots, it could be that the antibody is not ideal for UGT8 detection in either Western blot or IFA experiments. The abundance of UGT8 in Huh7 cells is also relatively low, so it could be that it is hard to accurately detect because the level of expression could be at or below the limit of detection. One final possibility is that the UGT8 protein is very stable and does not have frequent turnover, so the effects of knockdown may be limited.

2.5.5 Addition of exogenous GalCer to Huh7 cells

Methods:

We were curious if adding exogenous GalCer to cells would affect the DENV2 life cycle and have a similar phenotype to overexpressing UGT8. To address this question, we reconstituted C18 Galactosyl(ß) Ceramide (d18:1/18:0) (Avanti Polar Lipids, catalog # 860844P-5mg) in DMSO to achieve a stock concentration of 5 mg/mL (the maximum concentration based on the solubility of 1-5 mg/mL as reported by Avanti Polar Lipids customer support). Huh7 cells were seeded at 20,000 cells per well in two 96 well plates. Two-fold serial dilutions of GalCer was made in media containing 2% FBS from concentrations ranging from 0.781 µM to 25 µM. The controls included a cells only (no treatment) control and three DMSO only controls (0.09%, 0.18%, and 0.36% DMSO). The media was removed from the cells and the media containing GalCer or DMSO only was added to the cells and the plates were incubated for 2 hours at 37°C. The media containing the GalCer or DMSO was removed and saved on ice, while DENV2-infection and mock-infection was performed on each of the two plates. Infection was performed by adding 100 µl of virus (or PBS only for mock infection) for 1 hour and allowing plates to rock at room temperature. After 1 hour, virus or PBS was removed, cells were washed with 1XPBS, and the media containing the GalCer or DMSO was re-added to the plates. At 24 hours post-infection, an Alamar Blue Cell Viability assay (described in 2.4.3) was performed on the mock-infected plate and viral supernatants were collected from the DENV2-infected plate and titered on BHK cells (as described in 2.2.1).

Results:

We observed no significant difference in the DENV2 titer in any of the GalCer treated cells relative to the controls (S6A). This could mean that addition of GalCer does not affect DENV2 titer. Alternatively, it could be that the amount of GalCer added was too low to result in a change, the cells did not take up the GalCer, and/or the timing of GalCer addition was not appropriate. We also observed no changes to the cell viability in the Alamar Blue assay (S6B).

Supplemental Figures

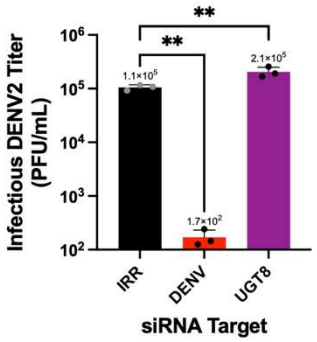

Supplemental Figure A.1: UGT8 knockdown was validated in a A549 cells. Human lung adenocarcinoma (A459) cells were transfected with a pool of four siRNAs targeting UGT8, a negative control irrelevant siRNA (IRR), or a positive control siRNA specific to the dengue virus used for infection (DENV). Forty-eight hours following transfection, cells were infected DENV2 (MOI = 0.3) for 24 hr. At 24 hpi, viral supernatants were collected and analyzed via plaque assays. Viral titer was significantly increased by 2-fold following UGT8 knockdown. One-way ANOVA with Dunnett's multiple comparison's test: ** = p≤0.01. Results are expressed as mean values with standard deviation indicated by error bars.

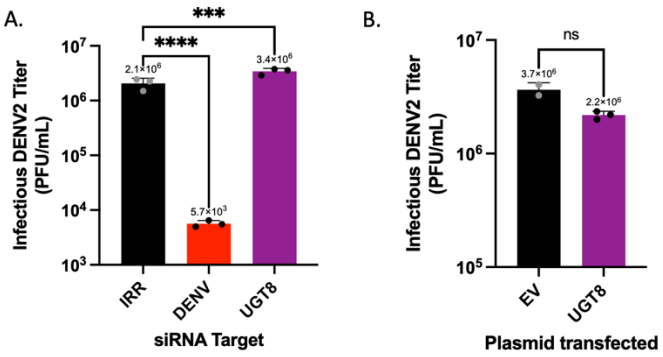

Supplemental figure A.2. Modulating UGT8 expression affects DENV2 titer at 48 hpi A. Huh7 cells were transfected with a pool of four siRNAs targeting UGT8, a negative control irrelevant siRNA (IRR), or a positive control siRNA specific to the dengue virus used for infection (DENV). Forty-eight hours following transfection, cells were infected DENV2 (MOI = 0.3) for 48 hours. At 48 hpi, viral supernatants were collected and analyzed via plaque assays. Viral titer was significantly increased by 1.62-fold following UGT8 knockdown. **B**. Huh7 cells were transfected with a plasmid containing the UGT8 gene and an empty vector control. Forty-eight hours following transfection, cells were infected DENV2 (MOI = 0.3) for 48 hr. At 48 hpi, viral supernatants were collected and analyzed via plaque assays. There was no significant difference in viral titer following UGT8 overexpression at 48 hpi. One-way ANOVA with Dunnett's multiple comparison's test: ns = $p \geq 0.05$, *** = $p \leq 0.001$, **** = $p \leq 0.0001$. Results are expressed as mean values with standard deviation indicated by error bars.

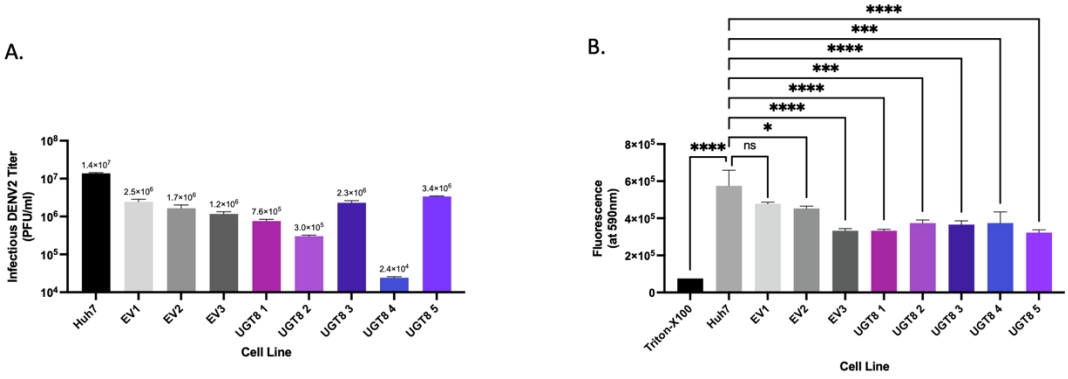

Supplemental figure A.3. Infection of clonal Huh7 cell lines and cell viability. Clonal Huh7 cell lines were infected DENV2 (MOI = 0.3) or mock-infected for 24 hours. **A.** At 24 hpi, viral supernatants were collected and analyzed via plaque assays. **B.** Mock infected cells were used in an Alamar Blue Cell Viability assay. All clonal cell lines had varying degrees of cytotoxic effects except for EV1 when compared to wild type Huh7 cells. One-way ANOVA with Dunnett's multiple comparison's test: ns = $p \geq 0.05$, *** = $p \leq 0.001$, **** = $p \leq 0.0001$.

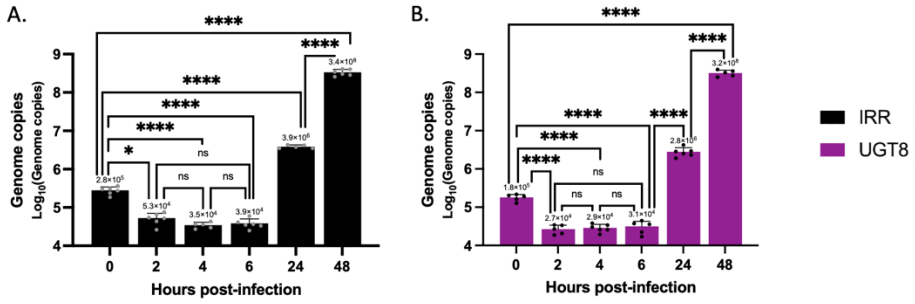

Supplemental Figure A.4. Results of a Student's unpaired T test for the entry experiment data. A-B. Genome copy values for IRR supernatant displayed in S4A and genome copy values for UGT8 supernatant displayed in S4B. For both groups, the statistical relationships are consistent. The 0 hpi time point is significantly different from all other time points. There is no significant difference between the 2-, 4-, and 6-hpi time points when compared to each other for both IRR and UGT8 groups. The 24- and 48-hpi time points are significantly different from each other and all other time points. Student's unpaired T test: ns = $p \geq 0.05$, * = $p \leq 0.05$, *** = $p \leq 0.001$, **** = $p \leq 0.0001$.

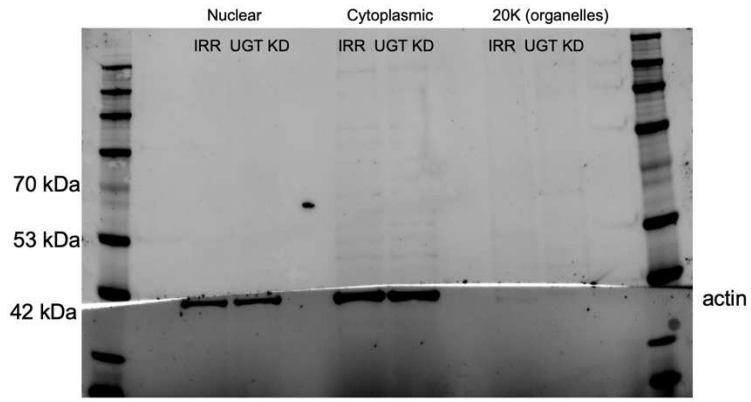

Supplemental Figure A.5A. A representative image of a Western blot to confirm protein knockdown following siRNA knockdown. A NuPAGE™ Bis-Tris Mini Protein Gel was used to analyze protein samples from Huh7 cells transfected with either the IRR control siRNA or the UGT8 siRNA. Proteins were fractionated to run the nuclear, cytoplasmic, and 20K fractions separately. The UGT8 polyclonal antibody from ThermoFisher was utilized and no protein was detected. Actin was detected at 42 kDa in the nuclear and cytoplasmic fractions but only faintly in the 20K fraction.

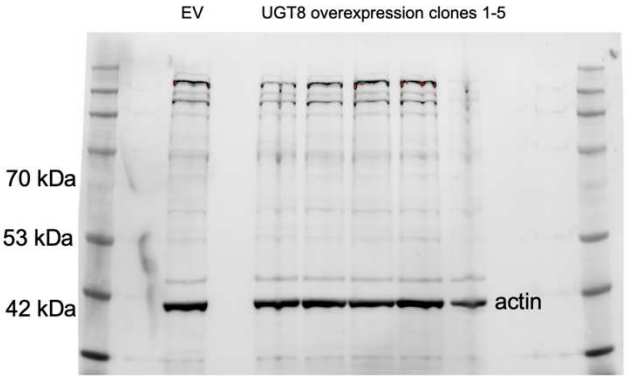

Supplemental Figure A.5B. A representative image of a Western blot to confirm protein overexpression in the Huh7 clonal cell lines.
A NuPAGE™ Bis-Tris Mini Protein Gel was used to run whole cell lysates from the Huh7 clonal cell lines. Samples include the empty vector (EV) control and five UGT8 overexpression clones were loaded. The Anti-UGT8 rabbit polyclonal antibody from ProteinTech was used to detect UGT8 and showed abundant non-specific staining but no clear band at the anticipated size of 61 kDa. Actin was detected and served as a loading control.

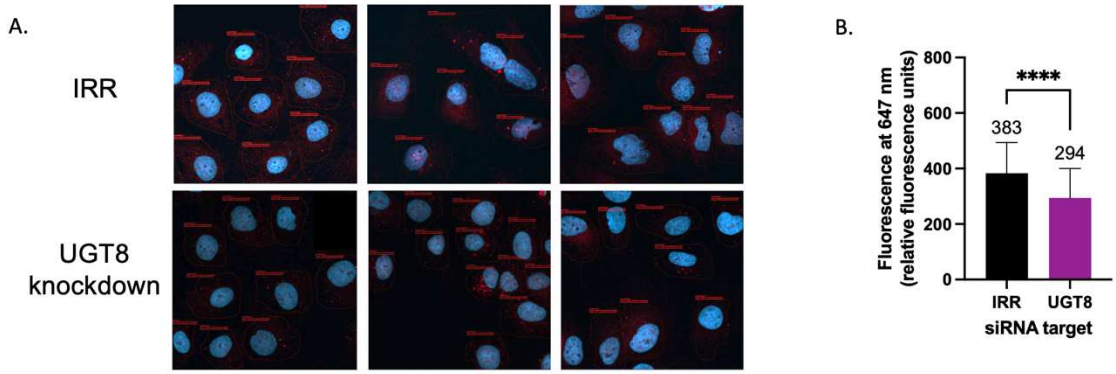

Supplemental Figure A.6. Immunofluorescence assay to confirm UGT8 protein knockdown.
Huh7 cells transfected with either IRR or UGT8 siRNA were evaluated 72 hours following mock-infection. Cells were stained with UGT8 polyclonal antibody and counterstained with AlexaFluor 647 (red) and then stained with DAPI (blue). **A.** Fluorescence was quantified in each cell using the ZEISS Confocal LSM 900 software. Cells were encircled and fluorescence data was reported. **B.** Average fluorescence intensity for 100 cells from each group showed a 24% decrease in fluorescence intensity for cells transfected with UGT8 siRNA. One-way ANOVA with Dunnett's multiple comparison's test: **** = p≤0.0001.

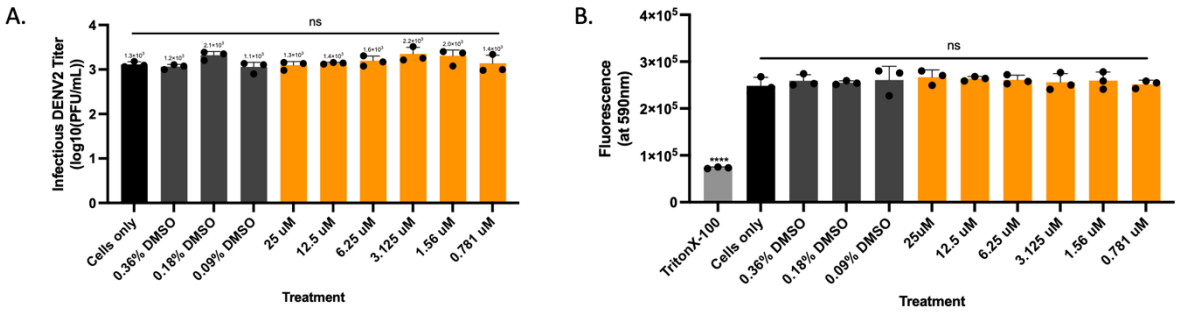

Supplemental Figure A.7. Addition of exogenous GalCer had no effect on DENV2 titer or cell viability.
A. There was no effect on DENV2 titer at any concentration of GalCer. **B**. No concentration of GalCer or DMSO affected cell viability. One-way ANOVA with Dunnett's multiple comparison's test: ns = p ≥ 0.05.

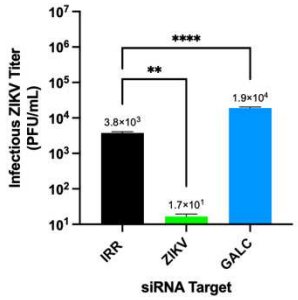

Supplemental Figure A.8. Huh7 cells were transfected with siRNAs targeting GALC, a non-targeting irrelevant (IRR) negative control, or a ZIKV-specific positive control siRNA (ZIKV). 48 hours following transfection, cells were infected DENV2 (MOI = 0.3) for 24 hr. At 24 hpi, cells were collected and analyzed via plaque assays. Results are represented as viral titers compared to the IRR control. siRNA knockdown of GALC shows a 5-fold increase in ZIKV titer. (A one-way ANOVA with Dunnett's multiple comparison's test: ** = p≤0.01, **** = p≤0.0001; results are expressed as mean values with standard deviation indicated by error bars) [Abbreviations: IRR, irrelevant, non-targeting siRNA; ZIKV, ZIKV-specific siRNA; GALC, galactocerebrosidase].